Development of a Physically Based Sediment Transport Model for Green Bay, Lake Michigan

Hector Bravo¹, Bahram Khazaei¹, Eric J Anderson², and J. Val Klump¹

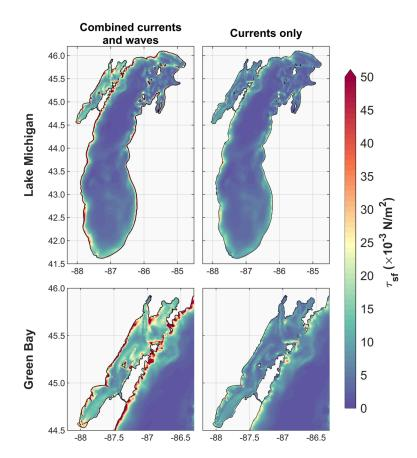
¹University of Wisconsin-Milwaukee

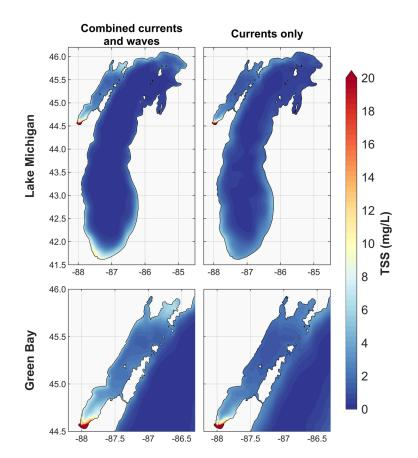
²National Oceanic and Atmospheric Administration (NOAA)

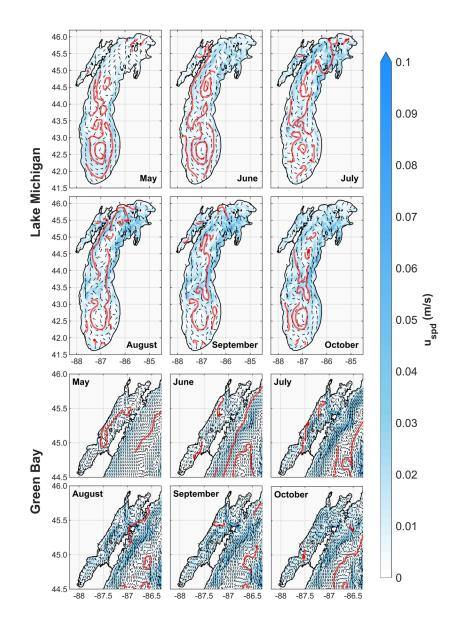
November 23, 2022

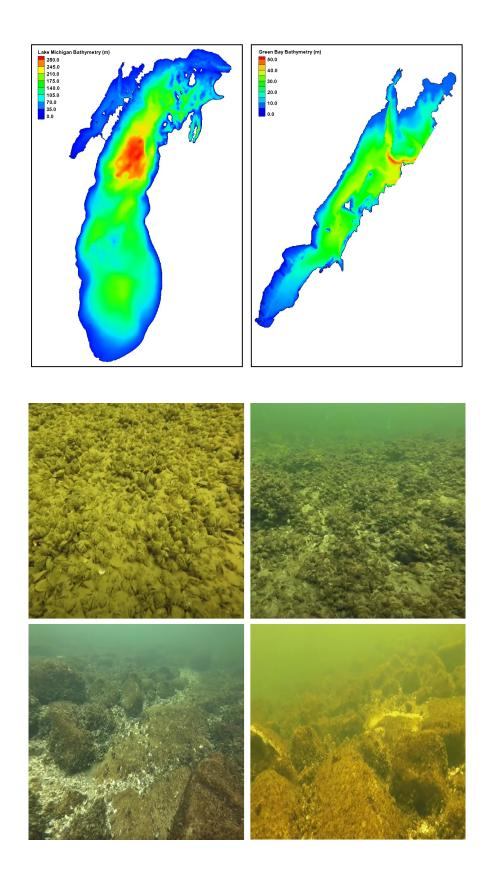
Abstract

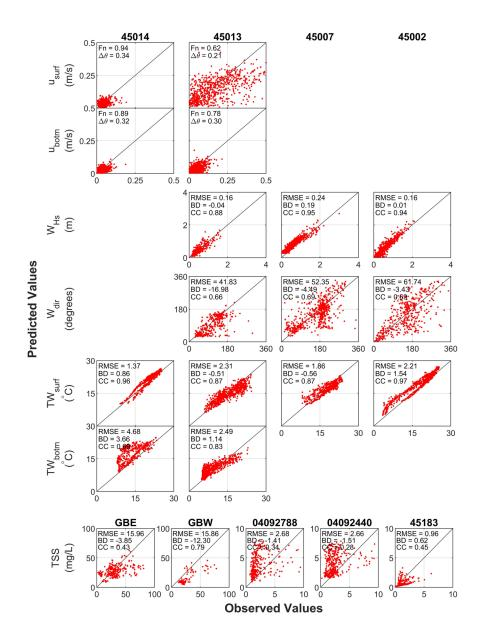
Green Bay is the largest freshwater estuarine system on earth, drains one-third of the Lake Michigan basin and delivers onethird of the lake's phosphorus load. Southern Green Bay is a designated area of concern (AOC) due to ecosystem degradation that includes eutrophication, harmful algal blooms (HABs), hypoxia, lost or altered habitat, and reduced water quality. While marine estuaries are subject to tidal influence and saltwater intrusion, this freshwater estuary is subject to lake intrusion of freshwater with different quality parameters. Understanding the simultaneous effects of tributary flows and lake intrusions is crucial to comprehend the dynamics of freshwater estuaries. A single hydrodynamic, wind-wave, and sediment transport model was developed for the lake and its estuary. This approach provides fine resolution in the estuary and simulates directly the combined effects of tributary flows and lake intrusions. The approach overcomes open-boundary limitations of nested models, and of whole-lake models that lack sufficient resolution or wind-wave and sediment transport simulation. The model confirms findings of previous studies and demonstrates how the circulation, thermal regime, wave action, and sediment transport in the estuary depend on meteorological forcing, tributary flows, and lake intrusions. The stage is set to apply this approach to study biogeochemical processes in lakes and estuaries.











2	Development of a Physically Based Sediment Transport Model for
3	Green Bay, Lake Michigan
4	
5	Bahram Khazaei ^{1,2} , Hector R. Bravo ¹ , Eric J. Anderson ³ , and Jeffrey V. Klump ⁴
6	¹ Department of Civil and Environmental Engineering, University of Wisconsin-Milwaukee
7	² Research Applications Laboratory, National Center for Atmospheric Research
8	³ Great Lakes Environmental Research Laboratory, National Oceanic and Atmospheric Administration
9	⁴ School of Freshwater Sciences, University of Wisconsin-Milwaukee
10	
11	Corresponding author: Hector R. Bravo (hrbravo@uwm.edu)
12	
13	
14	Key Points:
15	• Understanding the simultaneous effects of tributary flows and lake intrusions is crucial to
16	comprehend the dynamics of freshwater estuaries
17	• The circulation, thermal regime, wave action, and sediment transport in the estuary
18	depend on meteorological forcing, tributary flows, and lake intrusions
19	• The stage is set to apply this approach to study biogeochemical processes in lakes and
20	estuaries
21	

22 Abstract

23 Green Bay is the largest freshwater estuarine system on earth, drains one-third of the Lake 24 Michigan basin and delivers one-third of the lake's phosphorus load. Southern Green Bay is a 25 designated area of concern (AOC) due to ecosystem degradation that includes eutrophication, 26 harmful algal blooms (HABs), hypoxia, lost or altered habitat, and reduced water quality. While 27 marine estuaries are subject to tidal influence and saltwater intrusion, this freshwater estuary is 28 subject to lake intrusion of freshwater with different quality parameters. Understanding the 29 simultaneous effects of tributary flows and lake intrusions is crucial to comprehend the dynamics 30 of freshwater estuaries. A single hydrodynamic, wind-wave, and sediment transport model was 31 developed for the lake and its estuary. This approach provides fine resolution in the estuary and 32 simulates directly the combined effects of tributary flows and lake intrusions. The approach 33 overcomes open-boundary limitations of nested models, and of whole-lake models that lack 34 sufficient resolution or wind-wave and sediment transport simulation. The model confirms 35 findings of previous studies and demonstrates how the circulation, thermal regime, wave action, 36 and sediment transport in the estuary depend on meteorological forcing, tributary flows, and lake 37 intrusions. The stage is set to apply this approach to study biogeochemical processes in lakes and 38 estuaries.

39 Keywords: Green Bay, freshwater estuaries, sediment transport, physically-based models.

40 Plain Language Summary

41 Green Bay is a unique ecosystem located in the largest freshwater system on earth, the 42 Laurentian Great Lakes. Almost one-third of tributary waters to Lake Michigan flow through 43 Green Bay. Human activities in the watershed produce excessive amounts of contaminated 44 and/or nutrient-rich sediments that are discharged to the bay. Sediments are not efficiently 45 transported to Lake Michigan due to physical conditions in Green Bay, leading to ecosystem degradation, environmental and public health risks. We studied the movement, transport, and fate 46 47 of sediments in Lake Michigan, with a special attention to Green Bay, by developing a 48 physically-based, 3D sediment transport model. This model development effort helps to predict 49 circulation of contaminants and nutrients that are attached to the sediments, their settlement and 50 burial, and the detachment from the bottom during storm events. The knowledge gained in this 51 study will enhance our understanding of water quality conditions and nutrient recycling in 52 freshwater estuaries, and will improve future restoration efforts and management plans.

53 **1 Introduction**

54 Green Bay is the largest freshwater estuarine system on earth, drains one-third of Lake 55 Michigan basin and delivers one-third of the lake's total phosphorus load (Klump et al., 2018). 56 The International Joint Commission designated southern Green Bay as an area of concern (AOC) 57 in the 1980s due to several instances of ecosystem degradation including (but not limited to) 58 eutrophication, harmful algal blooms (HABs), hypoxia, lost or altered habitat, and reduced water 59 quality.

Green Bay has stimulated a significant amount of widely relevant research on the fate and behavior of toxics, biogeochemistry, habitat, biodiversity, and ecological processes. In particular, previous research relevant to hydrodynamics and sediment transport in Green Bay includes studies carried out on Green Bay, studies done on Lake Michigan and the Laurentian Great Lakes watershed, and studies done on marine estuaries. We will first concisely list those previous studies, then briefly explain how the present study differs in geophysical terms, present the focus and goals of this research, and describe its place within current research needs in Green Bay.

67 Relevant previous research to hydrodynamics and sediment transport in Green Bay 68 include studies on sediment resuspension and particle settling velocities (Eadie et al., 1991), 69 measurement of horizontal sediment transport (Hawley & Niester, 1993), on patterns of mass 70 sedimentation and of deposition of sediment contaminated by PCBs (Manchester-Neesvig et al., 71 1996), on sedimentary phosphorus (Klump et al., 1997), modeling hydrodynamics, sediment 72 transport and sorbent dynamics (HydroQual Inc., 1999), on benthic carbon and nitrogen mass 73 balances (Klump et al., 2009), explaining the role of circulation and heat fluxes in the formation 74 of stratification leading to hypoxia in Green Bay (Hamidi et al., 2015), a biogeochemical 75 analysis of hypoxia in Green Bay (Labuhn, 2017), analysis of the physical drivers of the 76 circulation and thermal regime impacting seasonal hypoxia in the bay (Bravo et al., 2017), 77 satellite-based estimations of surficial sediment transport (Hamidi et al., 2017), quantifying the 78 influence of cold-water intrusions in Green Bay (Grunert et al., 2018), and estimation of 79 transport timescales (Bravo et al., 2019). Previous relevant research done on Lake Michigan and 80 the Laurentian Great Lakes watershed include studying influences of suspended sediments on the 81 ecosystem in Lake Michigan (Chen et al., 2004; Ji et al., 2002), a 3D coupled bio-physical 82 modeling experiment on the St. Clair River, Lake St. Clair, and Detroit River System (Anderson

83 et al., 2010), relationships between wind-driven and hydraulic flow in Lake St. Clair and the St. 84 Clair River Delta (Anderson & Schwab, 2011), simulating a phytoplankton bloom in Lake 85 Michigan using a coupled physical-biological model (Luo et al., 2012), predicting the oscillating 86 bi-directional exchange flow in the Straits of Mackinac (Anderson & Schwab, 2013), modeling 87 the climatology of seasonal general circulation and thermal structure in the Great Lakes (Bai et 88 al., 2013), modeling the effect of invasive quagga mussels on the spring phytoplankton bloom in 89 Lake Michigan (Rowe et al., 2015), investigating the thermal response to meteorological forcing in a hydrodynamic model of Lake Superior (Xue et al., 2015), modeling Escherichia coli at 90 91 Beaches in Southern Lake Michigan (Safaie et al., 2016), modeling of dreissenid mussel impacts 92 on Lake Michigan (Shen, 2016), modeling wind-waves from deep to shallow waters in Lake 93 Michigan (Mao & Xia, 2017), biophysically modeling the influence of invasive quagga mussels, 94 phosphorus loads, and climate on spatial and temporal patterns of productivity in Lake Michigan 95 (Rowe et al., 2017), a study on the dynamics of wave-current-surge interactions in Lake 96 Michigan (Mao & Xia, 2020), and an investigation of the drivers of warmings in deep-waters of 97 Lake Michigan (Anderson et al., 2021).

98 There is vast research on marine estuaries, so we will just mention as examples the book 99 Estuarine Ecohydrology by Wolanski & Elliott (2015), a study on the impact of tides and winds 100 on estuarine circulation in the Pearl River Estuary (Lai et al., 2018), a study on the influence of 101 suspended sediment front on nutrients and phytoplankton dynamics off the Changjiang Estuary 102 (Ge et al., 2020), and an article on estuarine ecohydrology study of sediment transport in coastal 103 zones by (Ouillon, 2018). Wolanski & Elliott (2015) defined an estuary as a semi-enclosed body 104 of water connected to the sea as far as the tidal limit or the salt intrusion limit and receiving 105 freshwater runoff, recognizing that the freshwater inflow may not be perennial (i.e., it may occur 106 only for part of the year) and that the connection to the sea may be closed for part of the year 107 (e.g., by a sand bar), and that the tidal influence may be negligible. Sediments determine the 108 estuarine bed habitats (i.e., the fundamental niche for the fauna and flora on the bottom) and they 109 influence organisms in the water column. Sediments are mobile and their dynamics occur at time 110 scales of millennia, of intermediate timescales due to the tides, of storms, of river floods, of the 111 seasons, and of turbulence.

112 The Green Bay estuary is a semi-enclosed body of water connected to the freshwater 113 Lake Michigan as far as the limit of lake intrusion and receiving freshwater runoff. The

114 circulation, thermal regime, wave regime, and sediment transport in Lake Michigan and its 115 Green Bay estuary are driven by the momentum flux generated by wind, the heat flux across the 116 water surface, the Earth's rotation, thermal stratification, and topography (Bravo et al., 2017). 117 While marine estuaries are subject to tidal influence and saltwater intrusion, in freshwater 118 estuaries like Green Bay, the tidal influence is relatively smaller and salinity effects are 119 nonexistent. The role of the large receiving and exchanging large body of water is played by lake 120 water intrusion of currents, waves, and transport of waters with very different quality parameters 121 such as density, temperature, and conductivity. Understanding the simultaneous effects of 122 tributary flows and lake water intrusions is vital to comprehend the dynamics of freshwater 123 estuaries.

124 Previous hydrodynamic and transport modeling of Green Bay was done either by 125 employing nested models of the bay that represent the exchange of mass, energy, and momentum 126 with Lake Michigan using potentially problematic open boundary conditions, generally obtained 127 from low-resolution lake models (Hamidi et al., 2015; HydroQual Inc., 1999), or else using 128 whole-lake models that lack the desired high resolution in the bay (Lee et al., 2005, 2007; Mao & 129 Xia, 2017; Rowe et al., 2015; Rowe et al., 2017; Safaie et al., 2016; Shen, 2016). The study 130 presented herein bypasses the use of open boundary conditions by developing a single 131 hydrodynamic, wave, and sediment transport model of the lake that has high resolution in the 132 bay and in the exchange zone between the open lake and the bay.

133 The purposes of this research were to: a) use the existing database of hydrodynamic, 134 wave, and sediment field data to develop a predictive model of sediment transport in Lake 135 Michigan, with an emphasis on Green Bay; b) use the sediment transport model to contribute to 136 understanding ecological and environmental problems in the bay, and to recommend long-term 137 solutions; and c) analyze summertime patterns of circulation, wave action, current and wave-138 induced bottom shear stress, thermal structure, and sediment transport in Lake Michigan, with 139 special attention to Green Bay. The sediment transport model is designed to be a compatible 140 component of the NOAA Lake Michigan-Huron Operational Forecast System (LMHOFS) for 141 future water quality and shoreline protection applications for Lake Michigan and other Great 142 Lakes.

143 Green Bay represents a true "proving ground" for adaptive restoration. Among the main 144 recommendations of a recent summit on the "Ecological and Socio-Economic Tradeoffs of 145 Restoration in the Green Bay Ecosystem" was the creation of a "Green Bay Ecosystem 146 Simulation and Data Consortium" serving as a data clearing house, building upon the significant 147 progress to date, and developing a modeling framework and visualization tools, furthering public 148 outreach efforts, and ensuring a sustained growth in scientific expertise (Klump et al., 2018). 149 Gaps in biogeochemistry and hydrodynamics identified during the restoration summit include 150 incorporation of wind-wave models and an understanding of resuspension and its role in carbon 151 and phosphorus cycling, the delineation of diagenetic vs. rapid carbon remineralization and its 152 influence on sediment and water column respiration, the role of denitrification and nitrogen-153 fixation in the overall nitrogen budget for the bay and its link to nutrient stoichiometry and 154 phytoplankton and cyanobacterial production. Extending models to multiple-year simulations, 155 linking to refined watershed models, and engaging a complete range of downscaled regional climate scenarios to assess the magnitude of projected variability for the 21st century are 156 157 necessary to provide more robust projections and guide expectations for adaptive management 158 efforts (Klump et al., 2018). The present study addressed the incorporation of physical processes 159 including wind-wave dynamics and sediment transport, will be used to extend models to 160 multiple-year simulations, will engage downscaled regional climate scenarios to assess variability during the 21st century, and sets the stage for future work on other biogeochemical 161 162 modeling gaps listed above.

163 2 Model Components and Formulation

164 Physically-based sediment transport modeling is essential in Green Bay due to 165 complicated conditions of the system dynamics. Previous efforts intended to understand physical 166 processes and particle dynamics in Green Bay faced obstacles in model development. Major 167 obstacles included the use of Cartesian structured rectangular grids in POM-based models that 168 limits the representation of small-scale shoreline features in Green Bay, and difficulties in 169 modeling thermal structures and stratified flows in the shallow estuarine systems, especially 170 during upwelling or downwelling events. Challenges in the implementation of Environmental 171 Fluid Dynamics Code (EFDC) models were difficult documentation and neglected wind-wave effects. Additionally, those models are computationally expensive and not very efficient if ahigh-resolution grid in a large domain such as Lake Michigan is implemented.

To overcome those obstacles, a state-of-the-art modeling approach, the Finite-Volume Community Ocean Model (FVCOM) was used in this research. FVCOM's features such as the use of an unstructured-grid solver and a parallel mode computation option make it a suitable candidate for the Green Bay sediment transport model. FVCOM is also equipped with several water quality tools that can integrate different physical and biogeochemical processes and enhance the implementation of transport models in restoration applications.

180

2.1 Circulation Model: FVCOM

181 Developed by Chen et al. (2003), FVCOM is a free-surface, primitive-equation ocean 182 model and is a powerful numerical solution of the conservation of mass, momentum, and energy 183 principles that solves for currents, temperature, salinity, density, and other hydrodynamic 184 variables as follows:

$$\frac{\partial u}{\partial t} + u \frac{\partial u}{\partial x} + v \frac{\partial u}{\partial y} + w \frac{\partial u}{\partial z} - fv = -\frac{1}{\rho_W} \frac{\partial p}{\partial x} + \frac{\partial}{\partial z} \left(K_V \frac{\partial u}{\partial z} \right) + F_u$$
(1)

$$\frac{\partial v}{\partial t} + u \frac{\partial v}{\partial x} + v \frac{\partial v}{\partial y} + w \frac{\partial v}{\partial z} + fu = -\frac{1}{\rho_W} \frac{\partial p}{\partial x} + \frac{\partial}{\partial z} \left(K_V \frac{\partial v}{\partial z} \right) + F_v$$
(2)

$$\frac{\partial w}{\partial t} + u \frac{\partial w}{\partial x} + v \frac{\partial w}{\partial y} + w \frac{\partial w}{\partial z} = -\frac{1}{\rho_W} \frac{\partial p}{\partial x} + \frac{\partial}{\partial z} \left(K_V \frac{\partial w}{\partial z} \right) + F_w$$
(3)

$$\frac{\partial u}{\partial x} + \frac{\partial v}{\partial y} + \frac{\partial w}{\partial z} = 0$$
(4)

$$\frac{\partial TW}{\partial t} + u \frac{\partial TW}{\partial x} + v \frac{\partial TW}{\partial y} + w \frac{\partial TW}{\partial z} = \frac{\partial}{\partial z} \left(K_H \frac{\partial TW}{\partial z} \right) + F_{TW}$$
5)

$$\rho_W = \rho_W(TW, p)$$

185 where (u, v, w) are the components of the current in (x, y, z) Cartesian grid space, ρ_W is 186 the water density, p is the pressure, TW is the water temperature, f is the Coriolis coefficient, K_V 187 and K_H are the vertical eddy viscosity and thermal diffusion coefficients, and F_{u} , F_v , F_w , and F_{TW} 188 represent the momentum and thermal diffusion terms. FVCOM uses a modified MY-Level 2.5

6)

turbulence closure scheme (Mellor & Yamada, 1982) for vertical mixing calculations and
Smagorinsky's (1963) eddy scheme for horizontal mixing.

191 FVCOM has several features that make it an efficient computational tool for the physical 192 modeling of large lakes. FVCOM runs based on unstructured sigma-coordinated (terrain-193 following) grids, in which the 3D domain is discretized into triangular finite volumes. That 194 feature increases model flexibility in representing irregular geometry of shorelines in the Green 195 Bay estuary and preserves fine features of several peninsulas and islands that restrict physical 196 processes in the bay. Additionally, FVCOM is computationally efficient because it runs in 197 parallel and also adopts a split mode numerical scheme, in which it first calculates the water 198 surface elevation and depth-averaged currents in the external mode and then solves for the 199 vertical diffusive transport in a 3D internal mode.

200 FVCOM has been successfully implemented in various hydrodynamic applications such 201 as coastal modeling (e.g., Chen et al., 2003, 2007; Huang et al., 2008; B. Li et al., 2017; J. Li et 202 al., 2018; Zhang et al., 2018), Great Lakes studies (e.g., Anderson et al., 2010; Anderson & 203 Schwab, 2011; Bai et al., 2013; Mao et al., 2016; Mao & Xia, 2020; Read et al., 2010; Shore, 204 2009; Xue et al., 2015), and modeling rivers, straits, and channels (e.g., Anderson & 205 Phanikumar, 2011; Anderson & Schwab, 2013; Guerra et al., 2017; Lai et al., 2018). It has also 206 been coupled with water quality and biogeochemical models in various case studies (e.g., Luo et 207 al., 2012; Rowe et al., 2015; Rowe et al., 2017; Safaie et al., 2016; Shen, 2016). In this study, we 208 used FVCOM version 4.1 to develop the physical circulation model of Lake Michigan.

209

2.2 Wave Model: FVCOM-SWAVE

Sediment movement is primarily due to advective-diffusive transport in the water column; however, sediment processes near the bottom are significantly affected by the wave interactions. Therefore, the implementation of wave actions in the sediment model is an important step toward simulations of more realistic current-wave-sediment interactions in the bottom boundary layer. Simulating WAves Nearshore (SWAN) model is adopted by FVCOM (FVCOM-SWAVE) as the wave simulator. SWAN was developed by Booij et al. (1999) and models wave evolution using transport equations to solve for wave action density *N* as follows:

$$\frac{\partial N}{\partial t} + \frac{\partial c_x N}{\partial x} + \frac{\partial c_y N}{\partial y} + \frac{\partial c_\sigma N}{\partial \sigma} + \frac{\partial c_\theta N}{\partial \theta} = \frac{S_w}{\sigma}$$
⁽⁷⁾

where N is the energy density E divided by the relative frequency σ , $N(\sigma,\theta) = E(\sigma,\theta)/\sigma$, 217 218 (c_x, c_y) are the propagation velocities in the (x, y) Cartesian grid coordinates, σ and θ are the 219 intrinsic wave frequency and direction, c_{σ} is the propagation velocity due to variations in depth 220 and currents, c_{θ} is the propagation in wave direction, and S_{w} is acting as a source/sink term to 221 represent the effects of wind-wave generation, energy dissipation due to whitecapping, depth-222 induced wave breaking, and bottom friction, and nonlinear wave-wave interactions. Specific 223 details of the SWAN model formulation and validation are described in the literature (Booij et 224 al., 2004; Ris et al., 1999). SWAN is a structured-grid wave model and was converted to an 225 unstructured-grid finite-volume model to be consistent with FVCOM (Chen et al., 2013; Qi et 226 al., 2009).

SWAN has become popular in various applications including ocean wave simulations, engineering applications, modeling coastal and estuarine systems, and wave forecasting studies (Chen et al., 2018). SWAN is particularly adjusted for coastal regions with shallow waters, which makes it suitable for modeling sediment transport in Green Bay. Recent applications of the SWAN in studying Lake Michigan wave dynamics have also indicated good performance and applicability of the model for the Green Bay sediment transport studies (Mao et al., 2016; Mao & Xia, 2017).

234

2.3 Sediment Transport Model: FVCOM-SED

We used the FVCOM built-in sediment transport model (FVCOM-SED) in this study to model sediment processes in Green Bay and Lake Michigan. FVCOM-SED was developed based on the Community Sediment Transport Modeling Systems (CSTMS) by Warner et al. (2008) and was further modified to account for cohesive and mixed sediment dynamics (Sherwood et al., 2018). CSTMS was developed to be coupled with the structured-grid-based Regional Ocean Modeling System and was modified to be consistent with FVCOM unstructuredgrid solver (Chen et al., 2013).

FVCOM-SED accounts for several sediment mechanisms including suspended and bedload transport, layered bed dynamics, and erosion/deposition actions for an unlimited number of cohesive and non-cohesive sediment classes. Each sediment class is characterized by mean grain diameter, particle density, settling rates, and bed erosion characteristics. Each bed layer is defined based on the bulk characteristics of sediment classes in that layer and its initial thickness. The FVCOM-SED version 4.1 was only able to initiate the sediment transport model based on the uniform distribution of sediment classes in the entire domain. That seems to be an unrealistic assumption for Lake Michigan sediment stratigraphy. Therefore, we updated the code so that the model can take user-defined non-uniform distribution of sediment classes in the bed layer (Khazaei, 2020; Appendix A).

Bed layer characteristics, in particular thickness, is immediately affected by sediment actions such as erosion and deposition. In order to keep the number of bed layers constant throughout the simulation, an active layer is considered on top of sediment layers. The thickness of this active layer (z_a) is calculated in each time step based on the Harris and Wiberg's (2001) formulation as follows:

$$z_a = max[k_1(\tau_{sf} - \tau_{ce}), \quad 0] + k_2 D_{50}$$
⁸⁾

where τ_{sf} is the maximum bottom friction shear stress due to combined effects of currents and waves (N/m^2) , τ_{ce} is the critical shear stress for erosion (N/m^2) , D_{50} is the median grain diameter at the sediment-water interface (m), and k_1 and k_2 are empirical constants with values of 0.007 and 6.0, respectively. Sediment transport is limited to the mass available in the active layer in each time step.

The total load is the accumulated suspended load in the water column and bedload. FVCOM-SED calculates the suspended load by accounting for advective and diffusive concentration-based transport in the water column, as follows:

$$\frac{\partial C}{\partial t} + \frac{\partial uC}{\partial x} + \frac{\partial vC}{\partial y} + \frac{\partial wC}{\partial z} = \frac{\partial}{\partial x} \left(A_H \frac{\partial C}{\partial x} \right) + \frac{\partial}{\partial y} \left(A_H \frac{\partial C}{\partial y} \right) + \frac{\partial}{\partial z} \left(A_V \frac{\partial C}{\partial z} \right) + \frac{1}{H_z} C_{Source/sink}$$
9)

where *C* is the suspended sediment concentration, (u, v, w) are the three components of currents in the (x, y, z) Cartesian grid space, A_H and A_V are the horizontal and vertical eddy viscosity, and H_z is the thickness of grid cells. $C_{source/sink}$ accounts for additional vertical transport mechanisms due to settling and resuspension:

$$C_{source/sink} = -\frac{\partial \omega C}{\partial S} + E_s$$
10)

10

where ω is the settling velocity positive in the upwards direction (*m/s*) and E_s is the erosion rate ($kg/m^2/s$) in the vertical sigma coordinate direction *S*. Ariathurai and Arulanandan (1978) defined erosion rates of cohesive soils as a function of bed erodibility constant, sediment porosity (top layer sediment particles in this case), maximum bottom shear stress, and critical shear stress for erosion. Transport of suspended load is constrained to a zero-flux boundary condition at the surface of the water column and the net balance between erosion and deposition at the bottom.

While the suspended load includes the flux of sediment mass at the sediment-water interface and transport in the water column, the bedload is considered as the horizontal exchange within the top layer of the bed and is estimated based on the Hans Albert Einstein's definition of non-dimensional volumetric sediment flux:

$$q_{bl} = q_{s*} D_{50} \sqrt{(s-1)g} D_{50} \tag{11}$$

where q_{bl} is the horizontal bedload transport rate (m^2/s) and $s = \rho_s/\rho_w$ is the specific density of sediments in the water. q_{s^*} is the magnitude of the non-dimensional transport rate and could be determined based on the Meyer-Peter and Müller's (1948) scheme.

283 Mixed-sediment bed processes occur when both cohesive and non-cohesive sediments are 284 present and there is a considerable amount of mud (fine cohesive sediment) in the sediment layer 285 (Mitchener & Torfs, 1996). FVCOM-SED (and CSTMS) adopts a method similar to Le Hir et al. 286 (2011) and Mengual et al. (2017) to force resuspensions, in which mixed beds form when a mud 287 content of 3 to 30% is present in the sediment layer. Their strategy is tested and recommended 288 for implementation in real case 3D hydro-sedimentary modeling applications. This approach 289 means that in mixed-sediment bed conditions effective critical shear stress of the bottom ($\tau_{ce,eff}$) is 290 calculated based on a weighted combination of critical shear stresses of cohesive and non-291 cohesive portions of the bed:

$$\tau_{ce,eff} = max[P_c\tau_{cb} + (1 - P_c)\tau_{ce}, \tau_{ce}]$$
¹²

where τ_{ce} is the critical shear stress for each sediment class, τ_{cb} is the bulk critical shear stress for the sediment layer based on Sanford's (2008) approach, and P_c is the dimensionless cohesive behavior parameter. P_c is a function of the mud content in the bed layer with lower values denoting a non-cohesive behavior and vice versa. It is important to note that while the bed erodibility of non-cohesive sediment is treated as the property of individual sediment classes, the erodibility of cohesive sediment is treated as the bulk property of the bed. Following Sherwood et al. (2018), the equilibrium bulk critical shear stress $\tau_{cb,eq}$ is defined in terms of an exponential profile defined by a slope and offset:

$$\tau_{cb,eq} = a \exp\left[\frac{\ln(z_p) - \text{offset}}{\text{slope}}\right]$$
(13)

where z_p is mass depth defined as the cumulative dry mass of sediment overlying a given depth in the bed (kg/m^2) and $a = 1 Pa m^2/kg$ is a dummy coefficient that produces the correct units of critical shear stress. The parameter values of *offset* = 2 $ln(kg/m^2)$, *slope* = 5 $ln(kg/m^2)$, and timescale for consolidation $T_c = 8$ hours were based on the recommendations of the CSTMS and FVCOM-SED settings.

FVCOM-SED is fully coupled with the FVCOM ocean model and FVCOM-SWAVE to account for the current-wave-sediment interactions (Chen et al., 2013). More details of the CSTMS model, mixed sediment transport mechanisms, and model validation are provided in the literature (Sherwood et al., 2018; Warner et al., 2008). In section 3.3, we elaborate on the characterization of different sediment classes and their properties for the Lake Michigan sediment transport model.

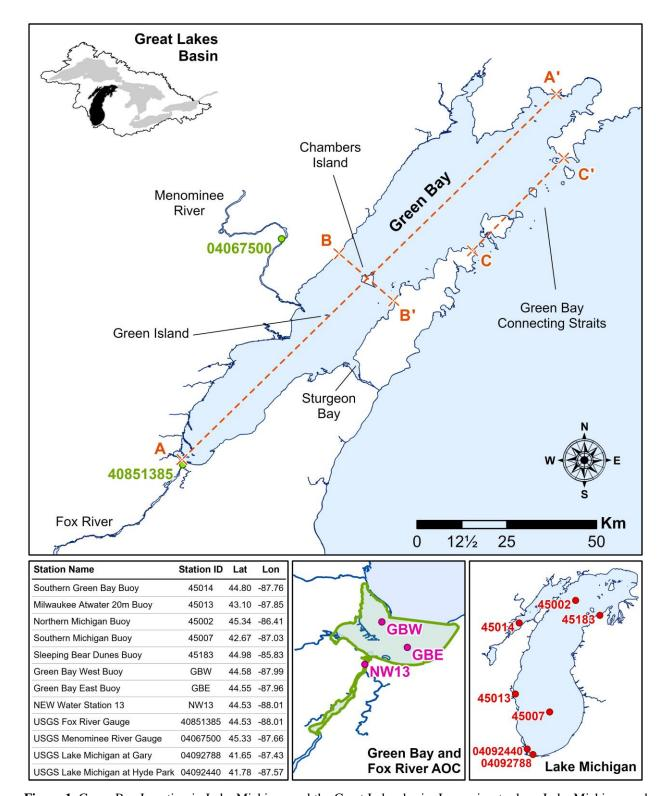
311 **3 Model Design**

312 3.1 Study Area

While the focus of the current study is Green Bay, to avoid the uncertainty and difficulty of obtaining internal or open-lake boundary conditions at the connection straits with Lake Michigan, a whole-lake model is developed. Green Bay is 190 km long in its longest axis and, on average, is about 20 km wide. With an average and maximum depths of approximately 20 m and 50 m, respectively, Green Bay is considered a shallow coastal water body. The maximum depth in Lake Michigan is about 280 m.

Chambers Island cross-section divides Green Bay into lower and upper sections. Lower Green Bay is the hotspot of environmental issues, where Fox River discharges runoff from the heavily developed and stressed Fox River watershed into the bay. The watershed is mostly

- 322 covered by vegetated areas (Khazaei & Wu, 2018), and the cities of Appleton and Green Bay,
- 323 large industrial sites, and farmlands impact the concentration and quality of particles running into
- 324 the river (Klump et al., 1997; Velleux et al., 1995). The Fox River alone contributes about two-
- thirds of the nutrient and particulate tributary loading into Green Bay and almost one-third of the
- total phosphorus load to Lake Michigan (Harris & Christie, 1987). Figure 1 shows the location of
- 327 Lake Michigan and Green Bay in the Great Lakes basin and Green Bay AOC.



³²⁸ 329

Figure 1. Green Bay Location in Lake Michigan and the Great Lakes basin. Lower insets show Lake Michigan and

the Green Bay Area of Concern (AOC). Buoy stations and USGS gauges used in this study and their abbreviations

are also shown in the Figure. Cross-sections A-A', B-B', and C-C' are used to look at transport patterns in different

locations across the bay.

333 3.2 Grid and Simulation Specifications

334 Circulation and transport mechanisms are very sensitive to the morphology of the system. 335 Shallow waters and the complex geometry of the Green Bay shorelines require a fine grid that 336 can resolve those detailed features (Figure S1 in the Supporting Information). Long Tail Point 337 and Little Tail Point Islands located on the western shore of lower Green Bay, Green and 338 Chambers Islands in the central bay areas, as well as Plum, Detroit, Washington, Rock, St. 339 Martin, Poverty, Summer, and Little Summer Islands in the exchange zone of the Lake Michigan 340 and Green Bay were incorporated in the grid (see Figure S2 in the Supporting Information). 341 Also, the coastline data was updated to include the Cat Island, a feature that is crucial in 342 modeling the circulation and transport in the Green Bay AOC.

Bathymetry and shoreline data, used to generate the Lake Michigan unstructured grid (Figure S3 in the Supporting Information), are based on NOAA datasets (National Geophysical Data Center, 2015; NOAA, 2017) and were updated in the southern Green Bay to represent recent changes of the bathymetry due to the dredging of navigational channel project.

347 The Lake Michigan grid in this study includes 52,574 triangular elements/cells, 28,985 348 nodes, and is vertically discretized to 20 σ -layers, i.e., layers follow terrain variations. The grid is 349 designed very dense in Green Bay, where element side length varies between 50 m to 1500 m 350 from the mouth of Fox River to upper Green Bay. Since the focus of our model is to simulate 351 sediment transport in Green Bay, a coarser grid resolution is used for the main body of Lake 352 Michigan for the sake of computational efficiency. Given the suggested summertime baroclinic 353 Rossby radius of 5 km in the Great Lakes, it is critical to use a grid size less than 5 km within the 354 8-10 km of the coastal areas (Beletsky et al., 1997, 2006b). Therefore, cell side length in the Lake 355 Michigan grid was designed to vary between 1000 m in the shorelines to about an average of 5 356 km in the central lake areas. A relatively fine grid is constructed near the connecting straits to be 357 able to accurately account for the exchanges between the lake and the bay.

FVCOM-SWAVE offers various options suitable for the simulation of waves in different physical conditions (Booij et al., 1999; Table 1). In this study, the wave model was adjusted by selecting from those options based on recommendations in the literature (Mao et al., 2016; Ris et al., 1999), and our comparisons of simulated results against the validation buoys in nearshore and deep-water areas of Lake Michigan. In this regard, the third generation of the SWAN wave model (Booij et al., 1999) with quadruplet wave-wave interactions of Hasselmann et al.'s (1985)
was adopted for this study. We also used Komen et al.'s (1984) formulation for wind growth and
whitecapping, Hasselmann et al.'s (1973) expressions for bottom friction, and Battjes & Janssen's
(1978) formulation for depth-induced breaking calculations. We also selected 60 as the number
of steps in the relative frequency space.

368

3.3 Sediment Classification and Properties

369 Sediment transport models require a set of standard parameters for model simulations, 370 which can be obtained through observations, lab experiments, and/or calibration. Those 371 important parameters include particle density (ρ_s), mean diameter (D_{50}), and porosity (φ). 372 Prediction of sediment transport is also very sensitive to erosion and deposition characteristics of 373 the particles such as critical shear stress for erosion (τ_{ce}) and settling rates (ω). A previous Lake 374 Michigan sediment transport model has found ~40% deviations in results by changing these 375 parameters (Lee et al., 2005), yet, the model had the most sensitivity to the fraction of fine-376 grained particles in the sediment mixture. Therefore, it is important in the first place to define the 377 distribution of sediment classes in the bed layer.

We extracted information from several studies to obtain a general understanding and reasonable estimates of sediment characteristics in Green Bay. The next steps included using soil classification methods/standards and consultation with experts to narrow down the ranges defined for each parameter in the literature. Finally, some of these model parameters were adjusted based on model calibration.

383 There are few studies of Green Bay sediment classes and their distribution. Field 384 observations and analysis of sediment samples (HydroQual Inc., 1999; Jones, 2000; Moore et al., 385 1973; Wisconsin DNR, 2000) have found clay, silt, and sand are the major constituting variables 386 of lower Green Bay. As we move from south, near the mouth of Fox River, to the north, near the 387 connecting straits, mud content decreases in the bed layer and the upper Green Bay bed is mostly 388 formed by sand and gravel. We compiled these findings with Lee et al.'s (2007) 389 recommendations for Lake Michigan and estimated bottom sediment stratigraphy as shown in 390 Figure S4 in the Supporting Information. These patterns are also consistent with distributions of 391 cohesive sediment in Green Bay (HydroQual Inc., 1999). It is important to mention that the 392 composition of the benthic zone in Lake Michigan has changed due to the invasion of Zebra and 393 Ouagga Mussels. Zebra mussels were first observed in Green Bay in 1991 and Ouaggas in 2003. 394 In lower Green Bay and the inner bay, the distribution of dreissenid mussels is patchy (Oualls et 395 al., 2013) and in the depositional areas of the bay they are absent. This is almost certainly due to 396 recurring summertime hypoxia in the mid and lower bay (Kaster et al., 2018; Klump et al., 397 2018). Hypoxic events have also been repeatedly observed from time series dissolved oxygen 398 sensors deployed recently in the shallow waters of the inner bay. The influence of dreissenids on 399 sediment resuspension is difficult to judge with certainty, but would appear minor relative to 400 physical processes. Those changes are neglected in the assignment of bottom sediment initial 401 conditions, yet have to be considered in future studies for improved simulations of sediment 402 transport when sufficient information becomes available (see Figure S5 in the Supporting 403 Information).

We identified six sediment classes for the current model development and determined sediment mean diameter based on the U.S. Department of Agriculture (USDA) soil classification standard (Yolcubal et al., 2004) as shown in Table 1. Density and porosity of different sediment classes were also estimated based on the analysis of sediment samples taken in Green Bay (Manchester-Neesvig et al., 1996; Wisconsin DNR, 2000).

409 Table 1. Sediment properties and erosion/deposition characteristics used in the Lake Michigan sediment transport410 model.

Sediment class	1	2	3	4	5	6	Source
Sediment type	Clay	Fine Silt	Coarse Silt	Fine Sand	Coarse Sand	Gravel	Moore et al. (1973), Wisconsin DNR (2000), and Lee et al. (2007)
$D_{50}(mm)$	0.001	0.008	0.05	0.1	0.5	2	Jones (2000) and Yolcubal et al. (2014)
$\rho_s (kg/m^3)$	2300	2300	2300	2450	2450	2450	Wisconsin DNR (2000)
Ф (%)	97.5	97.5	97.5	85	75	60	Manchester-Neesvig et al. (1996)
ω (mm/s)	0.001	0.02	1.01	4.95	57.04	175.31	Garcia (2008)
$ au_{ce} (N/m^2)$	0.008	0.029	0.09	0.18	0.25	1.10	Garcia (2008)
E_{θ} (kg/m ² /s)	0.0005	0.0025	0.005	0.005	0.005	0.005	Ariathurai and Arulanandan (1978)

Previous studies have shown wide ranges of sediment settling/fall velocity in Green Bay. NOAA sediment trap study found settling velocities of about 6-70 *mm/s* in stratified conditions (summertime) and 14-200 *mm/s* during unstratified periods. We used a method proposed by Soulsby (1998) that estimates fall velocity based on sediment mean diameter and density and viscosity of water. This method is suitable for fine-grained sediments, therefore, we used for coarser sediment classes a graphical method explained by García (2008, p. 42), which requires the same variables as Soulsby's method.

419 While settling velocity governs deposition, bottom erosion and resuspension events are 420 controlled by critical shear stress for erosion which we estimated based on the definition of 421 Shields non-dimensional critical shear stress (τ_c^*). τ_c^* can be found based on the modified Shields 422 diagram (Parker, 2004) or alternatively for finer particles based on Mantz's (1977) empirical 423 relationship. Critical shear stress for erosion is then a function of τ_c^* , particle density, and mean 424 sediment diameter according to the Shields formulation.

FVCOM-SED requires a bed erodibility constant (E_0) in order to estimate bottom sediment fluxes. A wide range of values is suggested in the literature for E_0 . Ariathurai and Arulanandan (1978) conducted several tests on more than 200 natural or lab-synthesized fine and cohesive sediment samples and suggested values between 5×10^{-4} and $5 \times 10^{-3} kg/m^2/s$. Analysis of those samples has shown that the slope of erosion rate curves increases proportionally to critical shear stress for erosion.

3.4 River Inputs

432 Tributary loadings are the major input fluxes into Green Bay. Required river inputs for 433 the circulation, wave, and sediment transport models are discharge, temperature, and total 434 suspended solids (TSS) at river mouth that were estimated in this study based on daily USGS 435 observational data. USGS observations during the 2011-2019 period show average inflowing discharge of 170, 24, 29, and 106 m^3/s and TSS concentrations of 24, 0.24, 0.03, and 3 mg/L for 436 437 the Fox, Oconto, Peshtigo, and Menominee Rivers, respectively. Those statistics indicate that the 438 Fox and Menominee Rivers have more influence on circulation and thermal regimes in Green 439 Bay, hence they were included as boundary conditions of the model.

440 It should be noted that riverine TSS loading into the bay is estimated based on empirical relationships developed using USGS observations of discharge and turbidity at the mouth of Fox 441 442 River (gage ID: 40851385) and cruise measurements of turbidity and TSS by the city of Green 443 Bay Sewerage district, now NEW Water, at this location (Khazaei, 2020; Khazaei et al., 2018; 444 NEW Water, 2017). The Fox River sediment load composition varies by flowrate. For the regular summertime flowrates in the Fox River (less than $\sim 300 \text{ m}^3/s$), observations by Jones 445 446 (2000) show that ~50% of Fox River sediments are very fine materials with mean diameter size less than 0.005 mm, ~40% are materials with a mean dimeter of 0.05 mm, and ~10% are coarser 447 448 materials. Therefore, we assumed 50% Clay, 35% Fine Silt, 10% Coarse Silt, 3% Fine Sand, and 449 2% Coarse Sand in the incoming river loads.

450

3.5 Field Data

451 Previous efforts in modeling physical and biogeochemical processes in Green Bay have 452 been challenged by the scarcity of relevant hydrodynamic and water quality observational data. 453 Recent data collection efforts, such as continuous monitoring of turbidity at Green Bay West and 454 East buoys in the southern bay (Miller, 2020), have made the development and validation of a 455 sediment transport model for Green Bay possible. As explained above, we used NEW Water 456 turbidity and TSS cruise data to convert turbidity observations into TSS time series. In addition, 457 seven buoy stations in Lake Michigan and Green Bay were used to validate hydrodynamic and 458 wave models, i.e., southern Green Bay, Atwater Beach in Milwaukee nearshore zone, Sleeping 459 Bear Dunes, North Michigan, and South Michigan buoys (see Figure 1).

External forcing inputs of the model are based on the interpolation of NOAA National Centers for Environmental Information (NCEI; NOAA, 2018) land-based and buoy stations in the Great Lakes basin. The interpolation scheme is based on a natural neighbor method developed by NOAA Great Lakes Environmental Research Laboratory for application in the Great Lakes forecasting models (Beletsky et al., 2003; Schwab & Beletsky, 1998) and accounts for adjustments of overland to overlake conditions whenever data from land-base stations were used (Beletsky & Schwab, 2001).

467 **3.6 Model Skill Criteria**

476

468 We use Root Mean Squared Error (*RMSE*), Bias Deviation (*BD*), and correlation 469 coefficients (*CC*) to assess model skills of scalar variables (e.g., temperature and *TSS*):

$$RMSE = \frac{1}{N} \left(\sum_{i=1}^{N} (e_i^2) \right)^{1/2}$$
(1)
4)

$$BD = \frac{1}{N} \sum_{i=1}^{N} (e_i)$$
(1)
5)

$$= \frac{\sum_{i=1}^{N} (x_{i,0} - x_{ave,0}) (x_{i,P} - x_{ave,P})}{(1 + 1)^{N}}$$

$$CC = \frac{\sum_{i=1}^{N} (x_{i,0} - x_{ave,0})^{2} (\sum_{i=1}^{N} (x_{i,0} - x_{ave,0})^{2})^{1/2} \left[\sum_{i=1}^{N} (x_{i,P} - x_{ave,P})^{2} \right]^{1/2}}{\left[\sum_{i=1}^{N} (x_{i,P} - x_{ave,P})^{2} \right]^{1/2}}$$
(1)

470 where *N* is the number of observation/prediction points, e_i is the deviation of the 471 predictions from observations (i.e., $e_i = x_{i,O} \cdot x_{i,P}$; where $x_{i,O}$ and $x_{i,P}$ are observational and 472 prediction values at point *i*, respectively), and $x_{ave,O}$ and $x_{ave,P}$ are the mean of observed and 473 predicted data, respectively.

474 To assess model skills for vector fields (e.g., currents) we use normalized Fourier norm 475 (F_n) and average angular difference ($\Delta \theta$):

$$F_{n} = \frac{\|V_{o}, V_{p}\|}{\|V_{0}, 0\|} = \frac{\left(\frac{1}{N}\sum_{i=1}^{N} |V_{i,o} - V_{i,p}|^{2}\right)^{1/2}}{\left(1 - \sum_{i=1}^{N} |V_{i,o} - V_{i,p}|^{2}\right)^{1/2}}$$
(1)

$$\left(\frac{1}{N}\sum_{i=1}^{N}|V_{i,o}-0|^{2}\right)$$

$$(1)$$

$$\Delta \theta = \frac{1}{\pi N} \sum_{i=1}^{N} \cos^{-1} \left(\frac{V_o \cdot V_p}{|V_o| |V_p|} \right) \tag{1}$$

where $V_{i,o}$ and $V_{i,p}$ denote observed and predicted vector fields at point *i*, respectively.

477 RMSE is used to assess model accuracy, i.e., zero indicates perfect model accuracy and as 478 the value increases, model accuracy decreases. BD shows model bias and smaller values close to 479 zero denote lower biased performance of the model. CC can be used as an indicator of model 480 performance in reproducing the temporal patterns of change in observational data. In this article, 481 *CC* is reported if significant at *p*-value ≤ 0.05 . *Fn* and $\Delta\theta$ assess model accuracy in the prediction 482 of vector fields magnitude and direction, respectively. F_n and $\Delta \theta$ equal to zero indicate a perfect 483 model, values between zero and one are in the acceptable range, and as the value increases, 484 model performance decreases.

485 **4 Simulation Details and Model Validation**

486 We ran the model for the 2016-2019 years and model simulations were limited to the 487 May-October period of each year to focus on the ice-free period in Lake Michigan and time of 488 active bottom layer sediment dynamics. Model stability requires simulations at a time step of 5 s. 489 The circulation model is initiated at rest, i.e., zero currents. 3D temperature fields are 490 interpolated from LMHOFS simulation in Lake Michigan at the initial condition. Also, the 491 model is run using realistic initial water surface elevation in Lake Michigan (NOAA, 2020). We 492 ignored major open boundary conditions around Lake Michigan, e.g., bi-directional flow at the 493 Straits of Mackinac and Chicago River diversion, because they do not have an immediate impact 494 on sediment transport in Green Bay, especially southern areas in the bay.

495 The bed layer and bottom sediment distribution are initialized in each year based on the 496 non-uniform distribution of different sediment classes defined in section 3.3 (see Figure S4 in 497 Supporting Information). Considering the average bottom distribution over the entire lake, the 498 portion of cohesive (Clay, Fine Silt, and Coarse Silt) and non-cohesive (Fine Sand, Coarse Sand, 499 and Gravel) sediment classes contributing to the bottom layer are 29% and 71%, respectively, 500 i.e., cohesive sediments are defined as the mixture of clay and silt (Wolanski, 2007). Analysis of 501 sediment samples in Green Bay showed that the average cohesive sediment depth in Green Bay 502 is ~0.5 m (Wisconsin DNR, 2000). Average erosion and deposition patterns in Green Bay, as 503 well as Lake Michigan (Lou et al., 2000), showed that bed changes do not exceed that value 504 during long-term simulations of semi-annual to annual scales. Therefore, we started the model 505 with a bed thickness of 0.5 m. We also conducted a sensitivity analysis of TSS simulations at 506 GBE and GBW and found that although results are slightly sensitive to initial bed thickness, 507 values in the range 0.25 m and 0.5 m result in a reasonable estimation of TSS simulations in 508 Green Bay.

509

4.1 Validation of Simulated Currents, Waves, and Temperature Fields

510 Currents are the main driver of transport mechanisms in hydrodynamic simulations. 511 Accurate simulations of sediment transport dynamics rely on accurate simulations of currents 512 near the bottom. Figure 2 compares the observed and predicted daily currents in N-S (*v* 513 component) and E-W (*u* component) directions during the May-October of 2016-2019 years. 514 Comparison plots and model skill criteria indicate reasonable agreement between model and 515 buoy observations at two selected locations, given the complex nature of the physical process 516 and the system. Our calculated model skill statistics for currents (or velocity fields) are 517 comparable and in some cases show slight improvements compared with previous Lake 518 Michigan hydrodynamic modeling efforts. For example, Fn values of 0.79-1.01 and 0.9-1.05 519 were reported respectively for barotropic (Schwab, 1983) and POM-based (Beletsky & Schwab, 520 2001) models of summertime circulation in Lake Michigan built on 5-km resolution grids. Rowe 521 et al. (2015) obtained improved performance in modeling summertime hydrodynamics by using 522 interpolated forcing and adopting FVCOM, and reported *Fn* values of 0.83-0.91. Schwab (1983) 523 and Rowe et al. (2015) have respectively reported values of 0.23-0.46 and 0.29-0.31 for $\Delta\theta$ in 524 modeling Lake Michigan currents direction. Wave action complements currents to force 525 sediment movement. Combined current-wave action produces stronger shear stresses at the 526 water-sediment interface and triggers more frequent and/or stronger episodes of resuspension. Hence, an accurate wave model will improve the understanding of sediment processes. 527

528 Figure 2 shows the comparison of observed and predicted significant wave heights (W_{Hs}) 529 and wave directions (W_{dir}) . W_{Hs} is defined as the average of the highest one-third of the waves, 530 measured between wave trough to crest. According to the figure and model skill statistics, 531 FVCOM-SWAVE simulations of wave height are in good agreement with observations at three 532 selected buoys. In particular, high correlations between observations and simulations implies that 533 patterns of the wave height variability are reproduced well by the model. However, wave 534 direction predictions are not as accurate as wave heights. Comparison of the model skill statistics 535 with previous wave models of Lake Michigan (Hawley et al., 2004; Mao et al., 2016) also 536 suggests a good (in some cases improved) performance by the FVCOM-SWAVE model and its 537 suitability for applications in modeling sediment transport.

538 We also validate predictions of temperature fields to assess the performance of the 539 physical model in simulating circulation and transport. Also, temperature governs 540 biogeochemical processes in the lake and is important for Green Bay restoration studies. As 541 shown in Figure 2, the temperature is predicted with high accuracy at four selected buoys, except 542 for over-estimation of mid-range bottom temperature at the location of Green Bay buoy station 543 45014. One possible explanation for that is the model's inability to fully capture cold water 544 intrusion from Lake Michigan into the southern bay. Denser cold water from the lake flows near 545 the bottom while warmer water, coming into the bay from rivers, flows on top; forming a two546 layered flow condition in Green Bay (Grunert et al., 2018). Yet, high correlations between 547 predicted and observed water temperature at this location, as well as other buoys, shows that the 548 model is capable of producing the patterns of variability in temperature profiles such as 549 upwelling events.

550

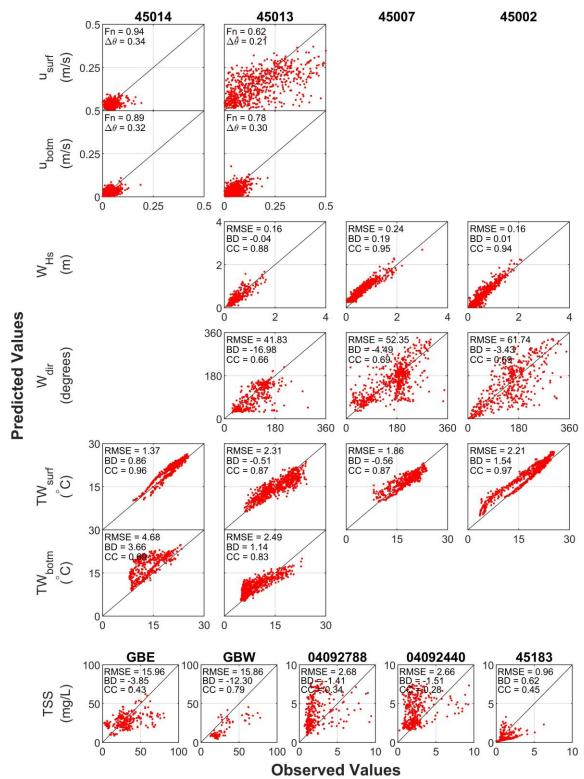




Figure 2. Comparison of the daily observed and predicted surface and bottom currents (u_{surf} and u_{botm}), significant wave height (W_{Hs}) and direction (W_{dir}), surface and bottom temperature (TW_{surf} and TW_{botm}), and total suspended solids (TSS) at the location of selected validation buoys during 2016-2019 years. Buoy locations are shown in Figure 1. CCs are reported if significant at P-value ≤ 0.05 .

556

4.2 Validation of Simulated Total Suspended Solids

557 Figure 2 compares predicted daily TSS against the observations at five different locations 558 in Green Bay and Lake Michigan, where turbidity observations are available in 2016-2019. 559 Turbidity times series obtained at those locations were converted into TSS concentration using 560 TSS-turbidity empirical functions for the estimation of river loadings (explained in section 3.4). 561 GBW and GBE buoys are located in very shallow areas of lower Green Bay (~1 m depth) and 562 sensor probes were placed at the mid-depth water column; therefore, observations represent the 563 bottom sediment conditions. USGS 04092788 and 04092440 buoys are located in southern and 564 southwestern Lake Michigan where multiple episodes of sediment resuspension events occur 565 during the May-October period. Great Lakes Observing System (GLOS) 45183 buoy is located 566 at Sleeping Bear Dunes in northeastern Lake Michigan with complex geomorphological 567 characteristics of the lake that complicates sediment dynamics. 04092788, 04092440, and 45183 568 buoy stations represent surface conditions.

569 Figure 2 implies a fairly good accuracy and overall satisfactory performance of the model 570 in modeling sediment transport in Green Bay AOC, given the physical complexity of the system. 571 Although the model is biased at GBW buoy, high correlations between observed and predicted 572 TSS values at GBW denotes model capability in the simulation of storm events and episodes of 573 resuspensions. Figure S6 of the Supporting Information illustrates examples of resuspension 574 events captured by the model at these two locations. In some cases, the model significantly 575 underestimated TSS observations at both buoys. Those underestimations may be explained by 576 sensor malfunction and/or sudden spikes of TSS concentrations due to construction activities near 577 the GBW buoy (e.g., Cat Island project), dredging of Fox River, and navigation channel project.

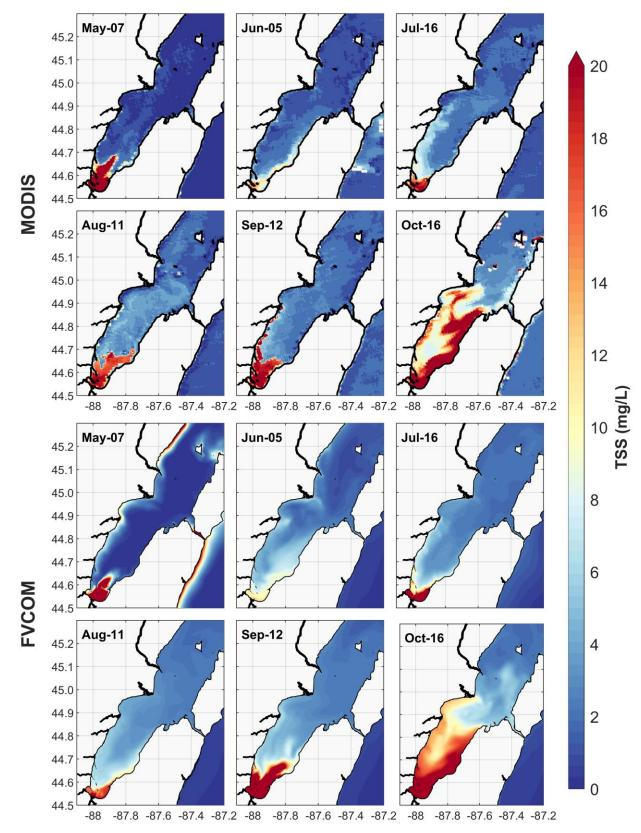
Although the sediment model is focused on Green Bay, *TSS* validations at southern Lake Michigan (04092788 and 04092440 buoys) and Sleeping Bear Dunes (45183 buoy) are fairly satisfactory (Figure 2). Supplementary Figure S6 also shows that the model is able to produce the patterns of high-turbidity episodes in these distinct locations in southern and northern basins of Lake Michigan, although the magnitude of high resuspension events is not completely accurate.

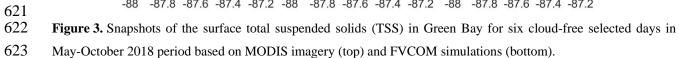
Figure 3 also compares the surface snapshots of *TSS* concentration based on FVCOM simulations and MODIS imagery for six selected days in 2018. MODIS-based *TSS* maps are estimated based on a procedure explained in Hamidi et al. (2017), using relationships developed 586 between simultaneous surface reflectance and NEW Water TSS observations at the location of 587 monitoring stations in lower Green Bay. We used MODIS product MYD09GA for the estimation 588 of surface TSS. We picked several days during the summer of 2018 by visual inspection, and 589 then used MYD09GA Surface Reflectance 500m Quality Assurance and 1km Reflectance Data 590 State QA layers to filter high-quality and cloud-free data. True-color visualization of raw 591 imagery data is presented in Figure S7 of Supporting Information. Except for small deviations in 592 August that could be explained by inaccurate estimation of TSS inputs and/or wind conditions, 593 the model-simulated spatiotemporal patterns of TSS in lower Green Bay and decreasing gradient 594 of suspended particles from Green Bay AOC towards Chambers Island match very well with the 595 results of the remote sensing method.

596 Besides these point and spatial validations of the model's ability to predict TSS, we 597 compared observed and predicted TSS profiles in lower Green Bay (45014 buoy) in 2018 to 598 assess model skills in the simulation of vertical sediment profiles (Figure 4). Observational TSS 599 profiles were inferred from the acoustic backscattering signal collected by Nortek Aquadopp 600 600 kHz Acoustic Doppler current profilers (ADCP) at 10 depth layers (GLOS, 2021). Backscattering 601 signal was converted from echo intensity based on a procedure explained and used in previous 602 studies (Deines, 1999; Lee et al., 2007). The backscattering signal was paired with turbidity data 603 from a deployment at the Green Bay buoy station 45014 in July 2016. Turbidity data were 604 collected by a WET Labs NTUSB turbidity sensor and were used to build relationships between 605 turbidity and ADCP backscattering signal. Those relationships are used to estimate turbidity 606 profiles, which were converted to TSS concentration profiles based on the empirical TSS-607 turbidity functions explained in section 3.4.

Figure 4 shows that the predicted *TSS* profiles resemble the patterns of the observed profiles and indicate the simultaneous occurrence of high-turbidity events, although the magnitude of *TSS* concentration deviates slightly during storm events. Comparison of the depthaveraged observed and predicted *TSS* profiles results in *RMSE*, *BD*, and *CC* skill metrics of 1.31 mg/L, -0.83 mg/L, and 0.47 at the Green Bay buoy station 45014. These model performance metrics show that the model is skillful in the simulation of *TSS* along the water column.

614 The array of validation methods used, including point validations of predicted *TSS* 615 concentration, assessment of model performance during the high-turbidity events, comparison of 616 the surface *TSS* patterns with satellite imagery data, and validation of model's capability in 617 reproducing the *TSS* profiles indicate a reasonable accuracy of the physical sediment transport 618 model. As we will discuss with more details in the next sections, our results also agree with the 619 findings of previous studies and qualitatively matches the patterns of the bottom shear stress 620 forces and sediment transport in Lake Michigan (Lee et al., 2005, 2007; Lou et al., 2000).





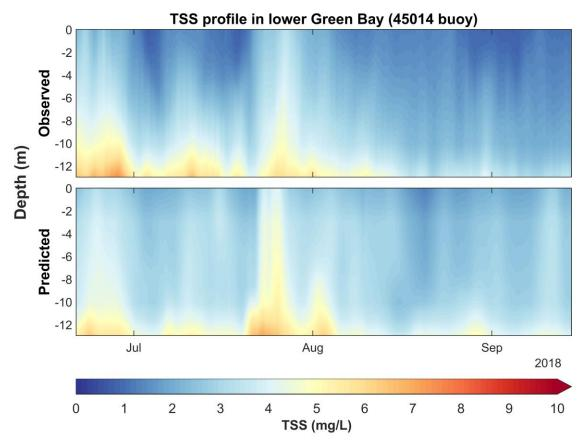


Figure 4. Comparison of the observed and predicted profiles of the total suspended solids (TSS) in lower Green Bay(45014 buoy) in 2018.

624

5 Results and Discussion: Summer Circulation and Transport Regimes in Lake Michigan and Green Bay

629 The summer circulation and transport regimes are analyzed in sections 5.1 to 5.4 in terms 630 of monthly average fields of wind-induced currents and waves action, bottom shear stress driven 631 by waves and currents, thermal structure, and sediment transport. The results of this study are 632 shown to complement previous modeling studies of Lake Michigan and to provide important 633 additional details on the circulation and transport regimes in Green Bay. Section 5.5 presents and 634 analyzes a climatological study of the summer circulation and transport regimes in Lake 635 Michigan. Section 5.6 summarizes previous studies on lake sediment dynamics, biogeochemical 636 interactions, HABs, and the role of mussels, and considers the potential application of the 637 approach developed in this study to investigate those processes.

638

5.1 Monthly-Averaged Wind-induced Circulation and Wave Action

639 Circulation and wave actions in Lake Michigan are predominantly wind-driven (Beletsky 640 et al., 2006b), and wind affects the exchange between Green Bay and Lake Michigan (Waples & 641 Klump, 2002). Figure 5 shows monthly-averaged wind patterns over Lake Michigan, with higher 642 resolution over Green Bay, during the 2016-2019 simulation period. The figure shows stronger 643 wind fields in northern Lake Michigan, as southerly winds accelerate over the approximately 500 644 km lake's longitudinal fetch. Winds are stronger in July-October with prevailing southwesterly 645 and southerly general regimes. Wind patterns over Green Bay are more uniform, yet consistent 646 with winds over Lake Michigan. Eastern winds dominate in May-June, and the wind fields shift 647 to southwesterly and southerly directions in July until October, when winds are the strongest. 648 Analyses of wind fields in the Great Lakes basin, including Lake Michigan, have shown 649 prevailing southwesterly winds during summer, with monthly and seasonal shifts in wind 650 direction/magnitude during 1980-1999 (Waples & Klump, 2002) and Green Bay during 2004-651 2008 (Hamidi et al., 2015).

652 In consistency with previous analyses of monthly averaged circulation in Lake Michigan 653 (Beletsky et al., 2006a), Figure 6 shows that cyclonic (counterclockwise) circulation dominates 654 Lake Michigan. Also, currents drive gyres in the lake, and the formation of gyres is more 655 common in the southern basin. Strong currents at the exchange zone affect water, heat, and 656 sediment fluxes between Lake Michigan and Green Bay. In consistency with wind patterns, 657 circulation is weaker in May and currents accelerate starting in June. Bimonthly analysis of 658 currents in the May-October period in Lake Michigan in 1982-1983 and 1994-1995 also suggests 659 that currents magnitude increase from May to October and currents move counterclockwise and 660 are stronger in the nearshore areas of the southern basin of the lake.

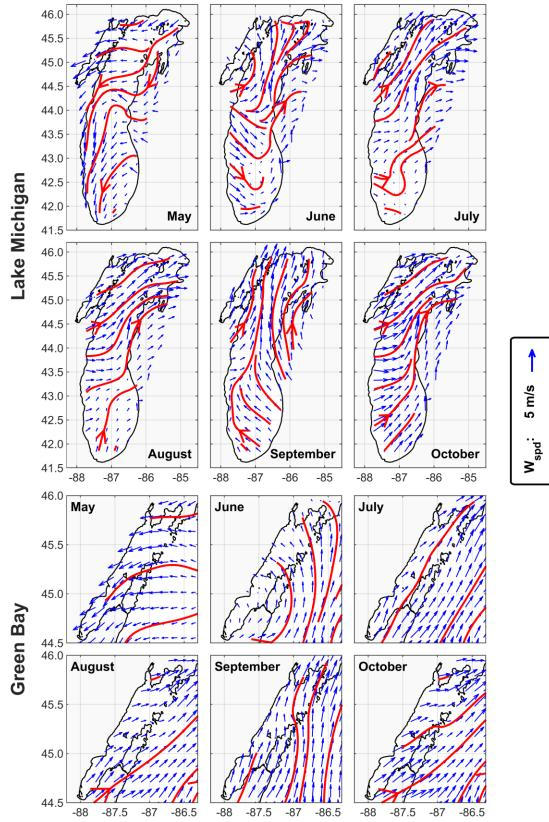
In Green Bay, the currents show more spatial variability than the wind fields, with the widespread formation of gyres, particularly north of Chambers Island and near the exchange zone with Lake Michigan, where strong currents are observed. Currents are generally in the north direction and stronger near the western shore of the bay. Most of these patterns, in particular stronger nearshore currents and frequent formation of gyres in Green Bay during summer, have shown by previous efforts in the simulation of currents in Green Bay for the 2004-2008 period using a POM-based circulation model (Hamidi et al., 2015). Those patterns are present along the water column, although currents are much stronger in the surface (Figures S8 and S9 in theSupporting Information).

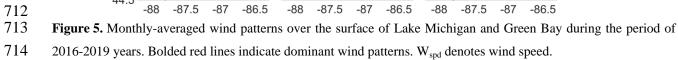
670 Current movement and transport in Green Bay are significantly restricted by morphology 671 and lake bottom terrain. Figure 7 shows monthly averaged horizontal current profiles, based on 672 2016-2019 simulations, along the three cross-sections shown in Figure 1. As illustrated in cross-673 section A-A' (where red colors show northward currents and blue colors show southward 674 currents along the section), the currents in southern Green Bay (i.e., south of Chambers Island, 675 located at km 85)—which play a main role in the transport of Fox River loads to the northern 676 bay—shift direction in June and move towards the south in the longitudinal cross-section A-A'. 677 The southward current pattern is driven by a combination of wind direction and cold-water 678 intrusion from the lake into the bay as mentioned above. Current profiles north of Chambers 679 Island and south of the exchange zone (between km 85 and km 130) are different from the rest of 680 the cross-section. Those patterns can be explained by the presence of gyres in that area, 681 especially away from the shorelines and in the central bay areas where cross-section A-A' cuts 682 through. Figures S8 and S9 in the Supporting information show clearly that the surface currents 683 in Green Bay are predominantly flowing north (especially near the shorelines) and bottom 684 currents flow towards the south, providing more evidence for the summertime stratified flow conditions in the bay. 685

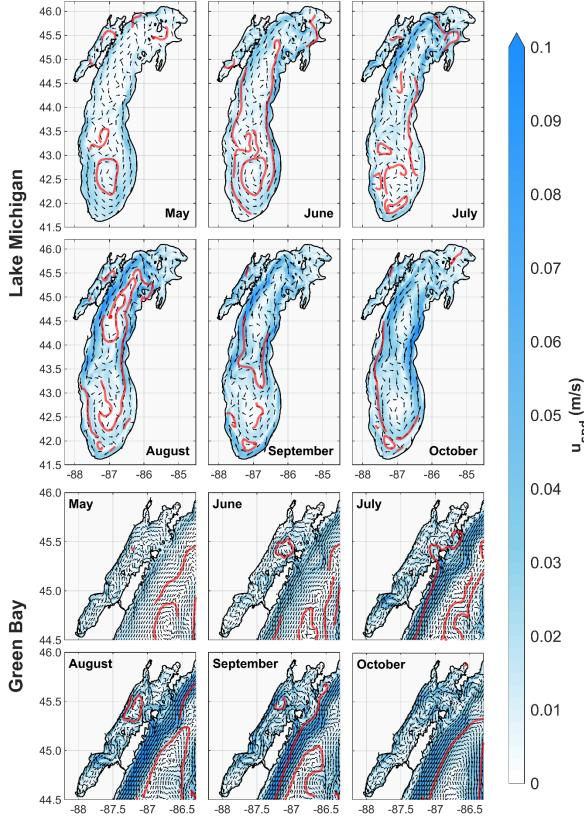
686 The current patterns in cross-section B-B' (where red colors show northward currents and 687 blue colors show southward currents perpendicular to the section) show that currents in the 688 western side of Chambers Island are strong and predominantly towards the south. The prevailing 689 southward and northward currents through the western and eastern sides of Chambers Island, 690 respectively, imply a counterclockwise circulation around the island, as shown in previous 691 studies based on field observations (Hawley & Niester, 1993). Cross-section B-B' shows that, 692 while surface currents are conveying water north, strong currents are moving towards the south 693 near the bottom. Current profiles at cross-section C-C' (where blue colors show currents flowing 694 into the bay and red colors show currents flowing out perpendicular to the section) also provide 695 evidence that lake cold-water intrusion into the bay occurs persistently through deeper sections 696 of the exchange zone profile. Similar to conditions in Chambers Island, currents are regularly 697 swirling around the small islands in this area.

698 Currents are the dominant driver of circulation and heat transfer in lake systems, yet 699 waves contribute significantly to sediment dynamics, through bottom interactions and 700 resuspension events. According to Figure 8, wave action in Lake Michigan is limited in May-701 August, gradually increases in September, and escalates in October. In general, the northern 702 basin of Lake Michigan experiences stronger waves, most probably due to dominant southern 703 winds during the modeling period. The wind-dependency of wave actions in Lake Michigan was 704 shown by previous modeling storm and surge peak events (Mao et al., 2016; Mao & Xia, 2017).

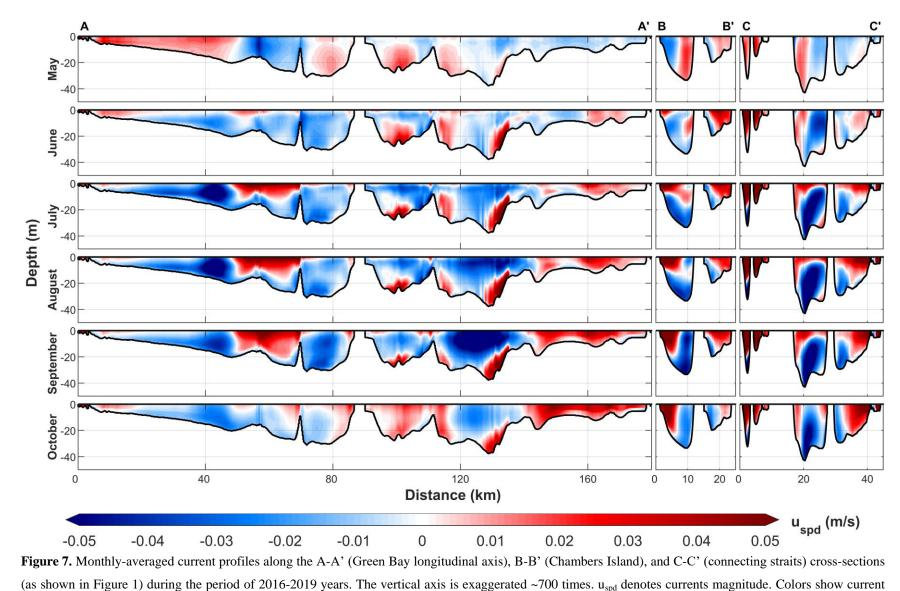
In concert with Lake Michigan, waves in the bay are stronger in September and October. Upper Green Bay and the exchange zone experience stronger waves probably due to rapid change in the bottom elevation in that area. As the incoming waves, originated in deep central areas of Lake Michigan, approach shallow waters of Green Bay and small islands at the connecting straits, water depth quickly starts to become less than the wavelength, reducing wave propagation velocity and leading to steepening of the waves and increased wave height.



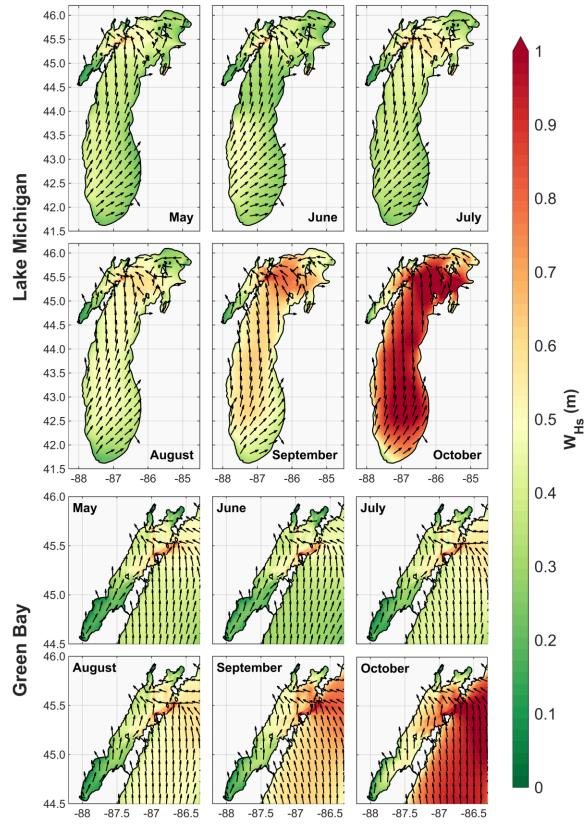




715 -88 -87.5 -87 -86.5 -88 -87.5 -87 -86.5 -88 -87.5 -87 -86.5
716 Figure 6. Monthly- and depth-averaged currents in Lake Michigan and Green Bay during the period of 2016717 2019 years. Bolded red lines indicate dominant circulation patterns. u_{spd} denotes currents magnitude.



(as shown in Figure 1) during the period of 2016-2019 years. The vertical axis is exaggerated ~700 times. u_{spd} denotes currents magnitude. Colors show current
 directions along the A-A' cross-section (red/blue indicates northward/southward) and perpendicular to B-B' and C-C' cross-sections (red/blue indicates into/out
 of cross-sections, respectively).



723 -88 -87.5 -87 -86.5 -88 -87.5 -87 -86.5 -88 -87.5 -87 -86.5 -88 -87.5 -87 -86.5 724 **Figure 8.** Monthly-averaged significant wave height (W_{Hs}) in Lake Michigan and Green Bay during the period of

725 2016-2019 years.

726 **5.2 Current-Wave Induced Bottom Shear Stress**

727 Bottom shear stress governs resuspension events and sediment availability in the water 728 column. Figure 9 shows the calculated monthly-averaged bottom shear stress due to the 729 combined effects of current-wave action. While higher shear stress near coastal areas is 730 associated with the stronger nearshore currents, increased wave action in September and October 731 results in augmented shear stress during those months. Western coastal regions, southern and 732 northern shallow areas, and the connecting straits experience higher stress in Green Bay. Also, 733 one would expect strong and frequent resuspension to occur in lower Green Bay in October, 734 produced by the bottom shear stress forcing patterns during that month. Increased shear stress in 735 southwestern Lake Michigan during May is probably associated with a lake-wide cyclonic gyre 736 in the southern basin driven by widespread and strong northerly winds in that area. Southwestern 737 coastal areas of Lake Michigan do not experience such strong wind regimes again until October. 738 Those patterns, in particular high shear stress in the southern and western nearshore areas of 739 Lake Michigan and southern, western, and northern Green Bay, compare well with current and 740 wave bed shear distribution during a March 1998 episode shown by Lee et al. (2007), as well as 741 average shear stress patterns in Lake Michigan during 1994-1995 (Lou et al., 2000).

742 To investigate the distinct contribution of waves and currents in driving physical forces in 743 the lake, we simulated bottom shear stress without waves (currents only) and compared the 744 results with the combined current-wave conditions. As expected, results indicated that for the 745 May-October period of 2016-2019 years, on average the bottom shear stresses were higher by 746 494%, 334%, and 296% in Lake Michigan, Green Bay, and lower Green Bay, respectively, when 747 combined physical processes are considered, compared to the case when only currents are 748 driving bottom shear stresses. Figure S10 and Table S1 in the Supporting Information compare 749 the average spatial patterns of bottom shear stress in Lake Michigan and Green Bay under the 750 two different physical forcing scenarios for the simulation period of 2016-2019 years. We expect 751 to observe similar impact on TSS patterns in the lake due to these different driving stress 752 scenarios. It is obvious that current-wave-induced forces play an important role in sediment 753 plume development and transport. As shown in previous studies, the effects of waves are 754 significant in shallow nearshore waters of Lake Michigan and Green Bay (Lou et al., 2000).

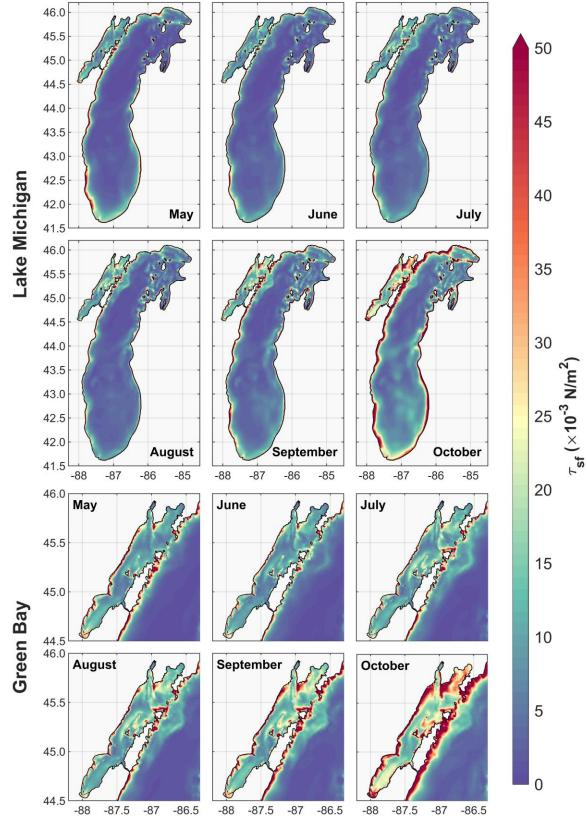


Figure 9. Monthly-averaged bottom shear stress (τ_{sf}) due to combined effects of currents and waves in Lake Michigan and Green Bay during the period of 2016-2019 years.

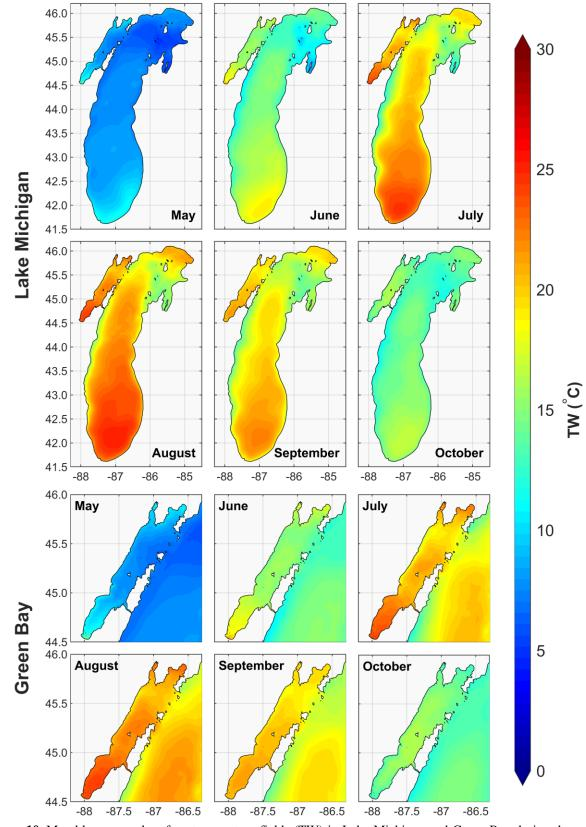
758 **5.3 Thermal Structure of the system**

759 Lake Michigan May-October monthly averages surface temperature fields are illustrated 760 in Figure 10, based on 2016-2019 simulations. The southern basin of Lake Michigan is generally 761 warmer than the rest of the lake. Driven by dominant wind direction and coastal upwellings, 762 western nearshore areas of the lake are often slightly colder than the open lake and eastern 763 coastlines. These patterns were also observed by POM-based simulations of thermal structure in 764 Lake Michigan during May-October of 1982-1983 and 1994-1995 (Beletsky & Schwab, 2001). 765 The thermal regime in Green Bay is significantly different than that of Lake Michigan. Warmer 766 temperatures in the bay can be explained by weaker mixing and shallower morphology. July-767 September are the months with more spatial variability, with higher temperatures in the southern 768 and northern shallow areas, and colder waters near the exchange zone with Lake Michigan, 769 predominantly due to cold water intrusions from the lake.

770 Stratification is an important aspect of the thermal regime and circulation, and 771 consequently of the ecological functioning of the bay. Figure 11 shows monthly average 772 temperature profiles, based on 2016-2019 simulations, along the three cross-sections shown in 773 Figure 1. The results of this study are consistent with the findings by Hamidi et al. (2015, 2013) 774 and Bravo et al. (2015), showing that stratification in Green Bay starts in June, peaks in July and 775 August, and starts to fade in September, resulting in a duration of about three months. Cross-776 section A-A' shows that vertical mixing of temperature occurs at faster rates in shallower areas, 777 as expected. The Fox River has a significant influence on the thermal distribution of the southern 778 Green Bay as shown in the first 50 km of the cross-section A-A' temperature profiles, closer to 779 the mouth of the Fox River. Cross-section B-B' shows that the temperature gradient is stronger 780 in the western side channel of Chambers Island section compared to the well-mixed, shallower 781 eastern channel. Stratification patterns are preserved at cross-section C-C', where Green Bay 782 meets Lake Michigan, but with a weaker gradient.

One advantage of FVCOM is its ability to capture upwelling events in coastal areas of Lake Michigan. A comparison of simultaneous wind fields, surface currents, and surface temperature fields indicates that northerly and southerly winds promote upwellings on the western and eastern coastal areas, respectively (Figure S12 in the Supporting Information). This

- 787 is an important quality when physical models are used to study biogeochemical processes in lake
- 788 systems.



789 790 Figure 10. Monthly-averaged surface temperature fields (TW) in Lake Michigan and Green Bay during the period

791 of 2016-2019 years.

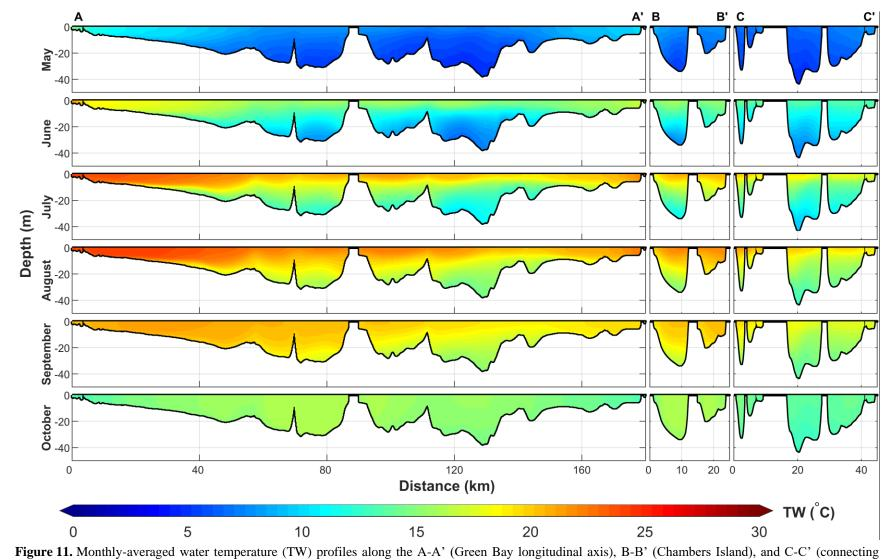


Figure 11. Monthly-averaged water temperature (TW) profiles along the A-A' (Green Bay longitudinal axis), B-B' (Chambers Island), and C-C' (connecting
 straits) cross-sections (as shown in Figure 1) during the period of 2016-2019 years. The vertical axis is exaggerated ~700 times.

797 **5.4 Sediment Transport**

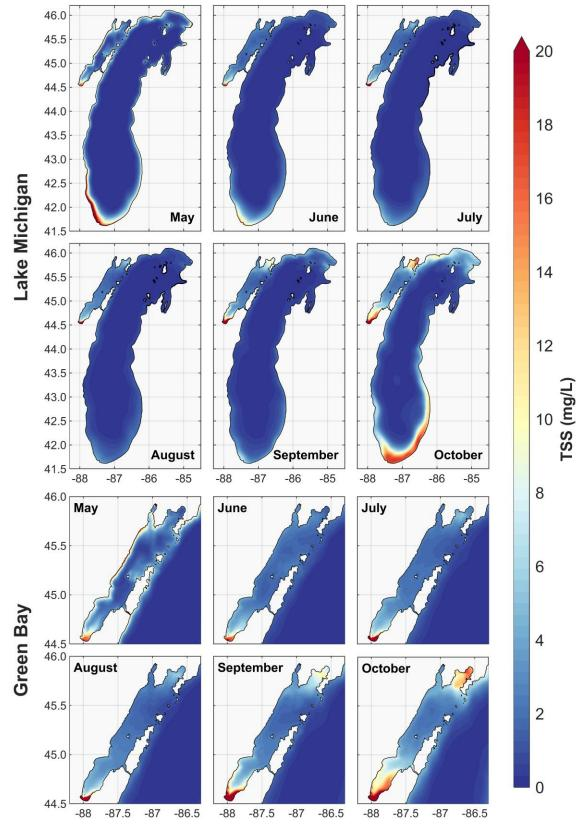
798 Figure 12 shows May-October monthly- and depth-averaged simulated TSS concentration 799 in Lake Michigan, with higher resolution in Green Bay, based on 2016-2019 simulations. 800 Consistent with shear stress patterns shown in Figure 9, TSS concentration patterns are relatively 801 uniform June through September, with higher concentrations in May and October in the 802 southernmost and northernmost Lake Michigan nearshore areas, as well as southern Green Bay. 803 Periods of resuspension in southwestern Lake Michigan during May are related to wind-driven 804 strong bottom shear stress and the availability of fine-grained sediments in those areas. In almost 805 every month southern Green Bay and southern Lake Michigan experience higher TSS 806 concentrations than the rest of the lake. These patterns are similar to those presented by Lee et al. 807 (2007) for March 1998 episodic events, based on physical simulations of sediment transport and 808 satellite imagery-based maps of sediment concentration (Figures 8 and 9 in that article). Also, 809 those patterns qualitatively resemble the predicted TSS concentration in southern Lake Michigan 810 during the 1994-1995 period (Lou et al., 2000).

811 Sediment transport in Green Bay shows significant differences with the transport patterns 812 in Lake Michigan. The Fox River acts as a point source of *TSS*, and the southern bay shows high 813 *TSS* concentrations every month, while the northern bay is more influenced by the Lake 814 Michigan patterns of transport. In Upper Green Bay the sediment transport is consistent with 815 shear stress patterns and mostly influenced by circulation and waves. The *TSS* spatial distribution 816 in the southern bay seems to be governed by the Fox River persistent and significant *TSS* 817 loading, and by the abundance of fine-grained sediments.

818 An interesting observation in the patterns of sediment circulation in Green Bay is that 819 TSS concentration is frequently higher in eastern nearshore areas of lower Green Bay, despite 820 higher current-wave driven shear stresses in the western shorelines. One possible explanation is 821 that the river plume tends to flow along the eastern shore because of the frequent 822 counterclockwise circulation in the southern bay driven by wind direction and the Coriolis effect. 823 In addition, several islands in western Green Bay (shown in Figure S2 in the Supporting 824 Information) cause less and/or weaker resuspensions in that area, therefore, the eastern shore 825 contains more sediments, produced mainly by resuspension, than waters near the western shore. 826 That model result is consistent with Klump et al.'s (1997) finding that currents carrying the plume of turbid Fox River water north along the eastern shore of the bay turn westward off Sturgeon Bay in a counterclockwise gyre that leaves behind a blanket of fine slit accumulating at rates of up to ~1 *cm/year* (160 $mg/cm^2/year$), 20 times faster than the average for the southern bay as a whole.

831 The TSS concentration profiles along the A-A' longitudinal cross-section of Green Bay, 832 shown in Figure 13, show more sediment dynamics near the mouth of Fox River (point A) and 833 higher TSS concentrations in the shallow southern and northern ends of the bay at points A and 834 A'. The model results show less variability in TSS concentration at the Chambers Island (B-B') 835 and connecting straits (C-C') cross-sections. Higher sediment concentration west of Chambers 836 Island cross-section (point B) is probably due to stronger currents near the western shoreline. 837 Results also showed higher sediment transport through channels on the north side of the 838 connecting straits (near point C'), probably due to higher shear stresses in that area.

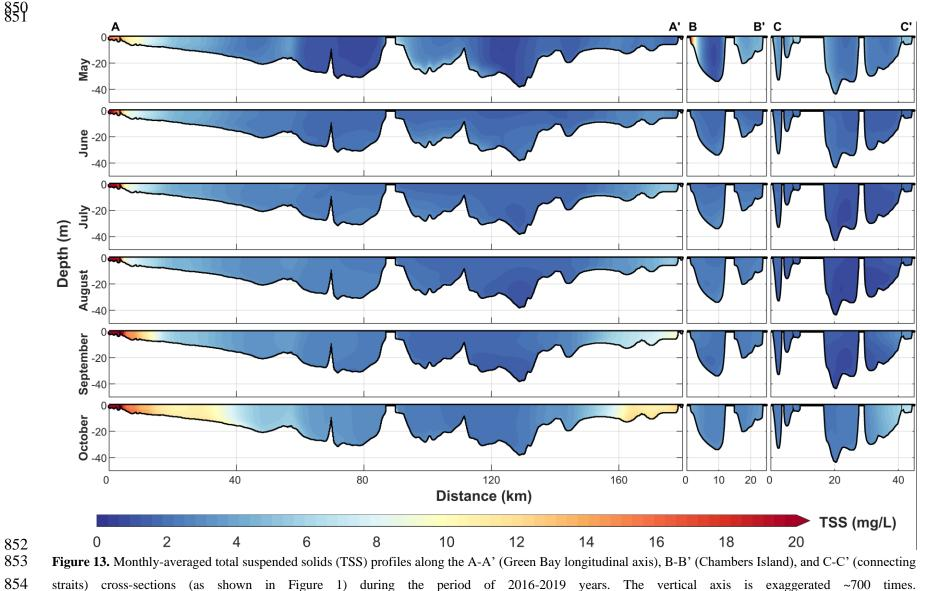
839 As we discussed in Section 5.4, combined current-wave actions drive stronger shear 840 stresses at the water-sediment interface, implying more intense resuspension and transport near 841 the bottom. Our analysis showed that on average during the May-October period of 2016-2019 842 years, considering current-wave combined effects results in 43%, 39%, and 32% higher depth-843 averaged TSS concentration, respectively, in Lake Michigan, Green Bay, and lower Green Bay 844 in comparison with the case when currents are the sole driver of physical forcing in the lake. TSS 845 patterns in Lake Michigan and Green Bay are illustrated with more details in Figure S11 and 846 Table S2 in the Supporting Information.



 847
 -88 -87.5 -87 -86.5
 -88 -87.5 -87 -86.5
 -88 -87.5 -87 -86.5

 848
 Figure 12. Monthly- and depth-averaged total suspended solids (TSS) in Lake Michigan and Green Bay during the

 849
 period of 2016-2019 years.



851

855 5.5 Climatological Summer Circulation and Sediment Transport Patterns in Lake 856 Michigan

857 This section aims to provide maps of summer transport of heat and sediment in Lake 858 Michigan, based simulations using the 2016-2019 meteorological forcing. Figure 14 shows that 859 in general, the prevailing wind direction is southwesterly, and winds are stronger in northern 860 Lake Michigan. The spatial distribution of bottom shear stress shows consistency from year to 861 year, with stronger stresses occurring in southwestern Lake Michigan, Green Bay, and nearshore 862 areas. The maps of surface temperature show a negative, gradual gradient from south to north 863 and a small decline in surface temperature in the southern basin of the lake from 2016 to 2019. 864 The climatological summer surface water temperature in Green Bay was fairly uniform during 865 the simulation period, except that it was somewhat colder near the exchange zone with Lake 866 Michigan.

The map of *TSS* concentration was fairly steady during the simulation period, but there was a small decrease in *TSS* concentration in southwestern Lake Michigan from 2016 to 2019. That temporal pattern was consistent with decreasing winds over the southern lake surface during that period. Northern Lake Michigan showed neither temporal variability in *TSS* patterns nor dependency on wind fields. Those results imply that sediment dynamics in the southern basin is more sensitive to wind and meteorological variability. That is an important pattern to be considered in coastal conservation and shoreline protection.

The maps of *TSS* concentration showed a different temporal trend in lower Green Bay compared to the whole lake. While *TSS* concentration showed a decreasing temporal trend in southern Lake Michigan, sediment concentration increased in lower Green Bay between 2016 and 2019. The increase is probably due to increased loading rates into the bay and confirms the importance of including the tributary loads, especially from the Fox River in modeling sediment transport and biogeochemical interactions in Green Bay.

The findings of this research confirm the results of previous studies by showing the importance of wind forcing in the circulation and transport in Lake Michigan. Wind forcing is a primary driver of circulation in Lake Michigan and Green Bay and can influence biogeochemical processes by governing the thermal structure of the lake and the fate and transport of sediments. Wind patterns should be given particular attention in restoration studies for Green Bay.

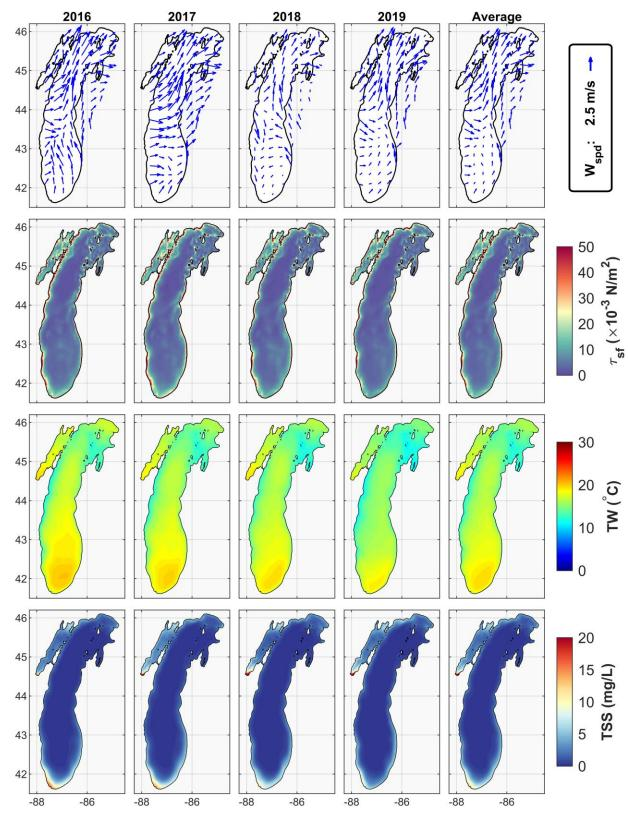


Figure 14. Average annual wind fields (W_{spd}), current-wave driven bottom shear stress (τ_{sf}), surface temperature fields (TW), and depth-averaged total suspended solids (TSS) in Lake Michigan during the period of 2016-2019 years. The last column shows the average for four simulated years.

5.6 Context and scope of this research

890 The 2017 "Summit on the Ecological and Socio-Economic Tradeoffs of Restoration in 891 the Green Bay, Lake Michigan Ecosystem" (Klump et al., 2018) looked at the state of 892 knowledge, gaps, and monitoring needs in the key areas of watershed modeling, biogeochemistry 893 and hydrodynamics, ecosystem modeling and trophic dynamics, habitat and diversity, and 894 socioeconomic and management issues. The introduction of this article summarized the gaps 895 identified in biogeochemistry and hydrodynamics and the intended contribution of this research. 896 This section summarizes previous studies on lake sediment dynamics, biogeochemical 897 interactions, HABs, and the role of mussels, and considers the potential expansion of this model 898 to study those processes. Bartlett et al.'s (2018) is the first study of its kind to assess the spatial 899 diversity of cyanotoxins in Green Bay, Lake Michigan. They characterized the diversity and 900 spatial distribution of toxic or otherwise bioactive cyanobacterial peptides (TBPs) in Green Bay. 901 They collected samples during three cruises in August 2014, and July and August 2015 at sites 902 spanning the mouth of the Fox River north to Chambers Island. They found that microcystins 903 (MCs) were positively correlated with chlorophyll (Chl) and negatively correlated with distance 904 to the Fox River in all cruises along a well-established south-to-north trophic gradient in Green 905 Bay. The influx of nutrients combined with shallow waters in the lower bay creates an ideal 906 environment for the proliferation of cyanobacteria and the formation of Cyanobacterial harmful 907 algal blooms (cyanoHABs).

908 Luo et al. (2012) simulated a 1998 spring phytoplankton bloom in Lake Michigan using a 909 coupled physical-biological model. Their biological model was a nutrient-phytoplankton-910 zooplankton-detritus (NPZD) model, that included phosphorus as the nutrient, phytoplankton, 911 zooplankton, and detritus. The biological model was coupled with the FVCOM physical model 912 and included a wind-wave mixing parametrization but no sediment transport. They searched for 913 the main physical and ecological mechanisms of this spring bloom formation and decay over a 914 long-time scale during March to May, differing from the previous studies of the short-term (5-7 915 days in March) bloom processes. They confirmed that the phytoplankton bloom was forced by 916 rapidly increasing temperature and light intensity in spring. The thermal front that developed in 917 spring inhibited the transport of nutrients and phytoplankton from the nearshore to the deeper 918 water. The wind-driven gyre circulation in southern Lake Michigan induced significant offshore 919 transport, which contributed to the establishment of the circular bloom. To test the importance of general circulation and interior source of ecological factors in the lake for sustaining the donutlike spring bloom, the phosphorus released from suspended sediments and rivers were excluded
from their study.

923 Shen (2016) applied a 1D biophysical model and FVCOM to investigate the ecosystem of 924 Lake Michigan, specifically to explore how invasive mussels affect the nutrient dynamics and 925 distribution of phytoplankton. Wave effects were considered in the 1D biophysical model, but 926 not in the 3D FVCOM simulations. Rowe et al. (2017) used a biophysical model to study the 927 influence of invasive quagga mussels, phosphorus loads, and climate on spatial and temporal 928 patterns of productivity in Lake Michigan. They applied the FVCOM hydrodynamic model, and 929 the FVCOM general ecosystem module (GEM) to implement the NPZD model with the addition 930 of a fifth compartment to represent benthic filter feeder (dreissenid mussel) biomass. They found 931 that although Chl-a and primary production declined over the quagga mussel invasion, their 932 results suggested that increased nutrient loads would increase lake-wide productivity even in the 933 presence of mussels; however, altered spatial and temporal patterns of productivity caused by 934 mussel filter feeding would likely persist. Rowe et al.'s (2017) model included neither a wave 935 model nor a sediment transport model.

936 Bravo et al. (2019) linked a previously built hydrodynamic model and a water quality 937 model developed by Fillingham (2015), extended to three dimensions to simulate the transport 938 and fate of phosphorus in the nearshore area of Lake Michigan. Their model accounted for the 939 interactions between phosphorus, Cladophora, mussels, and lake sediments in the nearshore 940 zone. They quantified the lake assimilative capacity by applying their model to estimate the area 941 required for mixing and diluting wastewater treatment plant outfall total phosphorus loadings to 942 the level of the lake target concentration during the Cladophora growing season. Their model 943 results compared well with empirical measurements of particulate and dissolved phosphorus as 944 well as Cladophora biomass and phosphorus content. The model was applied to test scenarios of 945 wastewater treatment plant phosphorus loading in two different years, in order to help establish 946 phosphorus discharge limits for the plant.

The stage is set to apply the approach developed in this study, which includes wave and sediment transport simulation, as follows: a) to study the spatial and temporal variability of cyanotoxins in Green Bay building upon Bartlett et al.'s (2018) spatial analysis; b) to study algal blooms in lakes following Luo et al.'s (2012) coupled physical-biological modeling approach; c)
to improve the study of the influence of invasive quagga mussels on lakes ecosystems pursuing
Rowe et al.'s (2017) modeling methods; and d) to study the interactions between phosphorus,
Cladophora, mussels, and lake sediments by using the biophysical concepts developed by Bravo
et al. (2019).

Ongoing research will apply the model to: a) to evaluate sediment dynamics in the bay under different climate conditions and loading scenarios in river/watershed management; b) predicting the short- and long-term effects of the Cat Island Chain restoration in altering flow, transport, deposition and benthic habitat in the Area of Concern (AOC); and c) to establish a sediment budget for lower- and entire Green Bay. One of the principal goals of the Cat Island Chain restoration project was to reestablish a barrier island complex and reduce wave energy in the inner bay as a means of reducing resuspension and increasing water clarity.

962 6 Conclusions

963 The hydrodynamic, wind-wave, and sediment transport model developed in this study 964 includes in a single platform of all the relevant geophysical drivers, namely the momentum flux 965 generated by wind, the heat flux across the water surface, the Earth's rotation, thermal 966 stratification, and topography. The single model of Lake Michigan and its Green Bay estuary has 967 high resolution in the bay and in the exchange zone between the open lake and the bay. The 968 single-model approach provides the desired resolution in the bay estuary and represents the 969 combined effects of tributary flows and lake intrusions. The model overcomes limitations of 970 previous nested models of the estuary that used potentially problematic open boundary 971 conditions to represent the exchange of mass, energy, and momentum with Lake Michigan, and 972 of previous whole-lake models that lacked the desired high resolution in the bay or did not 973 include physically-based wind-wave and sediment transport modules. The model confirms the 974 findings of previous studies on Lake Michigan and demonstrates how the circulation, thermal 975 regime, wind action, and sediment transport in the Green Bay estuary depend on meteorological 976 forcing, tributary flows, and lake water intrusions.

Winds are a primary driver of circulation and wave action in Lake Michigan. Easternwinds dominate in May-June, and the wind fields shift to southwesterly and southerly directions

manuscript submitted to Journal of Geophysical Research-Oceans

979 in July until October, when winds are the strongest. Cyclonic (counterclockwise) circulation 980 dominates Lake Michigan, and the formation of gyres is more common in the southern basin. In 981 consistency with wind patterns, circulation is weaker in May and currents accelerate starting in 982 June. Wave action in Lake Michigan is limited in May-August, gradually increases in 983 September, and escalates in October. The northern basin of Lake Michigan experiences stronger 984 waves due to dominant southern winds. Winds drive the fluxes of water, heat, and sediment 985 between the lake and the estuary. In Green Bay, the currents show more spatial variability than 986 the wind fields, with widespread formation of gyres. Surface currents in Green Bay flow 987 predominantly north (especially near the shorelines) and bottom currents flow predominantly 988 towards the south, providing evidence that the interaction of tributary flows and lake currents 989 force summertime stratified flow conditions in the bay. In concert with Lake Michigan, waves in 990 the bay are stronger in September and October. Upper Green Bay and the exchange zone 991 experience stronger waves due to rapid change in the bottom elevation in that area.

992 The southern basin of Lake Michigan is generally warmer than the rest of the lake. 993 Driven by dominant wind direction and coastal upwellings, western nearshore areas of the lake 994 are often slightly colder than the open lake and eastern coastlines. Analysis of simultaneous wind 995 fields, surface currents, and surface temperature fields indicates that northerly and southerly 996 winds promote upwellings on the western and eastern coastal areas, respectively. The model's 997 ability to capture upwelling events is an important quality in the study of biogeochemical 998 processes in lake systems. Warmer temperatures in the bay are explained by weaker mixing and 999 shallower morphology. Stratification in Green Bay starts in June, peaks in July and August, and 1000 starts to fade in September, resulting in a duration of about three months. Field data and model 1001 results showed that the Fox River has a significant influence on the thermal distribution of 1002 southern Green Bay.

Total suspended sediment (*TSS*) concentration fields in Lake Michigan are relatively uniform June through September, concentrations are higher in May and October in the southernmost and northernmost Lake Michigan nearshore areas, and in southern Green Bay. Sediment transport in the estuary is clearly shaped by both tributary loads and exchanges with Lake Michigan. The southern bay shows high *TSS* concentrations because the Fox River acts as a main point source of sediments. The Fox River plume tends to flow along the eastern shore because of counterclockwise circulation in the southern bay driven by wind direction and the

- 1010 Coriolis effect, and consequently, TSS concentration is normally higher in the eastern nearshore
- 1011 areas of lower Green Bay. Upper Green Bay is more influenced by current and wave exchanges
- 1012 with Lake Michigan. Sediment transport is higher through the channels on the north side of the
- 1013 connecting straits, because of higher shear stresses in that area.

1014 Acknowledgments

1015 This project was funded partially by the University of Wisconsin Sea Grant Omnibus 1016 Program Grant 144-AAG3496-UWMKE19A. We appreciate Jeff Houghton for assistance in the 1017 fieldwork, Jim Wagner and Jason Bacon for IT support, and Jessie Grow, Dr. Sarah Bartlett, and 1018 Dr. Todd Miller for providing field data in Green Bay and Lake Michigan.

1019 Lake Michigan bathymetry and shoreline data are obtained from NOAA National 1020 Geophysical Data Center (http://maps.ngdc.noaa.gov/viewers/bathymetry/). Input meteorological 1021 forcing data is based on NOAA National Centers for Environmental Information 1022 (https://www.ncei.noaa.gov/). Buoy observations were also downloaded from NOAA National 1023 Center (https://www.ndbc.noaa.gov/), Great Lakes Data Buoy Observing System 1024 (https://uwm.edu/glos/), lakestat monitoring program (http://www.lakestat.com/), and USGS 1025 National Water Information System (NWIS) database (https://waterdata.usgs.gov/nwis). River 1026 inputs are also based on the USGS NWIS database. Lake Michigan water level data is 1027 downloaded from NOAA Tides and Currents dataset (https://tidesandcurrents.noaa.gov/stations.html?type=Water+Levels). Turbidity and TSS in-situ 1028 1029 observations at the mouth of Fox River are provided based on personal communications with Dr. 1030 Sarah Bartlett at the NEW Water (http://newwater.us/programs-initiatives/aquatic-monitoring-1031 program/). MODIS imagery products are obtained from the NASA EARTHDATA platform 1032 (https://earthdata.nasa.gov/). This is GLERL contribution number XXXX.

1033 References

- Anderson, E. J., & Phanikumar, M. S. (2011). Surface storage dynamics in large rivers:
 Comparing three-dimensional particle transport, one-dimensional fractional derivative, and
 multirate transient storage models. *Water Resources Research*, 47(9).
 https://doi.org/10.1029/2010WR010228
- 1038 Anderson, E. J., & Schwab, D. J. (2011). Relationships between wind-driven and hydraulic flow

in Lake St. Clair and the St. Clair River Delta. Journal of Great Lakes Research, 37(1),

1040 147–158. https://doi.org/10.1016/J.JGLR.2010.11.007

- Anderson, E. J., & Schwab, D. J. (2013). Predicting the oscillating bi-directional exchange flow
 in the Straits of Mackinac. *Journal of Great Lakes Research*, *39*(4), 663–671.
 https://doi.org/10.1016/j.jglr.2013.09.001
- 1044 Anderson, E. J., Schwab, D. J., & Lang, G. A. (2010). Real-Time Hydraulic and Hydrodynamic
- Model of the St. Clair River, Lake St. Clair, Detroit River System. *Journal of Hydraulic Engineering*, *136*(8), 507–518. https://doi.org/10.1061/(ASCE)HY.1943-7900.0000203
- 1047 Anderson, E. J., Stow, C. A., Gronewold, A. D., Mason, L. A., McCormick, M. J., Qian, S. S., et
- 1048 al. (2021). Seasonal overturn and stratification changes drive deep-water warming in one of
- 1049 Earth's largest lakes. *Nature Communications*, 12(1), 1688. https://doi.org/10.1038/s41467-
- 1050 021-21971-1
- Ariathurai, R., & Arulanandan, K. (1978). Erosion Rates of Cohesive Soils. J Hydr Div, ASCE,
 1052 101(5), 635–639.
- 1053 Bai, X., Wang, J., Schwab, D. J., Yang, Y., Luo, L., Leshkevich, G. A., & Liu, S. (2013). 1054 Modeling 1993–2008 climatology of seasonal general circulation and thermal structure in 1055 the Ocean 65. 40-63. Great Lakes using FVCOM. Modelling, https://doi.org/10.1016/J.OCEMOD.2013.02.003 1056
- Battjes, J. A., & Janssen, J. P. F. M. (1978). Energy Loss and Set-Up Due to Breaking of
 Random Waves. In *Coastal Engineering 1978* (pp. 569–587). New York, NY: American
 Society of Civil Engineers. https://doi.org/10.1061/9780872621909.034
- Beletsky, D., & Schwab, D. J. (2001). Modeling circulation and thermal structure in Lake
 Michigan: Annual cycle and interannual variability. *Journal of Geophysical Research: Oceans*, *106*(C9), 19745–19771. https://doi.org/10.1029/2000JC000691
- 1063 Beletsky, D., O'Connor, W. P., Schwab, D. J., Dietrich, D. E., Beletsky, D., O'Connor, W. P., et
- al. (1997). Numerical Simulation of Internal Kelvin Waves and Coastal Upwelling Fronts*.
- 1065 *Http://Dx.Doi.Org/10.1175/1520-0485(1997)027<1197:NSOIKW>2.0.CO;2.*
- 1066 https://doi.org/10.1175/1520-0485(1997)027<1197:NSOIKW>2.0.CO;2
- 1067 Beletsky, D., Schwab, D. J., Roebber, P. J., McCormick, M. J., Miller, G. S., & Saylor, J. H.

- 1068 (2003). Modeling wind-driven circulation during the March 1998 sediment resuspension
 1069 event in Lake Michigan. *Journal of Geophysical Research: Oceans*, *108*(C2), n/a-n/a.
 1070 https://doi.org/10.1029/2001JC001159
- Beletsky, D., Schwab, D., & McCormick, M. (2006a). Modeling the 1998-2003 summer
 circulation and thermal structure in Lake Michigan. *Journal of Geophysical Research: Oceans*, *111*(10), 1–18. https://doi.org/10.1029/2005JC003222
- Beletsky, D., Schwab, D., & McCormick, M. (2006b). Modeling the 1998–2003 summer
 circulation and thermal structure in Lake Michigan. *Journal of Geophysical Research*, *111*(C10), C10010. https://doi.org/10.1029/2005JC003222
- Booij, N., Ris, R. C., & Holthuijsen, L. H. (1999). A third-generation wave model for coastal
 regions: 1. Model description and validation. *Journal of Geophysical Research: Oceans*, *104*(C4), 7649–7666. https://doi.org/10.1029/98JC02622
- Booij, N., Haagsma, I. J. G., Holthuijsen, L. H., Kieftenburg, A. T. M. M., Ris, R. C., van der
 Westhuysen, A. J., & Zijlema, M. (2004). SWAN Cycle III version 40.51 Technical
 documentation. Delft, The Netherlands.
- Bravo, H.R., Hamidi, S. A., Klump, J. V., & Waples, J. T. (2017). Physical Drivers of the
 Circulation and Thermal Regime Impacting Seasonal Hypoxia in Green Bay, Lake
 Michigan. In *Modeling Coastal Hypoxia* (pp. 23–47). Cham: Springer International
 Publishing. https://doi.org/10.1007/978-3-319-54571-4_2
- Bravo, Hector R., Hamidi, S. A., Anderson, E. J., Klump, J. V., & Khazaei, B. (2019).
 Timescales of Transport Through Lower Green Bay. *Journal of Great Lakes Research*, (In
 Press.). https://doi.org/https://doi.org/10.1016/j.jglr.2020.06.010
- Bravo, Hector R, Hamidi, S. A., Klump, J. V., & Waples, J. T. (2015). Currents and heat fluxes
 induce stratification leading to hypoxia in Green Bay, Lake Michigan. *E-Proceedings of the 36th IAHR World Congress*, (1985), 1–10.
- Chen, C., Liu, H., & Beardsley, R. C. (2003). An unstructured grid, finite-volume, threedimensional, primitive equations ocean model: Application to coastal ocean and estuaries. *Journal of Atmospheric and Oceanic Technology*, 20(1), 159–186.
 https://doi.org/10.1175/1520-0426(2003)020<0159:AUGFVT>2.0.CO;2

- 1097 Chen, C., Wang, L., Ji, R., Budd, J. W., Schwab, D. J., Beletsky, D., et al. (2004). Impacts of
 1098 suspended sediment on the ecosystem in Lake Michigan: A comparison between the 1998
 1099 and 1999 plume events. *Journal of Geophysical Research*, *109*(C10), C10S05.
 1100 https://doi.org/10.1029/2002JC001687
- Chen, C., Huang, H., Beardsley, R. C., Liu, H., Xu, Q., & Cowles, G. (2007). A finite volume numerical approach for coastal ocean circulation studies: Comparisons with finite difference models. *Journal of Geophysical Research*, *112*(C3), C03018.
- 1104 https://doi.org/10.1029/2006JC003485
- Chen, C., Beardsley, R. C., Cowles, G., Qi, J., Lai, Z., Gao, G., et al. (2013). An Unstructured *Grid*, Finite-Volume Community Ocean Model FVCOM User Manual. Retrieved from
 http://fvcom.smast.umassd.edu/
- Chen, T., Zhang, Q., Wu, Y., Ji, C., Yang, J., & Liu, G. (2018). Development of a wave-current
 model through coupling of FVCOM and SWAN. *Ocean Engineering*, *164*, 443–454.
 https://doi.org/10.1016/J.OCEANENG.2018.06.062
- Deines, K. L. (1999). Backscatter estimation using broadband acoustic Doppler current profilers.
 Proceedings of the IEEE Working Conference on Current Measurement, 249–253.
 https://doi.org/10.1109/ccm.1999.755249
- 1114 Eadie, B. J., Bell, G. L., & Hawley, N. (1991). Sediment Trap Study in the Green Bay Mass
- 1115 Balance Program: Mass and Organic Carbon Fluxes, Resuspension, and Particle Settling
- 1116 *Velocities.* NOAA Technical Memorandum ERL GLERL-75. Great Lakes Environmental
- 1117 Research Laboratory Ann Arbor, Michigan July 1991.
- Fillingham, J. (2015). Modeling Lake Michigan Nearshore Carbon and Phosphorus Dynamics.
 Theses and Dissertations. University of Wisconsin-Milwaukee. Retrieved from http://dc.uwm.edu/etd/871
- García, M. H. (2008). Sediment Transport and Morphodynamics. In M. H. García (Ed.),
 Sedimentation Engineering: Processes, Measurements, Modeling, and Practice (pp. 21–
- 1123163).Reston,VA:AmericanSocietyofCivilEngineers.1124https://doi.org/10.1061/9780784408148.ch02
- 1125 Ge, J., Torres, R., Chen, C., Liu, J., Xu, Y., Bellerby, R., et al. (2020). Influence of suspended

- sediment front on nutrients and phytoplankton dynamics off the Changjiang Estuary: A
- 1127 FVCOM-ERSEM coupled model experiment. Journal of Marine Systems, 204, 103292.
- 1128 https://doi.org/10.1016/j.jmarsys.2019.103292
- 1129 GLOS. (2021). Data | Great Lakes Observing System. Retrieved January 25, 2021, from
 1130 https://uwm.edu/glos/data/
- Grunert, B. K., Brunner, S. L., Hamidi, S. A., Bravo, H. R., & Klump, J. V. (2018). Quantifying
 the influence of cold water intrusions in a shallow, coastal system across contrasting years:
 Green Bay, Lake Michigan. *Journal of Great Lakes Research*, 44(5), 851–863.
 https://doi.org/10.1016/J.JGLR.2018.07.009
- Guerra, M., Cienfuegos, R., Thomson, J., & Suarez, L. (2017). Tidal energy resource
 characterization in Chacao Channel, Chile. *International Journal of Marine Energy*, 20, 1–
 https://doi.org/10.1016/J.IJOME.2017.11.002
- Hamidi, Sajad Ahamd, Bravo, H. R., & Klump, J. V. (2013). Evidence of Multiple Physical
 Drivers on the Circulation and Thermal Regime in the Green Bay of Lake Michigan. In *World Environmental and Water Resources Congress 2013* (pp. 1719–1726). Reston, VA:
 American Society of Civil Engineers. https://doi.org/10.1061/9780784412947.169
- Hamidi, Sajad Ahmad, Bravo, H. R., Val Klump, J., & Waples, J. T. (2015). The role of
 circulation and heat fluxes in the formation of stratification leading to hypoxia in Green
 Bay, Lake Michigan. *Journal of Great Lakes Research*, *41*(4), 1024–1036.
 https://doi.org/10.1016/j.jglr.2015.08.007
- Hamidi, Sajad Ahmad, Hosseiny, H., Ekhtari, N., & Khazaei, B. (2017). Using MODIS remote
 sensing data for mapping the spatio-temporal variability of water quality and river turbid
 plume. *Journal of Coastal Conservation*, 21(6), 939–950. https://doi.org/10.1007/s11852017-0564-y
- Harris, C. K., & Wiberg, P. L. (2001). A two-dimensional, time-dependent model of suspended
 sediment transport and bed reworking for continental shelves. *Computers & Geosciences*,
 27(6), 675–690. https://doi.org/10.1016/S0098-3004(00)00122-9
- Harris, V. A., & Christie, J. (1987). *The lower Green Bay Remedial Action Plan: nutrient and eutrophication management. Technical Advisory Committee report.* Publication No. WR-

- 1155 167-87. Wisconsin Department of Natural Resources. Madison, WI.
- Hasselmann, K., Barnett, T. P., Bouws, E., Carlson, H. K., Cartwright, D. E., Enke, K., et al.
 (1973). Measurements of wind-wave growth and swell decay during the Joint North Sea
 Wave Project (JONSWAP).
- Hasselmann, S., Hasselmann, K., Allender, J. H., & Barnett, T. P. (1985). Computations and
 Parameterizations of the Nonlinear Energy Transfer in a Gravity-Wave Specturm. Part II:
 Parameterizations of the Nonlinear Energy Transfer for Application in Wave Models. *Journal of Physical Oceanography*, *15*(11), 1378–1391. https://doi.org/10.1175/15200485(1985)015<1378:CAPOTN>2.0.CO;2
- Hawley, N., & Niester, J. (1993). Measurement of Horizontal Sediment Transport in Green Bay,
 May-October, 1989. *Journal of Great Lakes Research*, 19(2), 368–378.
 https://doi.org/10.1016/S0380-1330(93)71225-3
- Hawley, N., Lesht, B. M., & Schwab, D. J. (2004). A comparison of observed and modeled
 surface waves in southern Lake Michigan and the implications for models of sediment
 resuspension. *Journal of Geophysical Research*, *109*(C10), C10S03.
 https://doi.org/10.1029/2002JC001592
- Le Hir, P., Cayocca, F., & Waeles, B. (2011). Dynamics of sand and mud mixtures: A
 multiprocess-based modelling strategy. *Continental Shelf Research*, *31*(10 SUPPL.), S135–
 S149. https://doi.org/10.1016/j.csr.2010.12.009
- Huang, H., Chen, C., Cowles, G. W., Winant, C. D., Beardsley, R. C., Hedstrom, K. S., &
 Haidvogel, D. B. (2008). FVCOM validation experiments: Comparisons with ROMS for
 three idealized barotropic test problems. *Journal of Geophysical Research*, *113*(C7),
 C07042. https://doi.org/10.1029/2007JC004557
- HydroQual Inc. (1999). *Hydrodynamics, Sediment Transport, and Sorbent Dynamics in Green Bay.* Report to Wisconsin Department of Natural Resources, Madison, Wisconsin.
- Ji, R., Chen, C., Budd, J. W., Schwab, D. J., Beletsky, D., Fahnenstiel, G. L., et al. (2002).
 Influences of suspended sediments on the ecosystem in Lake Michigan: A 3-D coupled biophysical modeling experiment. *Ecological Modelling*, 152(2–3), 169–190.
 https://doi.org/10.1016/S0304-3800(02)00027-3

Jones, C. A. (2000). An Accurate Model of Sediment Transport. University of California, Santa
Barbara.

1186 Kaster, J. L., Groff, C. M., Klump, J. V., Rupp, D. L., Iyer, S., Hansen, A., et al. (2018). 1187 Evaluation of lower Green Bay benthic fauna with emphasis on re-ecesis of Hexagenia 1188 nymphs. Journal of Great Lakes Research, 44(5), 895-909. mayfly 1189 https://doi.org/10.1016/J.JGLR.2018.06.006

- 1190 Khazaei, B. (2020). Development of a Hydrodynamic and Sediment Transport Model for Green
 1191 Bay, Lake Michigan. University of Wisconsin-Milwaukee.
- Khazaei, B., & Wu, C. (2018). Estimation of Vegetation Coverage Based on Seasonal
 Variabilities in MODIS-Based Vegetation Indices. In *World Environmental and Water Resources Congress 2018* (pp. 11–20). Reston, VA: American Society of Civil Engineers.
 https://doi.org/10.1061/9780784481400.002
- Khazaei, B., Hamidi, S. A., & Nabizadeh, A. (2018). An Empirical Approach to Estimate Total
 Suspended Sediment using Observational Data in Fox River and Southern Green Bay, WI.
 In *World Environmental and Water Resources Congress*. Minneapolis, MN, USA.
- Klump, J. Val, Fitzgerald, S. A., & Waplesa, J. T. (2009). Benthic biogeochemical cycling,
 nutrient stoichiometry, and carbon and nitrogen mass balances in a eutrophic freshwater
 bay. *Limnology and Oceanography*, 54(3), 692–712.
 https://doi.org/10.4319/lo.2009.54.3.0692
- Klump, J. Val, Bratton, J., Fermanich, K., Forsythe, P., Harris, H. J., Howe, R. W., & Kaster, J.
 L. (2018). Green Bay, Lake Michigan: A proving ground for Great Lakes restoration. *Journal of Great Lakes Research*, 44(5), 825–828.
 https://doi.org/10.1016/J.JGLR.2018.08.002
- Klump, J.V. V, Edgington, D. N. N., Sager, P. E. E., & Robertson, D. M. M. (1997).
 Sedimentary phosphorus cycling and a phosphorus mass balance for the Green Bay (Lake
 Michigan) ecosystem. *Canadian Journal of Fisheries and Aquatic Sciences*, 54(1), 10–26.
 Retrieved from http://www.nrcresearchpress.com/doi/10.1139/f96-247
- 1211 Klump, J. Val, Brunner, S. L., Grunert, B. K., Kaster, J. L., Weckerly, K., Houghton, E. M., et al.
 1212 (2018). Evidence of persistent, recurring summertime hypoxia in Green Bay, Lake

- 1213
 Michigan.
 Journal
 of
 Great
 Lakes
 Research,
 44(5),
 841–850.

 1214
 https://doi.org/10.1016/J.JGLR.2018.07.012
 https://doi.org/10.1016/J.JGLR.2018.07.012
 https://doi.org/10.1016/J.JGLR.2018.07.012
- Komen, G. J., Hasselmann, K., & Hasselmann, K. (1984). On the Existence of a Fully
 Developed Wind-Sea Spectrum. *Journal of Physical Oceanography*, *14*(8), 1271–1285.
 https://doi.org/10.1175/1520-0485(1984)014<1271:OTEOAF>2.0.CO;2
- Labuhn, S. L. (2017). *Dissolved oxygen dynamics within Green Bay in an effort to understand hypoxia Table of Contents*. University of Wisconsin-Milwaukee.
- Lai, W., Pan, J., & Devlin, A. T. (2018). Impact of tides and winds on estuarine circulation in the
 Pearl River Estuary. *Continental Shelf Research*, 168, 68–82.
 https://doi.org/10.1016/J.CSR.2018.09.004
- Lee, C., Schwab, D. J., & Hawley, N. (2005). Sensitivity analysis of sediment resuspension
 parameters in coastal area of southern Lake Michigan. *Journal of Geophysical Research C: Oceans*, *110*(3), 1–16. https://doi.org/10.1029/2004JC002326
- Lee, C., Schwab, D. J., Beletsky, D., Stroud, J., & Lesht, B. (2007). Numerical modeling of
 mixed sediment resuspension, transport, and deposition during the March 1998 episodic
 events in southern Lake Michigan. *Journal of Geophysical Research: Oceans*, *112*(2), 1–17.
 https://doi.org/10.1029/2005JC003419
- Li, B., Tanaka, K. R., Chen, Y., Brady, D. C., & Thomas, A. C. (2017). Assessing the quality of
 bottom water temperatures from the Finite-Volume Community Ocean Model (FVCOM) in
 the Northwest Atlantic Shelf region. *Journal of Marine Systems*, *173*, 21–30.
 https://doi.org/10.1016/J.JMARSYS.2017.04.001
- Li, J., Pan, S., Chen, Y., Fan, Y.-M., & Pan, Y. (2018). Numerical estimation of extreme waves
 and surges over the northwest Pacific Ocean. *Ocean Engineering*, *153*, 225–241.
 https://doi.org/10.1016/J.OCEANENG.2018.01.076
- Lou, J., Schwab, D. J., Beletsky, D., & Hawley, N. (2000). A model of sediment resuspension
 and transport dynamics in southern Lake Michigan. *Journal of Geophysical Research: Oceans*, 105(C3), 6591–6610. https://doi.org/10.1029/1999JC900325
- Luo, L., Wang, J., Schwab, D. J., Vanderploeg, H., Leshkevich, G., Bai, X., et al. (2012).
 Simulating the 1998 spring bloom in Lake Michigan using a coupled physical-biological

- 1242 model. J. Geophys. Res, 117, 10011. https://doi.org/10.1029/2012JC008216
- Manchester-Neesvig, J. B., Andren, A. W., & Edgington, D. N. (1996). Patterns of Mass
 Sedimentation and of Deposition of Sediment Contaminated by PCBs in Green Bay. *Journal of Great Lakes Research*, 22(2), 444–462. https://doi.org/10.1016/S03801330(96)70969-3
- Mantz, P. A. (1977). Incipient transport of fine grains and flakes by fluids-extended Shields
 diagram. *Journal of the Hydraulics Division*, *103*(HY6).
- Mao, M., & Xia, M. (2017). Dynamics of wave–current–surge interactions in Lake Michigan: A
 model comparison. *Ocean Modelling*, *110*, 1–20.
 https://doi.org/10.1016/J.OCEMOD.2016.12.007
- Mao, M., & Xia, M. (2020). Monthly and episodic dynamics of summer circulation in Lake
 Michigan. *Journal of Geophysical Research: Oceans*, 125(6).
 https://doi.org/10.1029/2019jc015932
- Mao, M., van der Westhuysen, A. J., Xia, M., Schwab, D. J., & Chawla, A. (2016). Modeling
 wind waves from deep to shallow waters in Lake Michigan using unstructured SWAN. *Journal of Geophysical Research: Oceans, 121*(6), 3836–3865.
 https://doi.org/10.1002/2015JC011340
- Mellor, G. L., & Yamada, T. (1982). Development of a turbulence closure model for geophysical
 fluid problems. *Reviews of Geophysics*, 20(4), 851.
 https://doi.org/10.1029/RG020i004p00851
- Mengual, B., Hir, P., Cayocca, F., & Garlan, T. (2017). Modelling Fine Sediment Dynamics:
 Towards a Common Erosion Law for Fine Sand, Mud and Mixtures. *Water*, 9(8), 564.
 https://doi.org/10.3390/w9080564
- 1265Meyer-Peter, E., & Müller, R. (1948). Formulas for Bed-Load transport. IAHSR 2nd Meeting,1266Stockholm, Appendix2.Retrievedfrom1267https://repository.tudelft.nl/islandora/object/uuid%3A4fda9b61-be28-4703-ab06-from
- 1268 43cdc2a21bd7
- 1269 Miller, T. R. (2020). Lakestat. Retrieved November 12, 2019, from http://www.lakestat.com/

- Mitchener, H., & Torfs, H. (1996). Erosion of mud/sand mixtures. *Coastal Engineering*, 29(1–2),
 1–25. https://doi.org/10.1016/S0378-3839(96)00002-6
- Moore, J. R., Meyer, R. P., & Morgan, C. L. (1973). *Investigation of the Sediments and Potential Manganese Nodule Resources of Green Bay, Wisconsin.* University of Wisconsin, Sea
 Grant College Program. Technical Report-WIS. WISCU-T-73-001.
- 1275 National Geophysical Data Center. (2015). Bathymetric Data Viewer. Retrieved January 1, 2017,
 1276 from http://maps.ngdc.noaa.gov/viewers/bathymetry/
- NEW Water. (2017). Aquatic Monitoring Program > NEW Water. Retrieved October 1, 2018,
 from http://newwater.us/programs-initiatives/aquatic-monitoring-program/
- NOAA. (2017). Bathymetry of Lake Michigan. Retrieved January 1, 2017, from
 https://ngdc.noaa.gov/mgg/greatlakes/michigan.html
- NOAA. (2018). National Centers for Environmental Information (NCEI). Retrieved November
 1, 2018, from https://gis.ncdc.noaa.gov/maps/ncei/cdo/hourly
- NOAA. (2020). Station Selection NOAA Tides & Currents. Retrieved January 5, 2020, from
 https://tidesandcurrents.noaa.gov/stations.html?type=Water+Levels
- Ouillon, S. (2018). Why and How Do We Study Sediment Transport? Focus on Coastal Zones
 and Ongoing Methods. *Water*, *10*(4), 390. https://doi.org/10.3390/w10040390
- 1287Parker, G. (2004). 1D Morphodynamics of Rivers and Turbidity Currents. Saint Anthony Falls1288Lab., Univ. of Minn., Minneapolis. [Available at1289http://hydrolab.illinois.edu/people/parkerg/morphodynamics_e-book.htm].
- Qi, J., Chen, C., Beardsley, R. C., Perrie, W., Cowles, G. W., & Lai, Z. (2009). An unstructuredgrid finite-volume surface wave model (FVCOM-SWAVE): Implementation, validations
 and applications. *Ocean Modelling*, 28(1–3), 153–166.
 https://doi.org/10.1016/J.OCEMOD.2009.01.007
- Qualls, T., Harris, H. J., & Harris, V. (2013). *The State of Green Bay: The Condition of the Bay of Green Bay/Lake Michigan 2013*. University of Wisconsin Sea Grant Institute. Retrieved
 from https://www.seagrant.wisc.edu/wp-content/uploads/2018/11/State-of-the-Bay-Report 2013.pdf

- Read, J., Klump, V., Johengen, T., Schwab, D., Paige, K., Eddy, S., et al. (2010). Working in
 Freshwater: The Great Lakes Observing System Contributions to Regional and National
 Observations, Data Infrastructure, and Decision Support. *Marine Technology Society Journal*, 44(6), 84–98. https://doi.org/10.4031/MTSJ.44.6.12
- Ris, R. C., Holthuijsen, L. H., & Booij, N. (1999). A third-generation wave model for coastal
 regions: 2. Verification. *Journal of Geophysical Research: Oceans*, *104*(C4), 7667–7681.
 https://doi.org/10.1029/1998JC900123
- Rowe, M.D., Anderson, E. J., Wang, J., & Vanderploeg, H. A. (2015). Modeling the effect of
 invasive quagga mussels on the spring phytoplankton bloom in Lake Michigan. *Journal of Great Lakes Research*, 41, 49–65. https://doi.org/10.1016/J.JGLR.2014.12.018
- Rowe, Mark D., Anderson, E. J., Vanderploeg, H. A., Pothoven, S. A., Elgin, A. K., Wang, J., &
 Yousef, F. (2017). Influence of invasive quagga mussels, phosphorus loads, and climate on
 spatial and temporal patterns of productivity in Lake Michigan: A biophysical modeling
 study. *Limnology and Oceanography*, 62(6), 2629–2649. https://doi.org/10.1002/lno.10595
- 1312 Safaie, A., Wendzel, A., Ge, Z., Nevers, M. B., Whitman, R. L., Corsi, S. R., & Phanikumar, M.
- 1313 S. (2016). Comparative Evaluation of Statistical and Mechanistic Models of *Escherichia*
- 1314 *coli* at Beaches in Southern Lake Michigan. *Environmental Science & Technology*, 50(5),
- 1315 2442–2449. https://doi.org/10.1021/acs.est.5b05378
- Sanford, L. P. (2008). Modeling a dynamically varying mixed sediment bed with erosion,
 deposition, bioturbation, consolidation, and armoring. *Computers and Geosciences*, *34*(10),
 1263–1283. https://doi.org/10.1016/j.cageo.2008.02.011
- Schwab, D.J., & Beletsky, D. (1998). Lake Michigan Mass Balance Study: Hydrodynamic
 Modeling Project. ERL GLERL-108. NOAA GLERL, Ann Arbor, MI.
- Schwab, David J. (1983). Numerical Simulation of Low-Frequency Current Fluctuations in Lake
 Michigan. *Journal of Physical Oceanography*, *13*(12), 2213–2224.
 https://doi.org/10.1175/1520-0485(1983)013<2213:NSOLFC>2.0.CO;2
- Shen, C. (2016). Modeling of dreissenid mussel impacts on Lake Michigan. ProQuest
 Dissertations and Theses. University of Wisconsin-Milwaukee. Retrieved from
 https://search.proquest.com/docview/1844987331?accountid=6180%0Ahttp://dw2zn6fm9z.

- 1327 search.serialssolution.com?ctx_ver=Z39.88-2004&ctx_enc=info:ofi/enc:UTF-
- 1328 8&rfr_id=info:sid/ProQuest+Dissertations+%26+Theses+Global&rft_val_fmt=info:ofi/fmt:
 1329 kev:mtx:dissertat
- 1330 Sherwood, C. R., Aretxabaleta, A. L., Harris, C. K., Paul Rinehimer, J., Verney, R., & Ferré, B.
- 1331 (2018). Cohesive and mixed sediment in the Regional Ocean Modeling System (ROMS
- 1332 v3.6) implemented in the Coupled Ocean-Atmosphere-Wave-Sediment Transport Modeling
- 1333 System (COAWST r1234). Geoscientific Model Development, 11(5), 1849–1871.
- 1334 https://doi.org/10.5194/gmd-11-1849-2018
- 1335 Shore, J. A. (2009). Modelling the circulation and exchange of Kingston Basin and Lake Ontario
- 1336
 with
 FVCOM.
 Ocean
 Modelling,
 30(2–3),
 106–114.

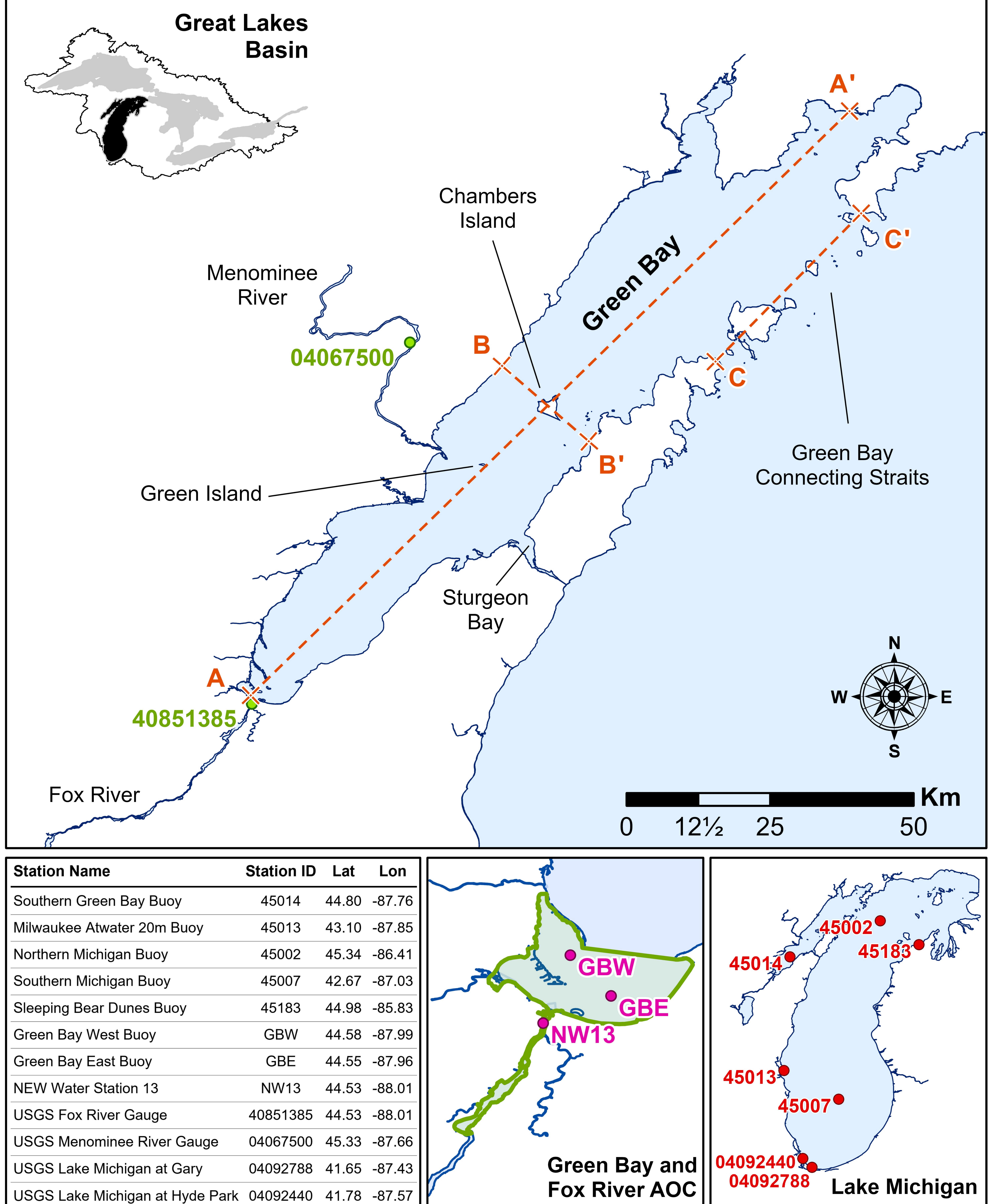
 1337
 https://doi.org/10.1016/J.OCEMOD.2009.06.007

 </t
- 1338 Smagorinsky, J. (1963). General circulation experiments with the primitive equations, I. The
- basic experiment. *Monthly Weather Review*, 91(3), 99–164. https://doi.org/10.1175/15200493(1963)091<0099:GCEWTP>2.3.CO;2
- 1341 Soulsby, R. L. (1998). Dynamics of marine sands.
- Velleux, M., Endicott, D., Steuer, J., Jaeger, S., & Patterson, D. (1995). Long-Term Simulation
 of PCB Export from the Fox River to Green Bay. *Journal of Great Lakes Research*, *21*(3),
 359–372. https://doi.org/10.1016/S0380-1330(95)71047-4
- Waples, J. T., & Klump, J. V. (2002). Biophysical effects of a decadal shift in summer wind
 direction over the Laurentian Great Lakes. *Geophysical Research Letters*, 29(8), 43-1-43–4.
 https://doi.org/10.1029/2001GL014564
- Warner, J. C., Sherwood, C. R., Signell, R. P., Harris, C. K., & Arango, H. G. (2008).
 Development of a three-dimensional, regional, coupled wave, current, and sedimenttransport model. *Computers* & *Geosciences*, 34(10), 1284–1306.
 https://doi.org/10.1016/J.CAGEO.2008.02.012
- Wisconsin DNR. (2000). Model Evaluation Workgroup Technical Memorandum 2f: Estimation
 of Sediment Bed Properties for Green Bay.
- Wolanski, E. (2007). Estuarine sediment dynamics. In *Estuarine Ecohydrology* (pp. 41–69).
 Elsevier. https://doi.org/10.1016/b978-044453066-0.50004-0

Wolanski, E., & Elliott, M. (2015). Estuarine Ecohydrology: An Introduction. Estuarine
 Ecohydrology. Elsevier. https://doi.org/10.1016/c2013-0-13014-0

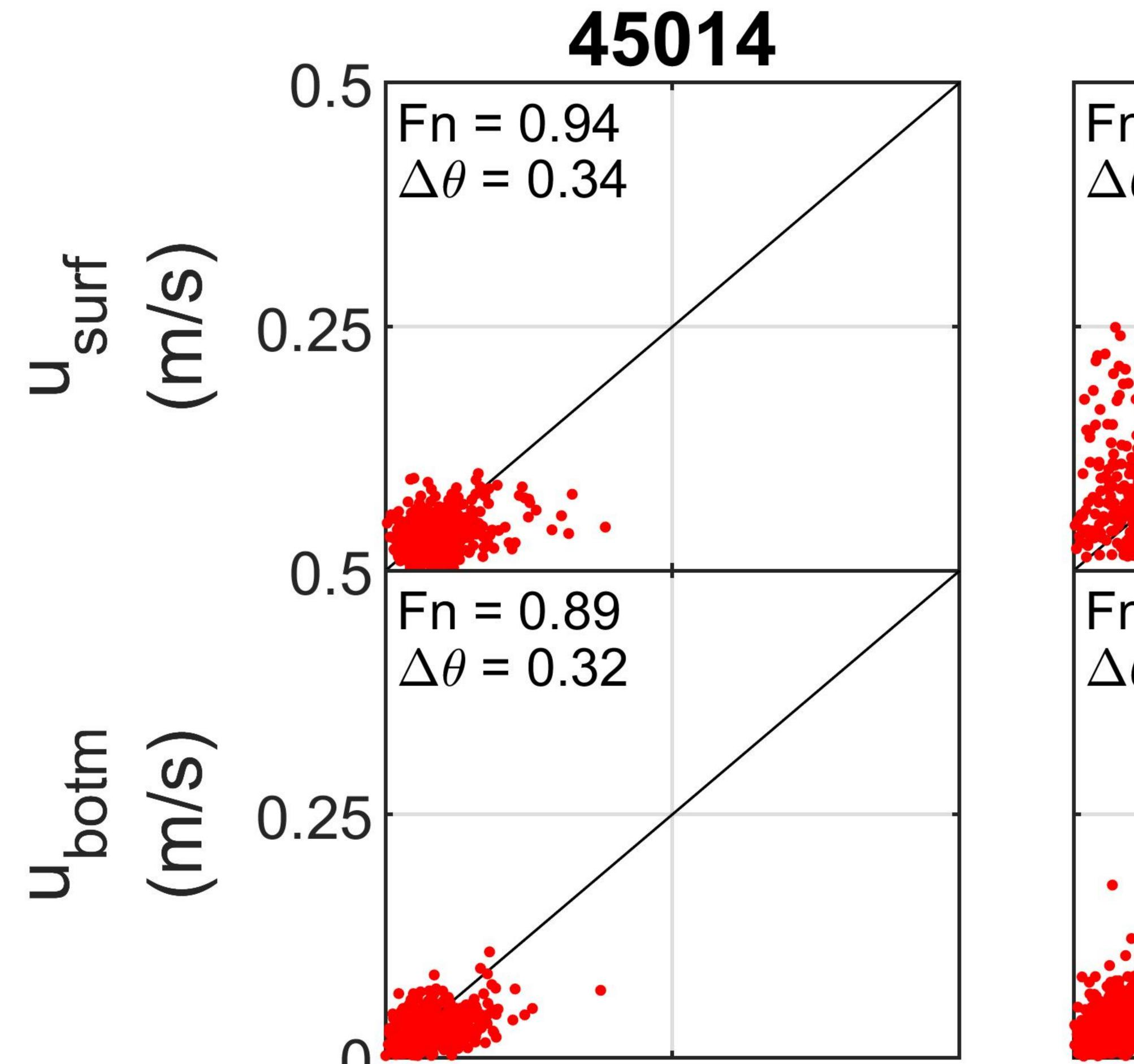
- Xue, P., Schwab, D. J., & Hu, S. (2015). An investigation of the thermal response to
 meteorological forcing in a hydrodynamic model of Lake Superior. Retrieved from
 https://www.semanticscholar.org/paper/An-investigation-of-the-thermal-response-to-
- 1361 forcing-Xue-Schwab/40eca7b276ebcad8589f9df017dbd724b1ffc00d
- Yolcubal, I., Brusseau, M. L., Artiola, J. F., Wierenga, P., & Wilson, L. G. (2004).
 ENVIRONMENTAL PHYSICAL PROPERTIES AND PROCESSES. *Environmental Monitoring and Characterization*, 207–239. https://doi.org/10.1016/B978-0120644773/50014-X
- 1366 Zhang, J., Xiong, M., Yin, C., & Gan, S. (2018). Inner shelf response to storm track variations
 1367 over the east LeiZhou Peninsula, China. *International Journal of Applied Earth*1368 *Observation and Geoinformation*, 71, 56–69. https://doi.org/10.1016/J.JAG.2018.03.011

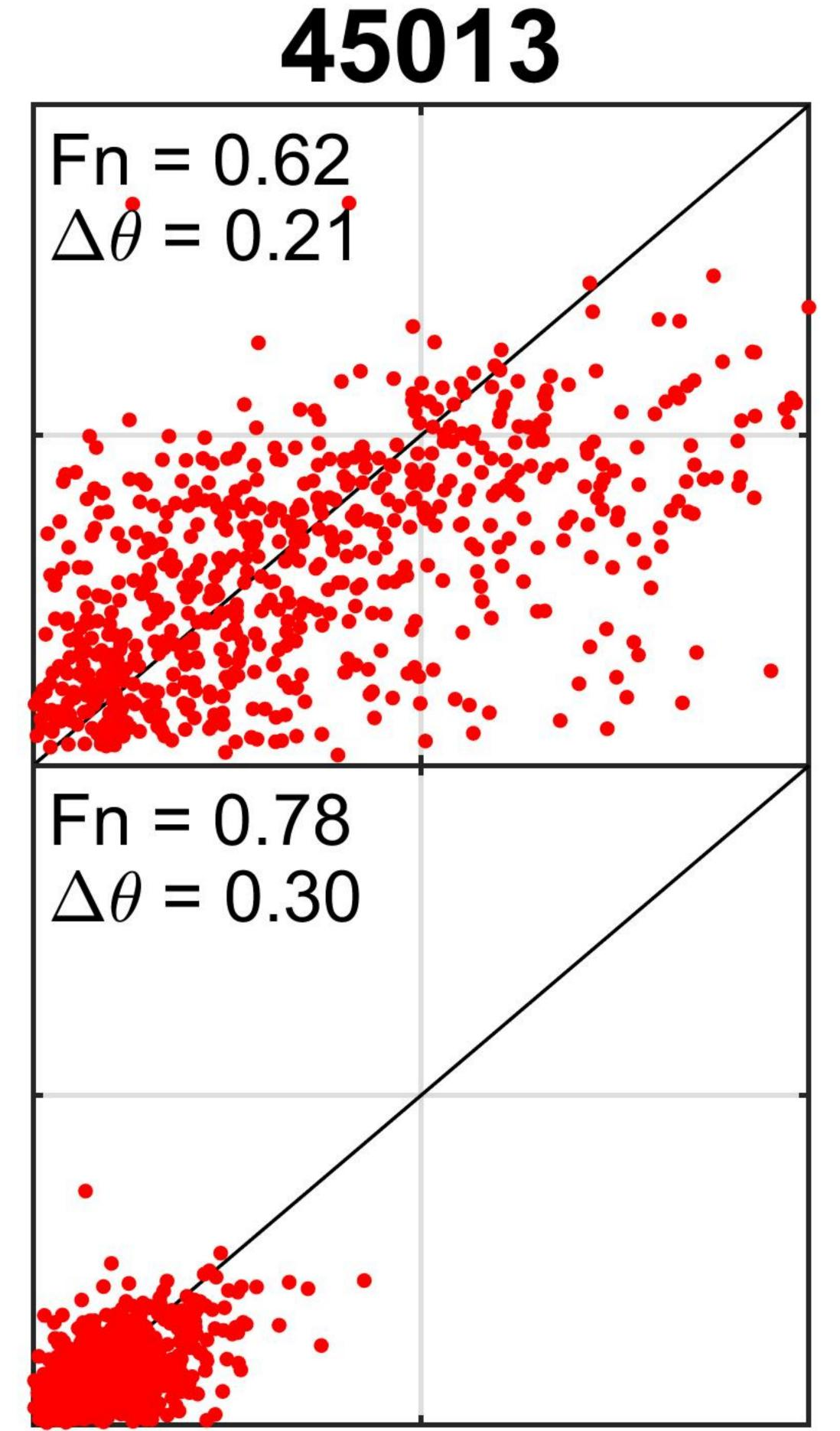
Figure 1.



Milwaukee Atwater 20m Buoy	45013	43.10	-87.85	
Northern Michigan Buoy	45002	45.34	-86.41	
Southern Michigan Buoy	45007	42.67	-87.03	
Sleeping Bear Dunes Buoy	45183	44.98	-85.83	
Green Bay West Buoy	GBW	44.58	-87.99	
Green Bay East Buoy	GBE	44.55	-87.96	
NEW Water Station 13	NW13	44.53	-88.01	
USGS Fox River Gauge	40851385	44.53	-88.01	
USGS Menominee River Gauge	04067500	45.33	-87.66	
USGS Lake Michigan at Gary	04092788	41.65	-87.43	
USGS Lake Michigan at Hyde Park	04092440	41.78	-87.57	

Figure 2.



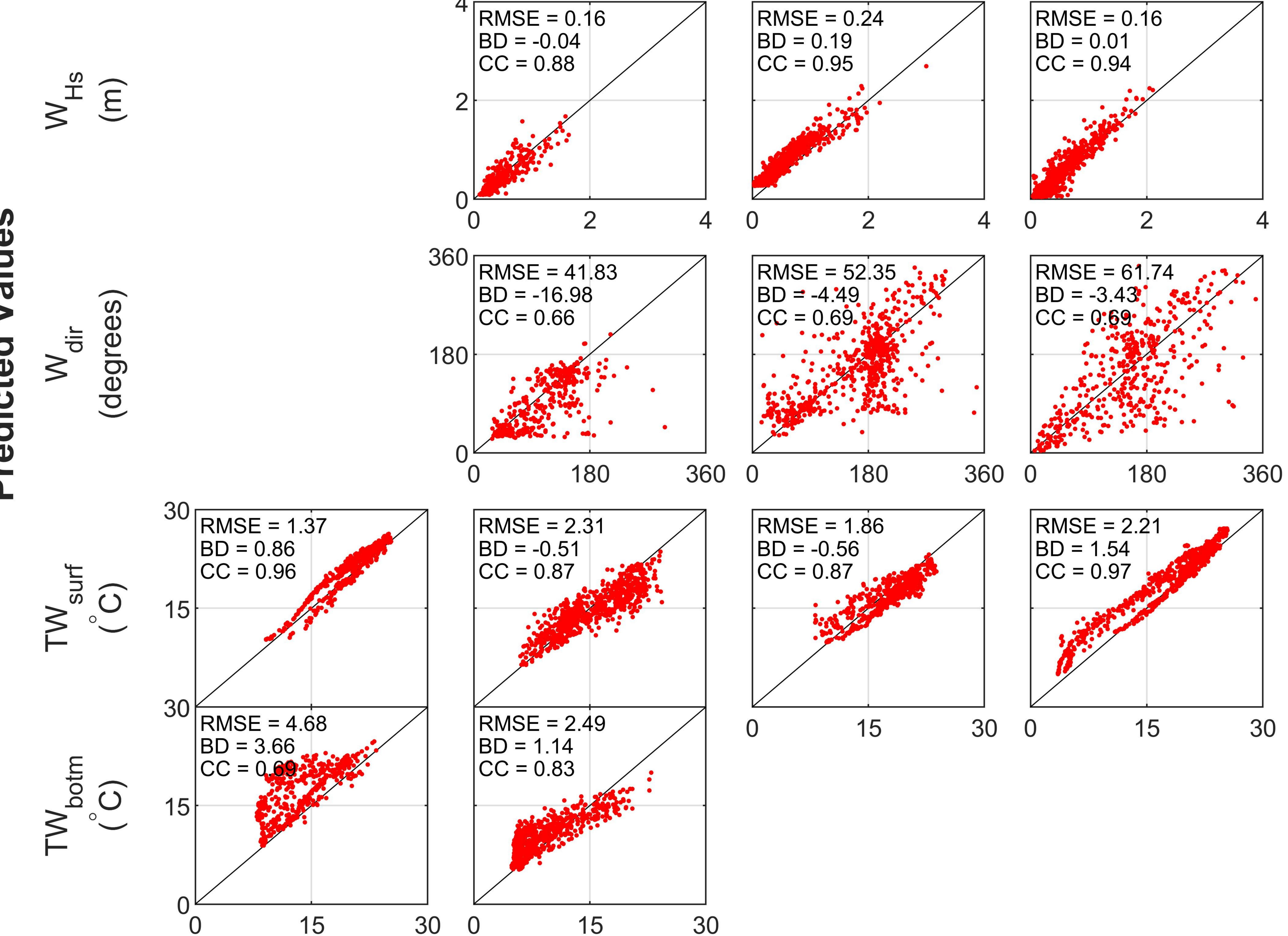


45002

 \mathbf{D}

S

0.25 0.25 0.5 0 0.5 U



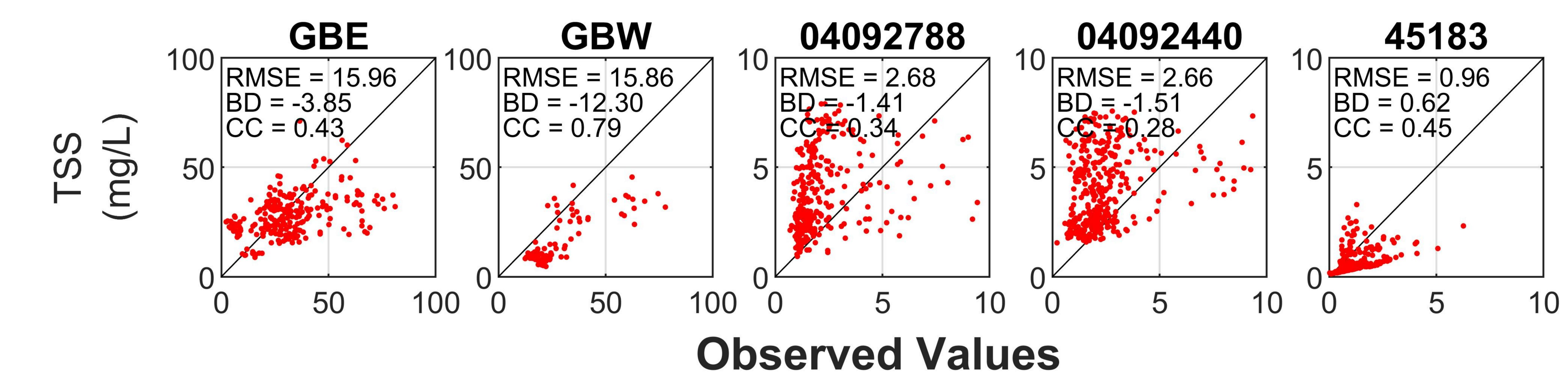
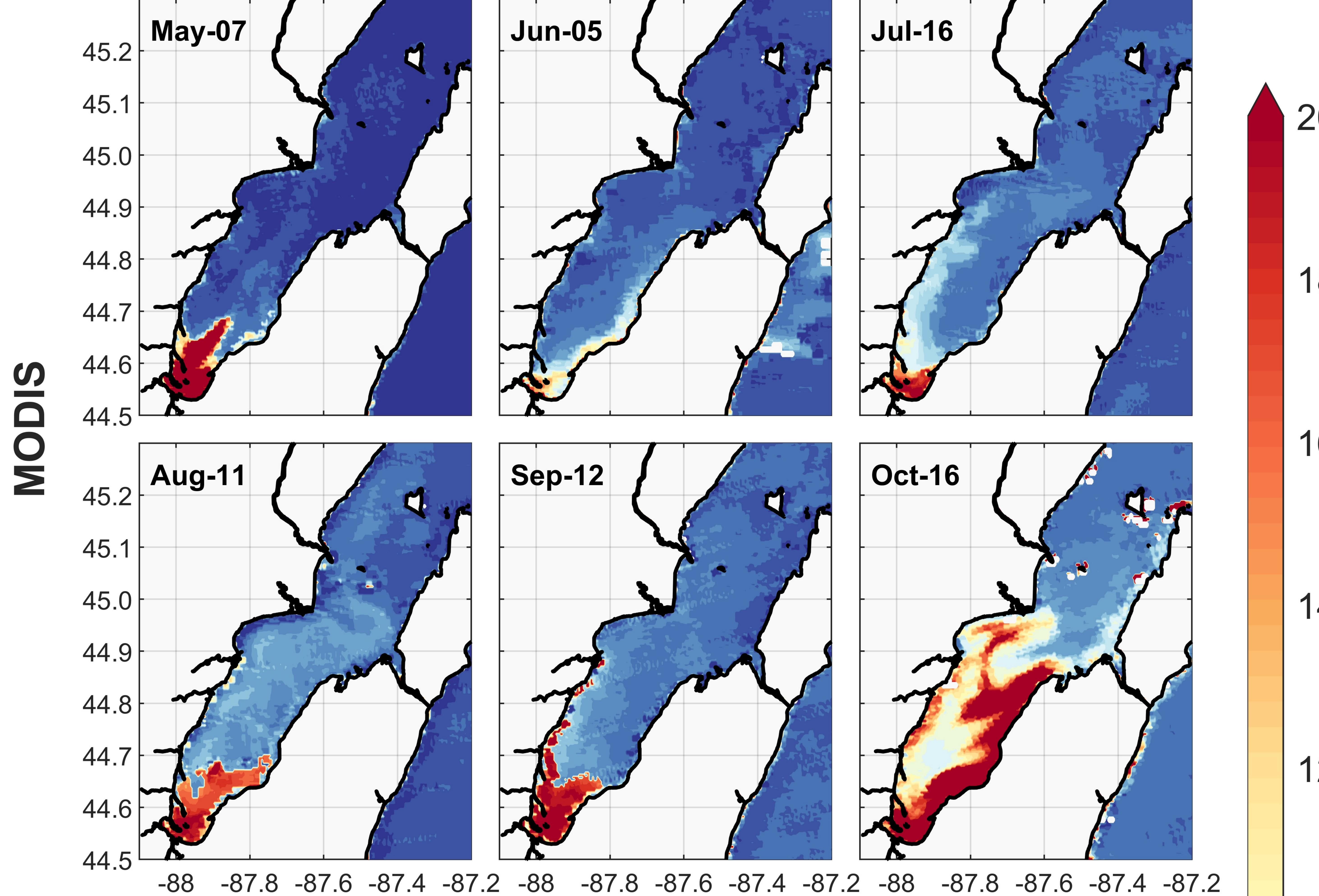


Figure 3.



 $\overline{}$

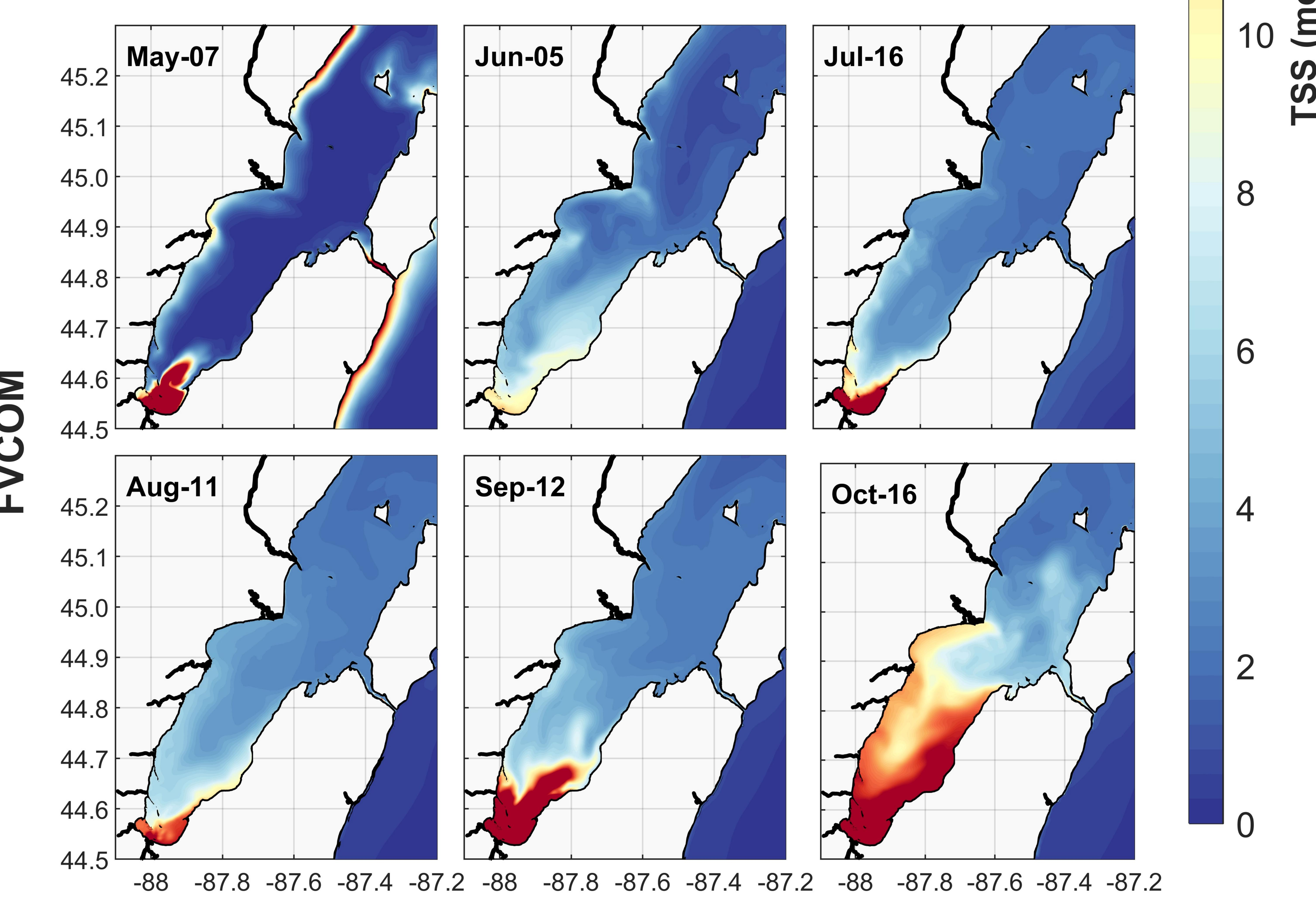
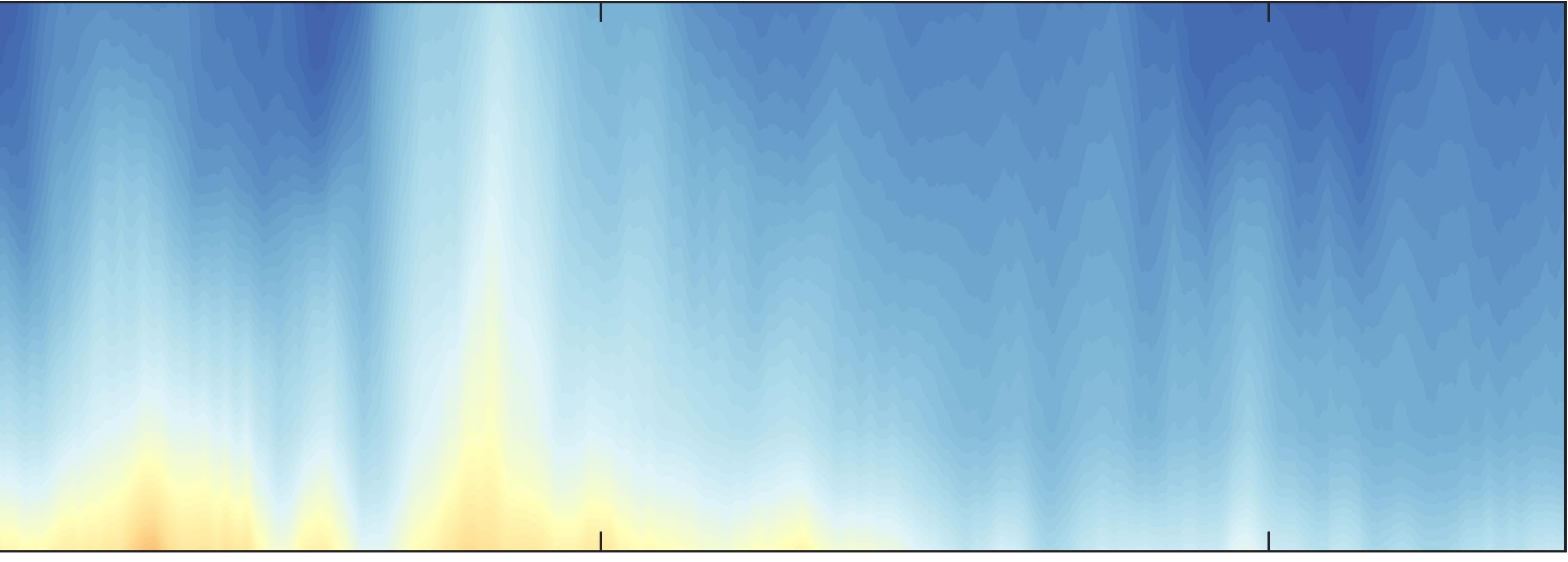


Figure 4.

		0	
Depth (m)		-2	
	60	-4	
	2	-6	
	D SO	-8	
	U	-10	
		-12	
		0	
		-2	
	te d	-4	
		-6	
	L D D	-8	
		-10	
		-12	
			Jul

TSS profile in lower Green Bay (45014 buoy)



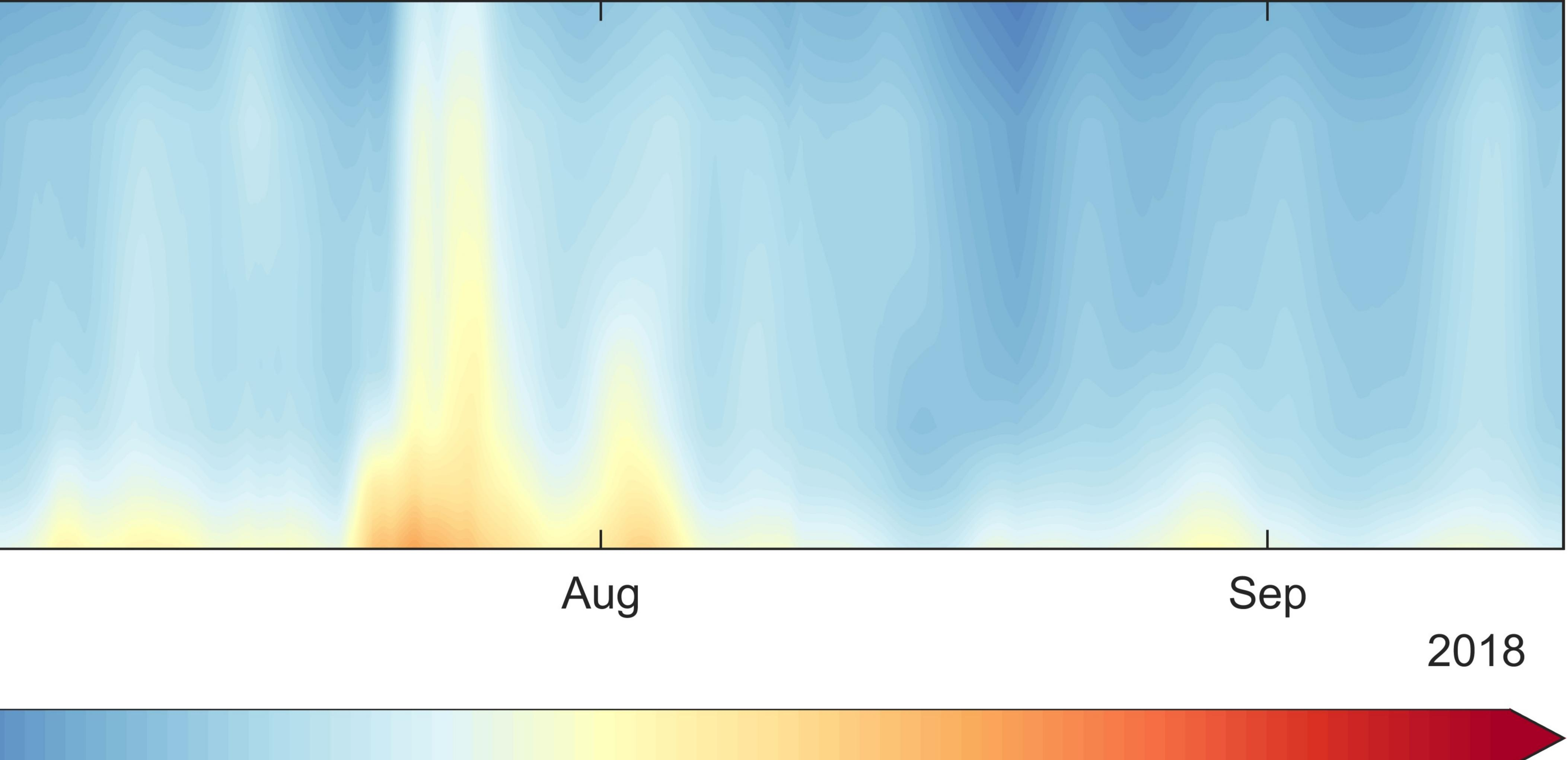






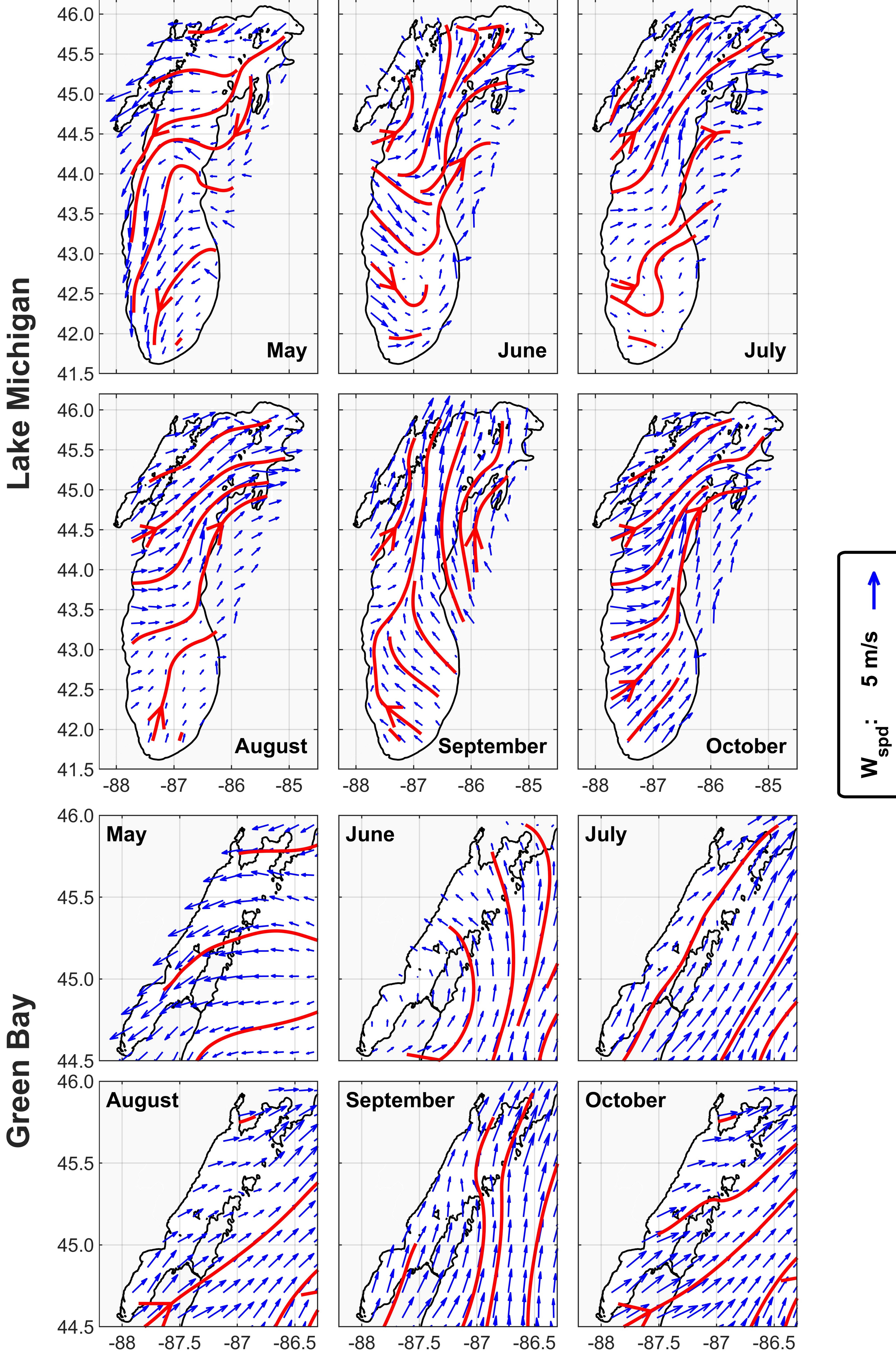








Figure 5.



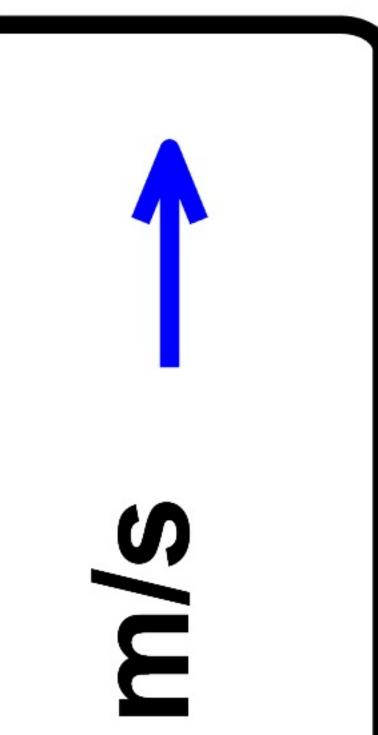
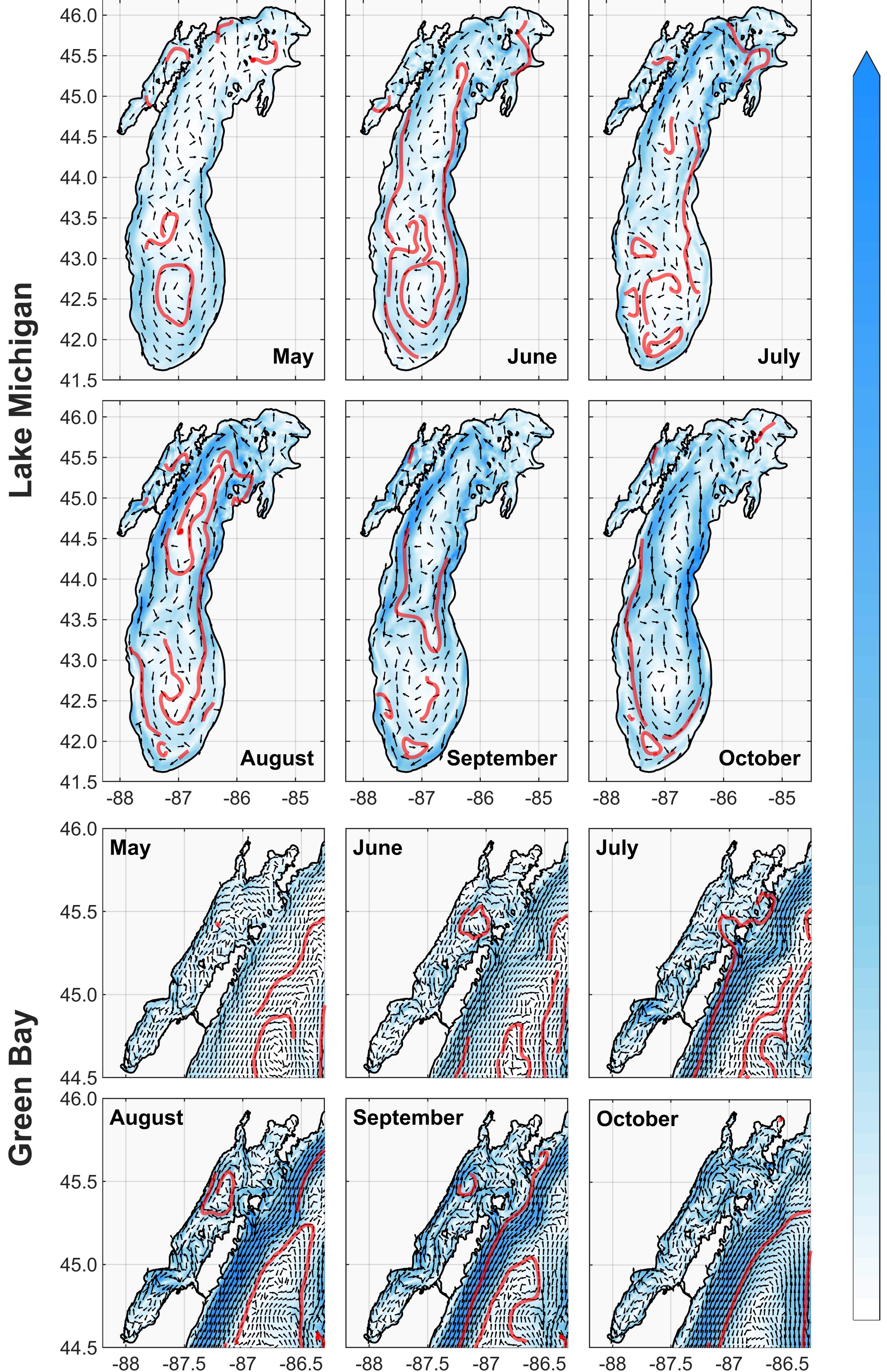


Figure 6.









0.07

0.06

0.05 Jods

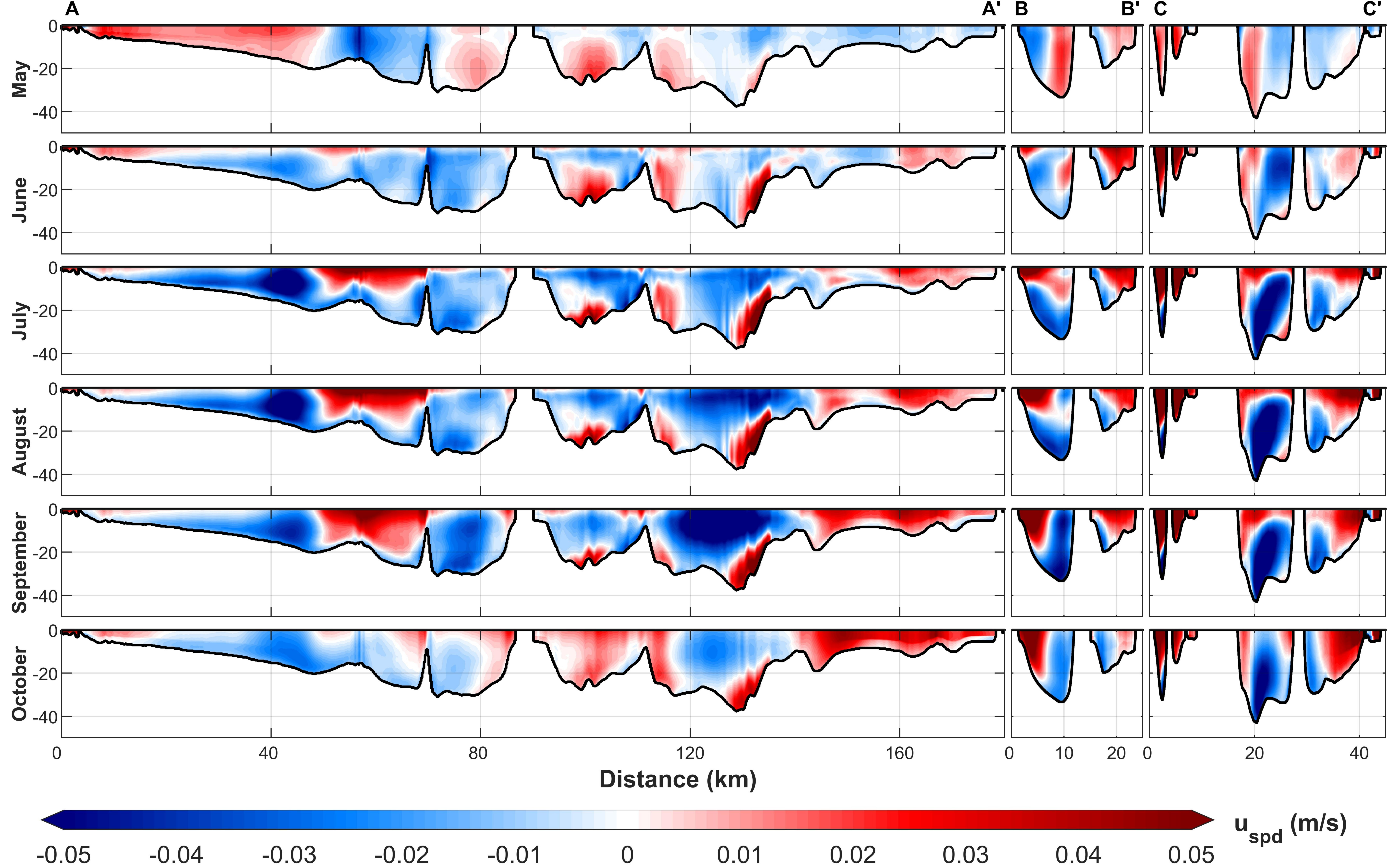
 $\widehat{\mathbf{0}}$

0.04

0.03

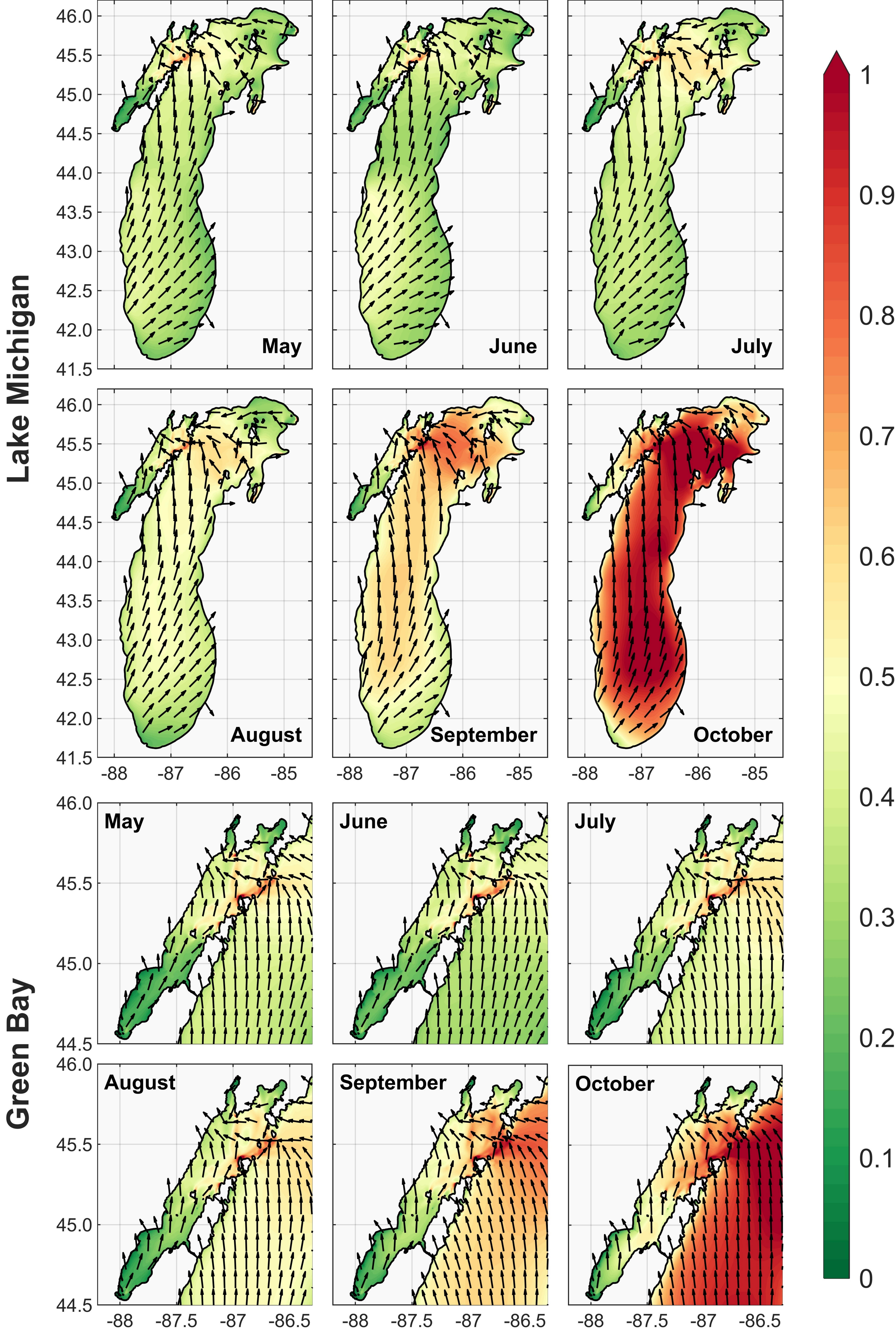
0.02

Figure 7.



-

Figure 8.



0.9

0.8

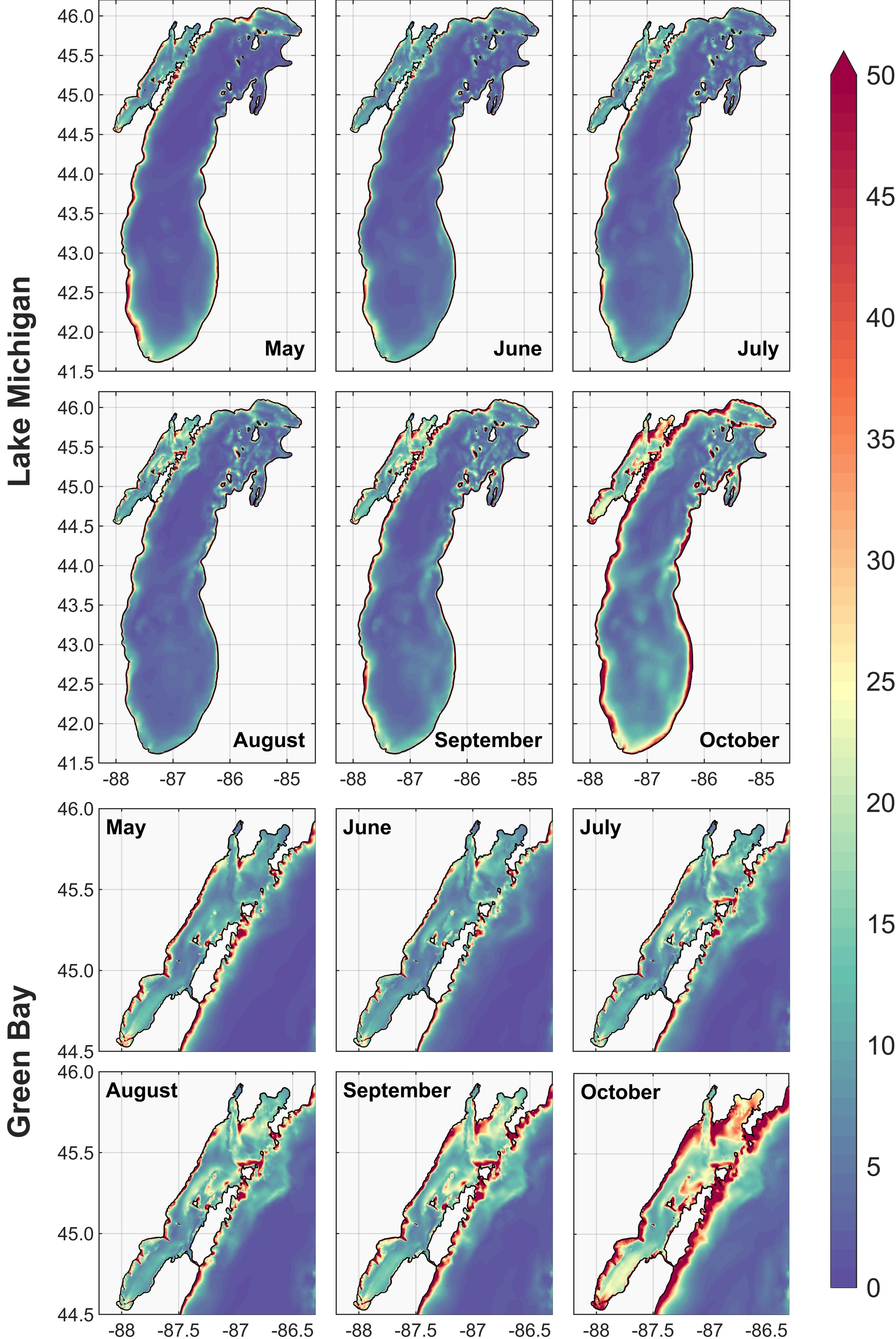


S

0.3

 $\mathbf{\Omega}$

Figure 9.









Ń **m**

0

C

4S

Figure 10.





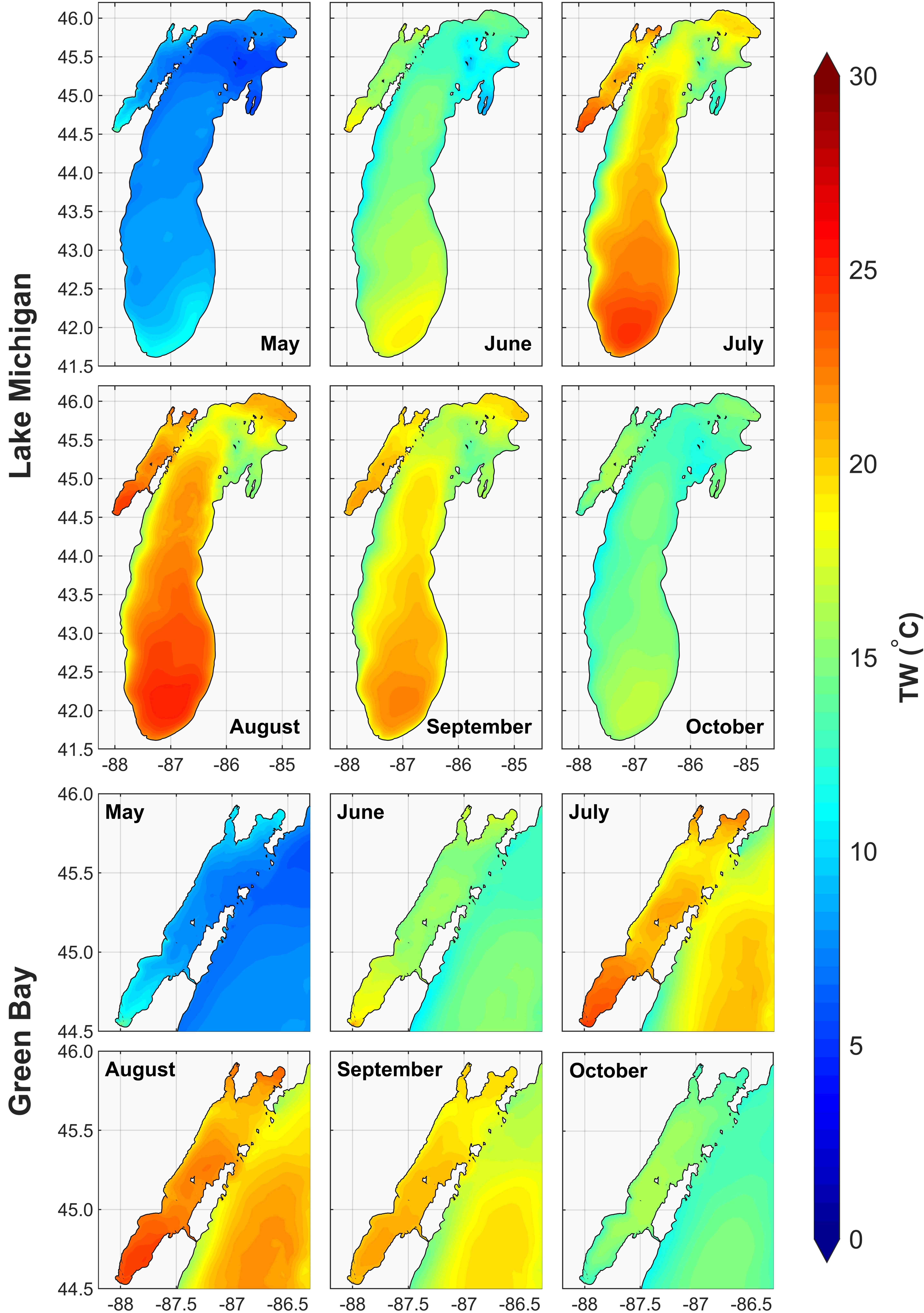


Figure 11.

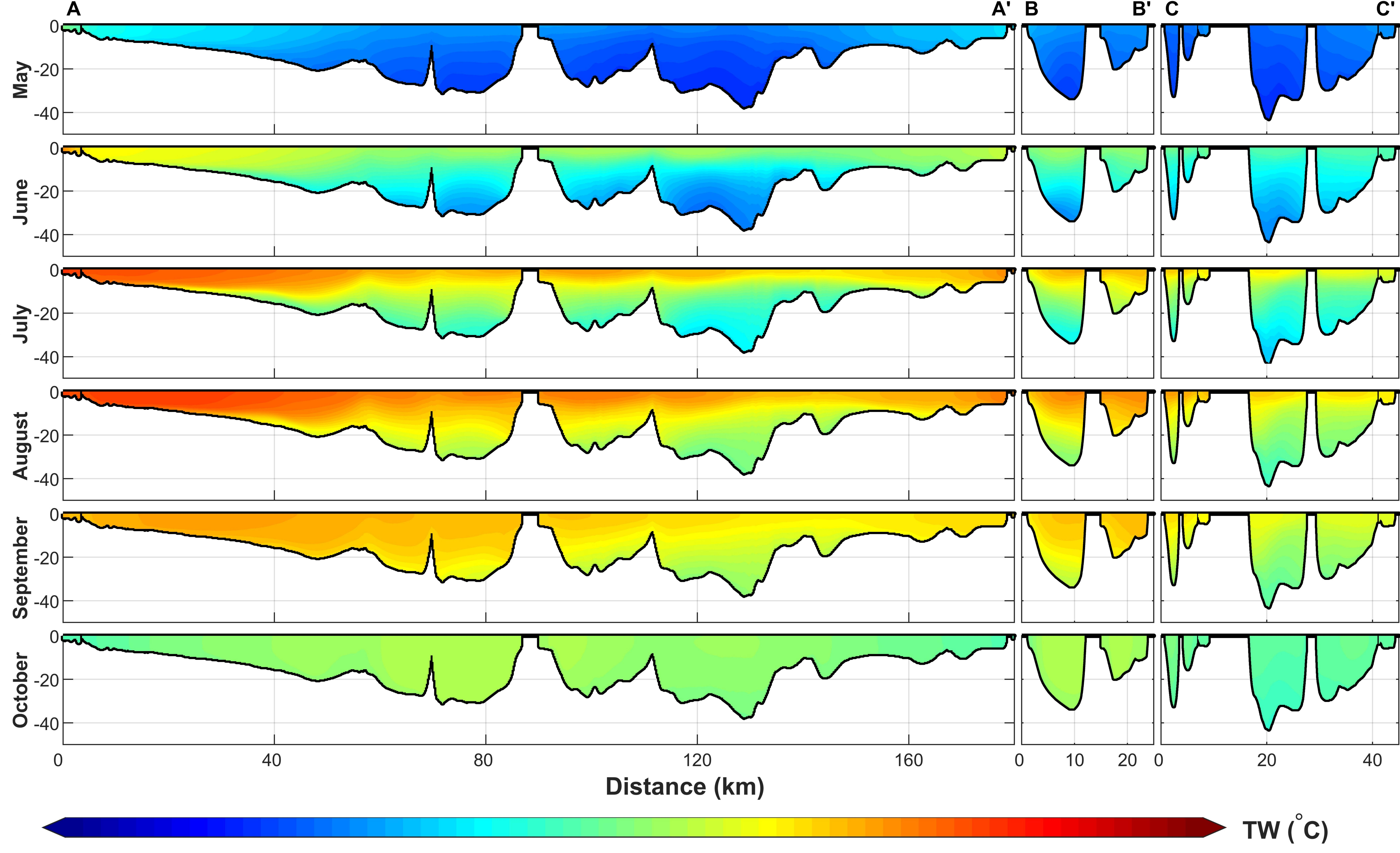


Figure 12.

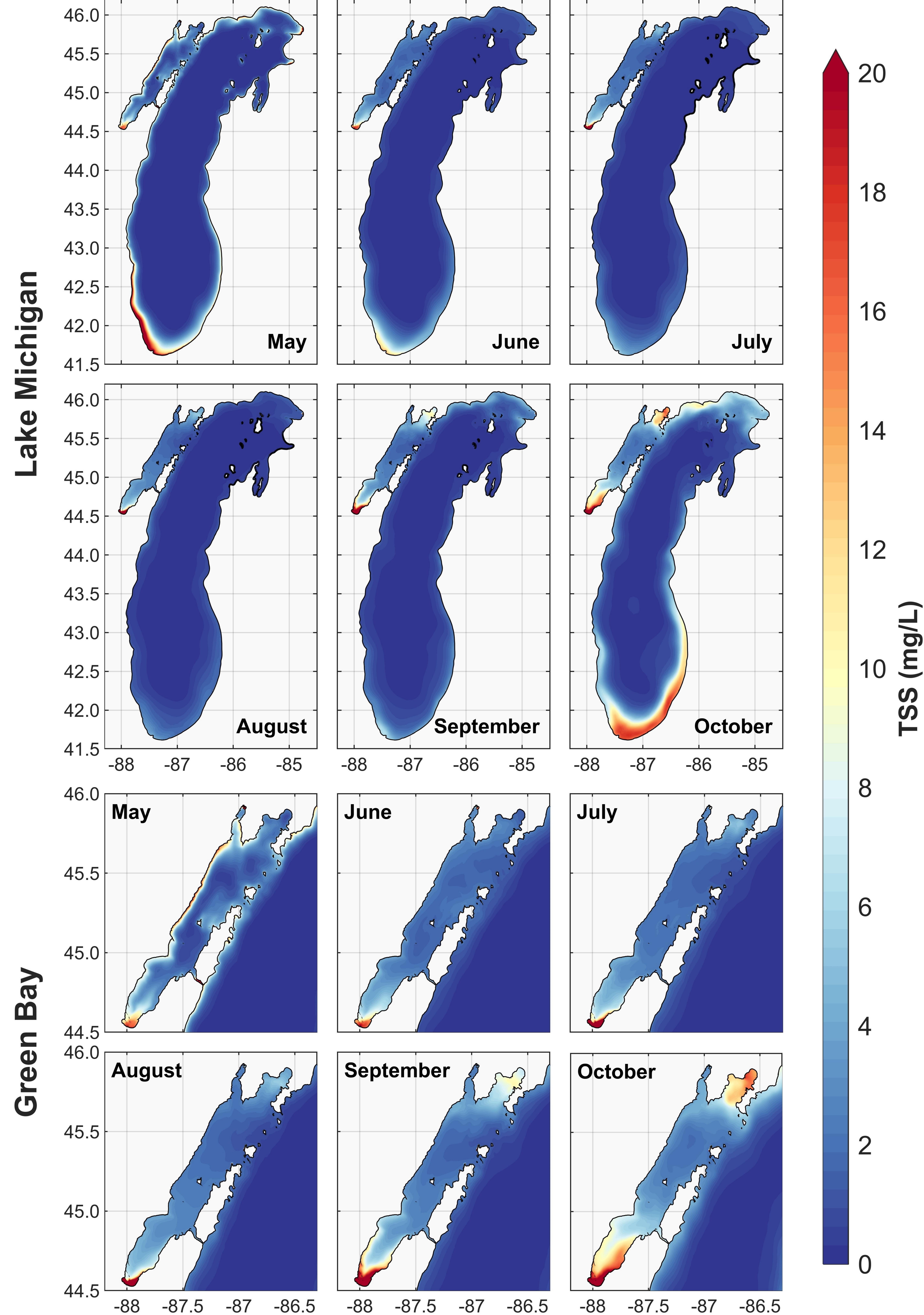




Figure 13.

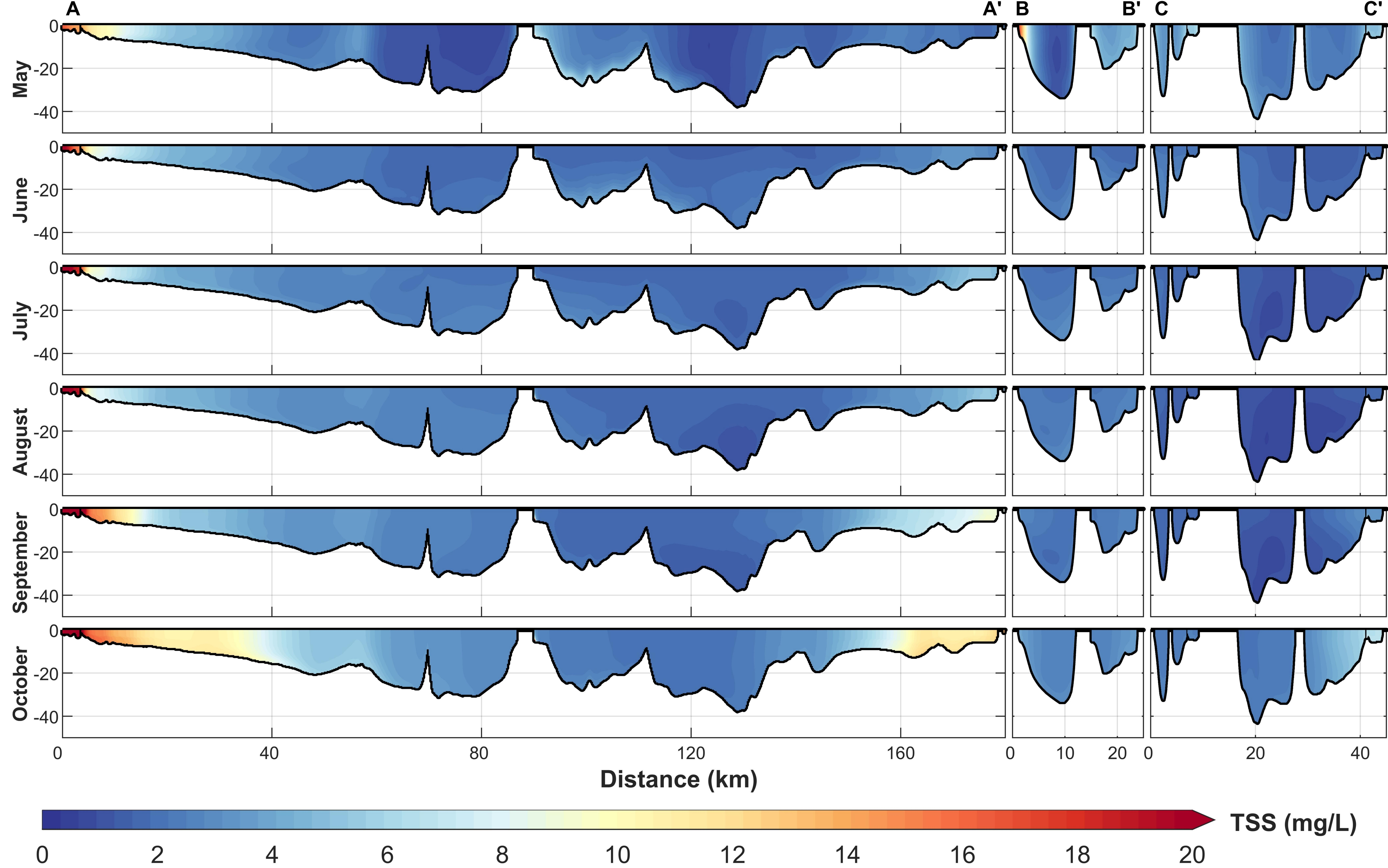
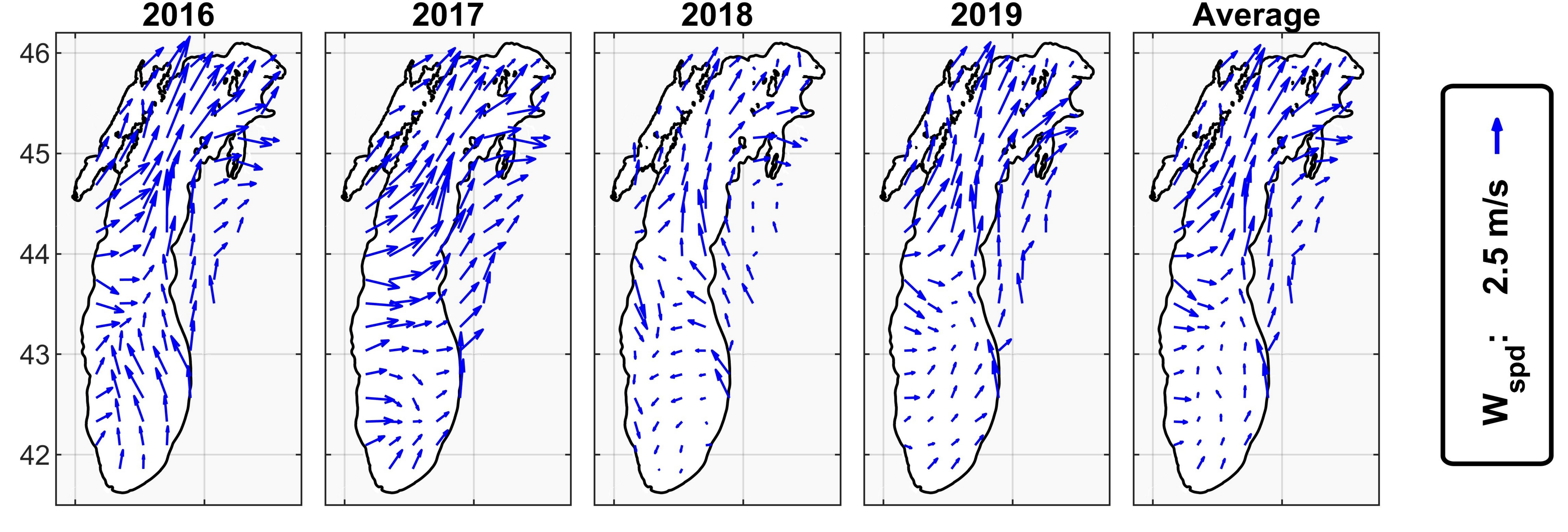
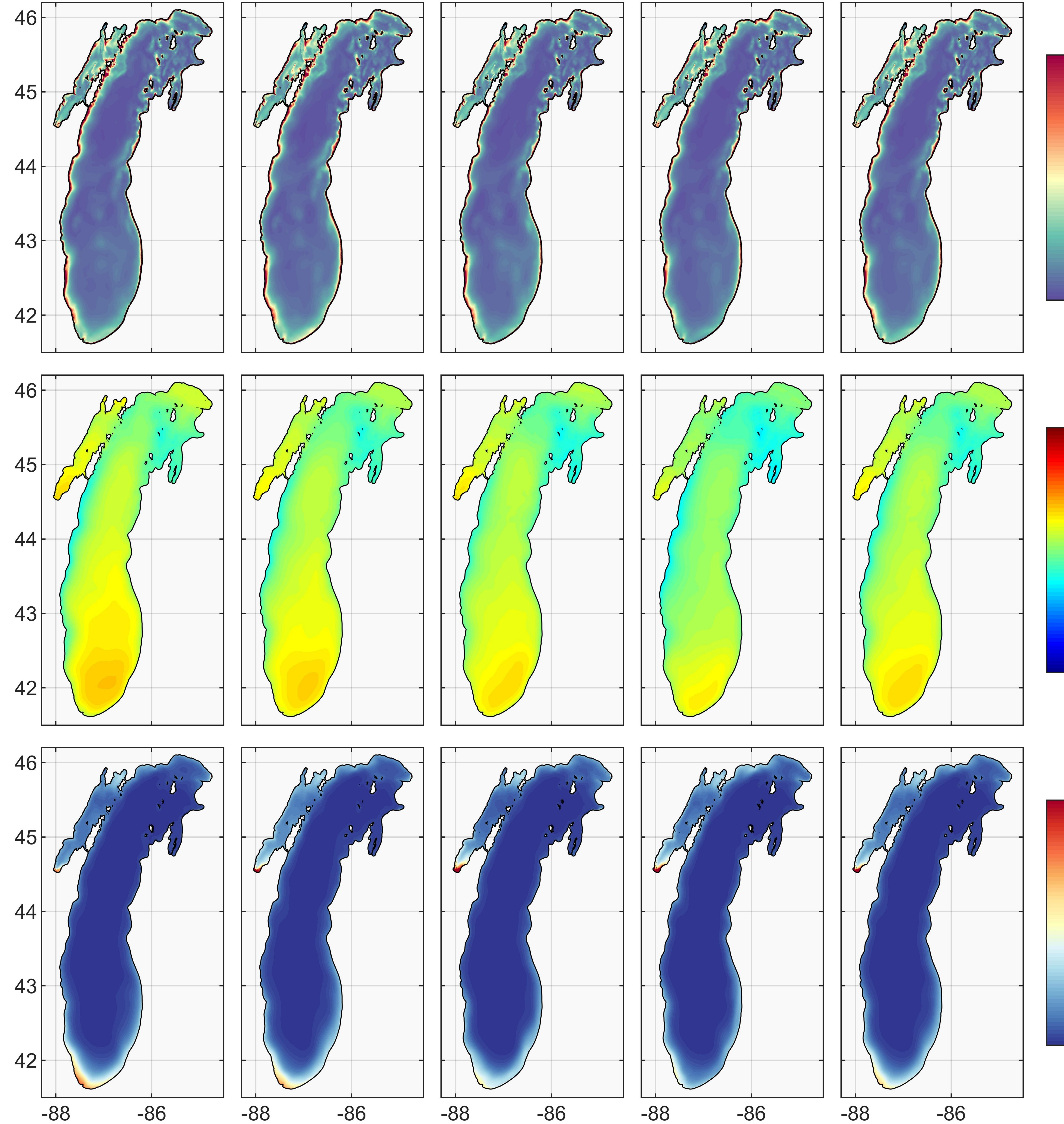
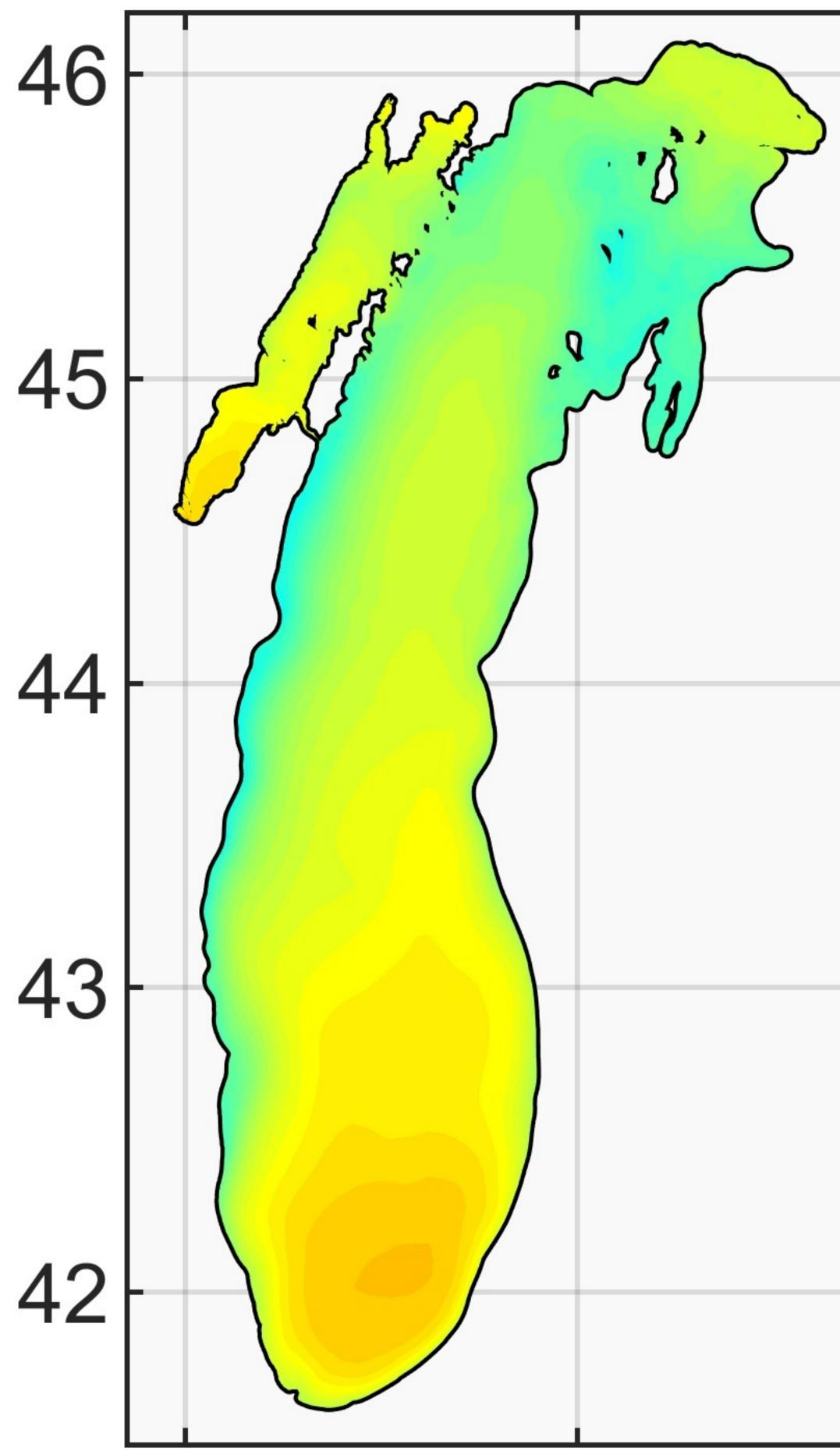
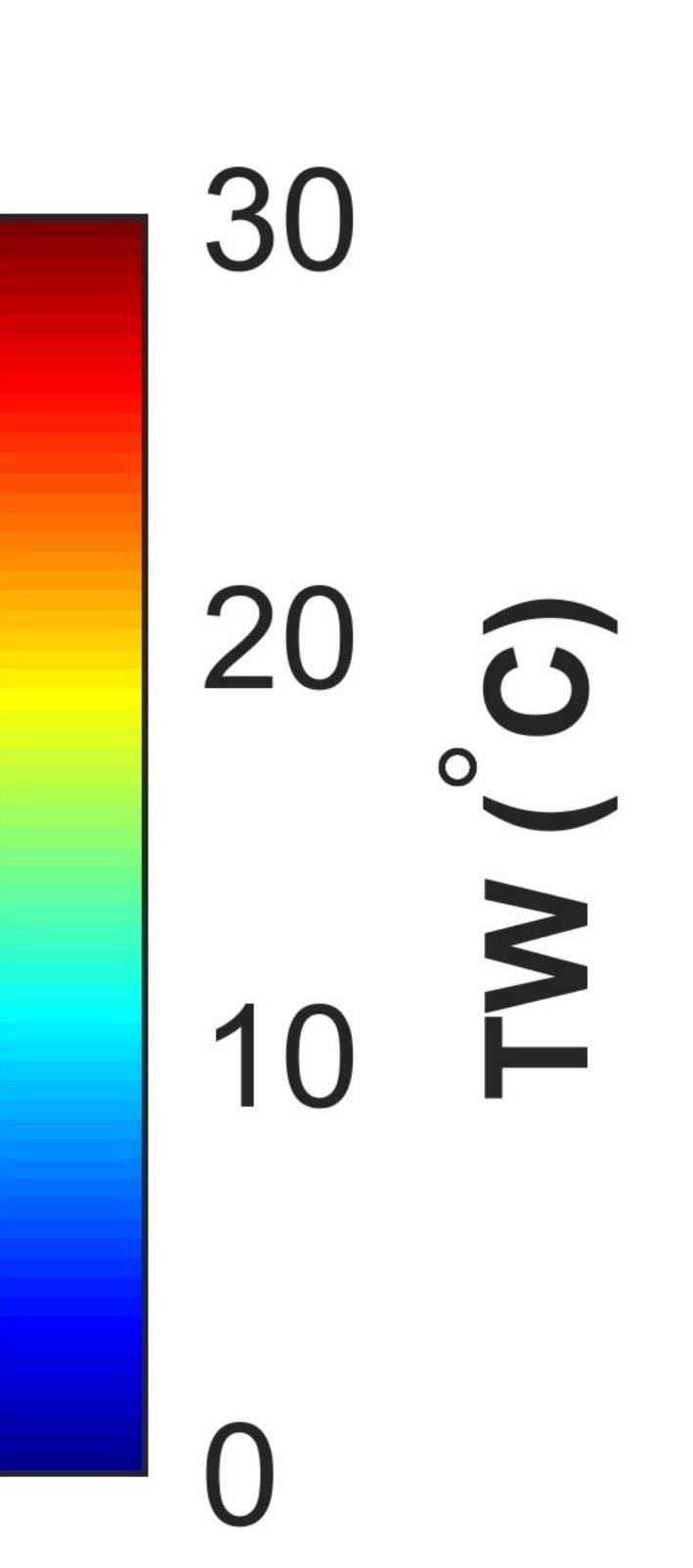


Figure 14.









 $\mathbf{\cap}$

Sf

 \mathbf{c}

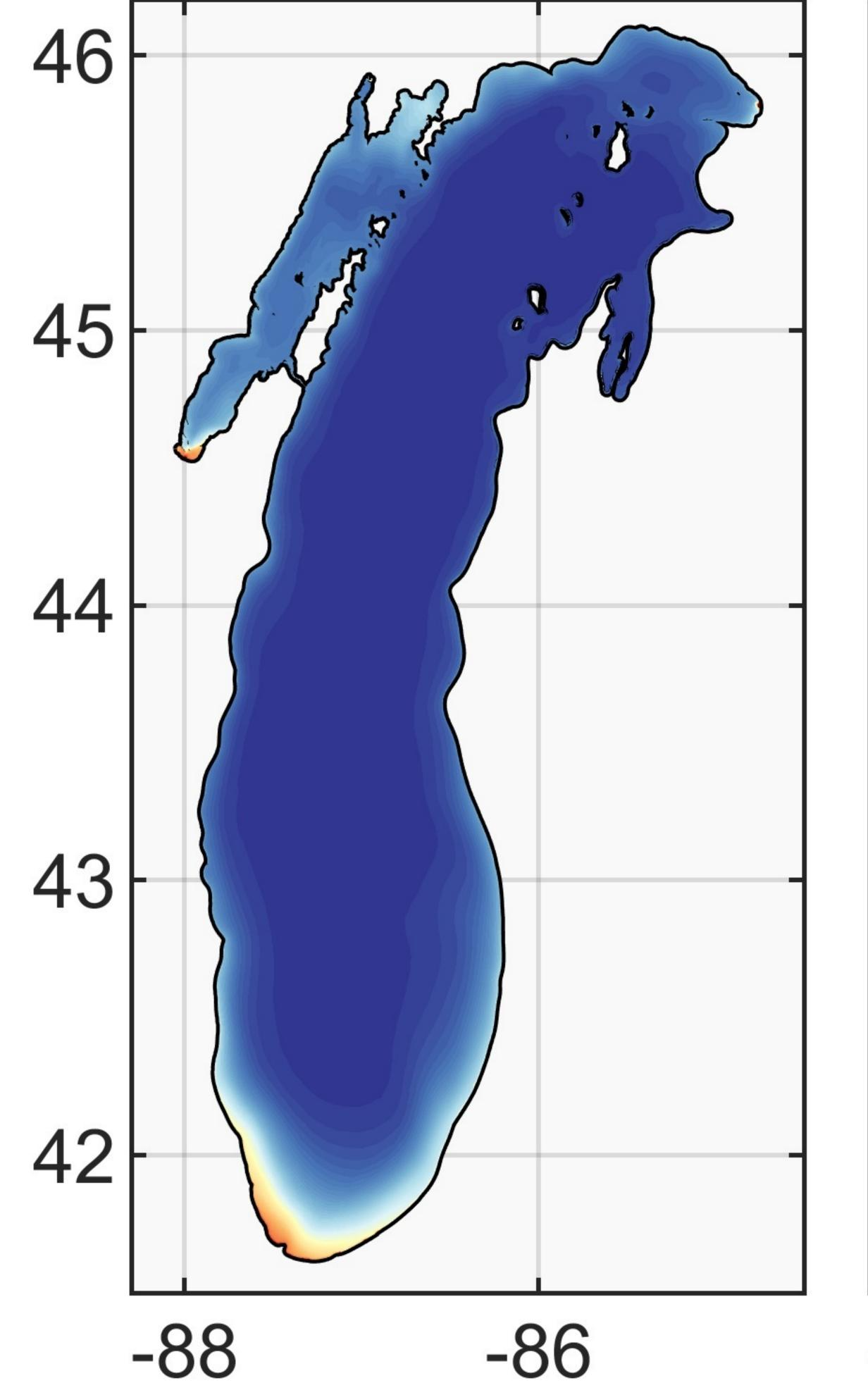


Figure S1.

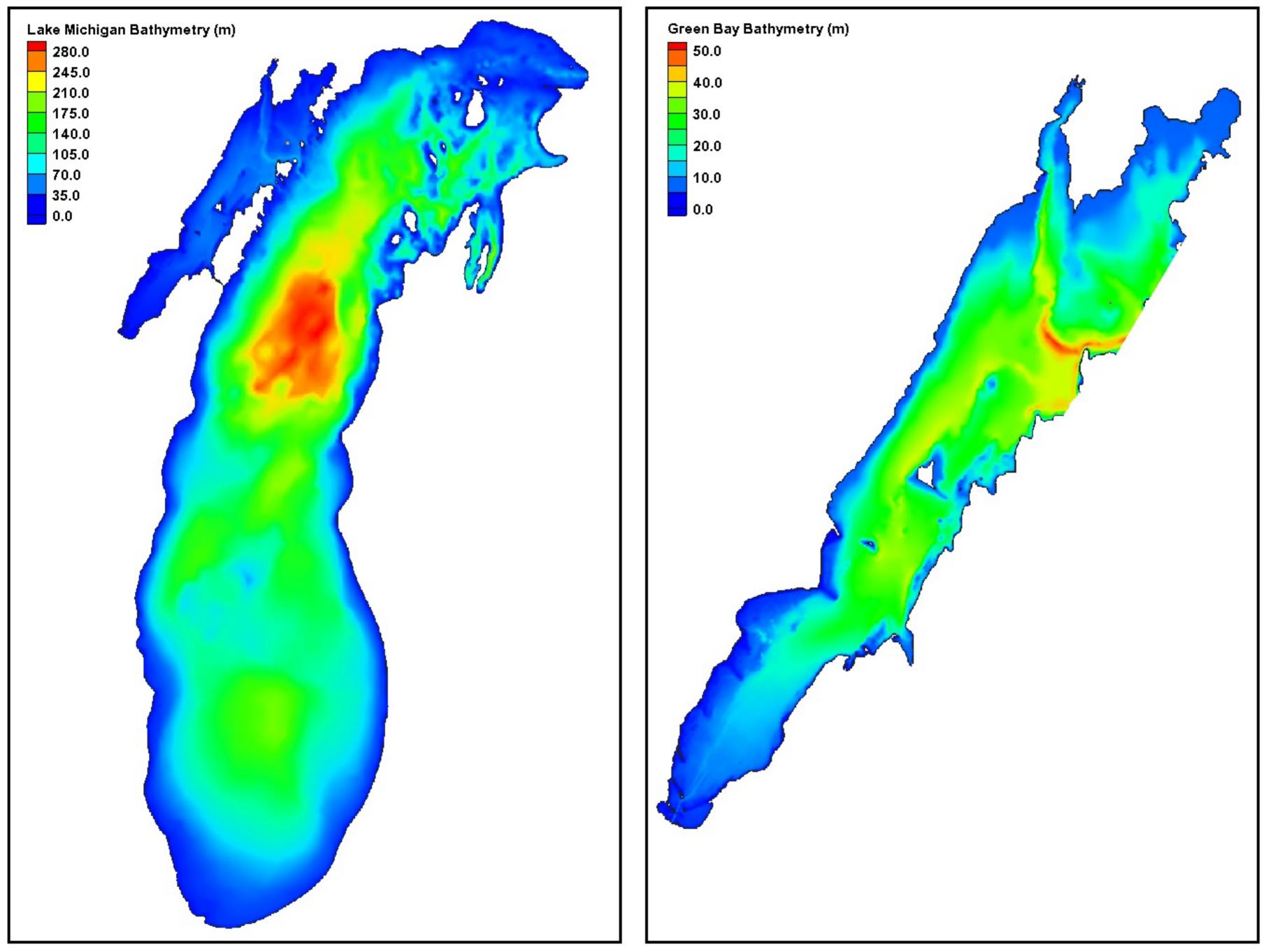


Figure S2.

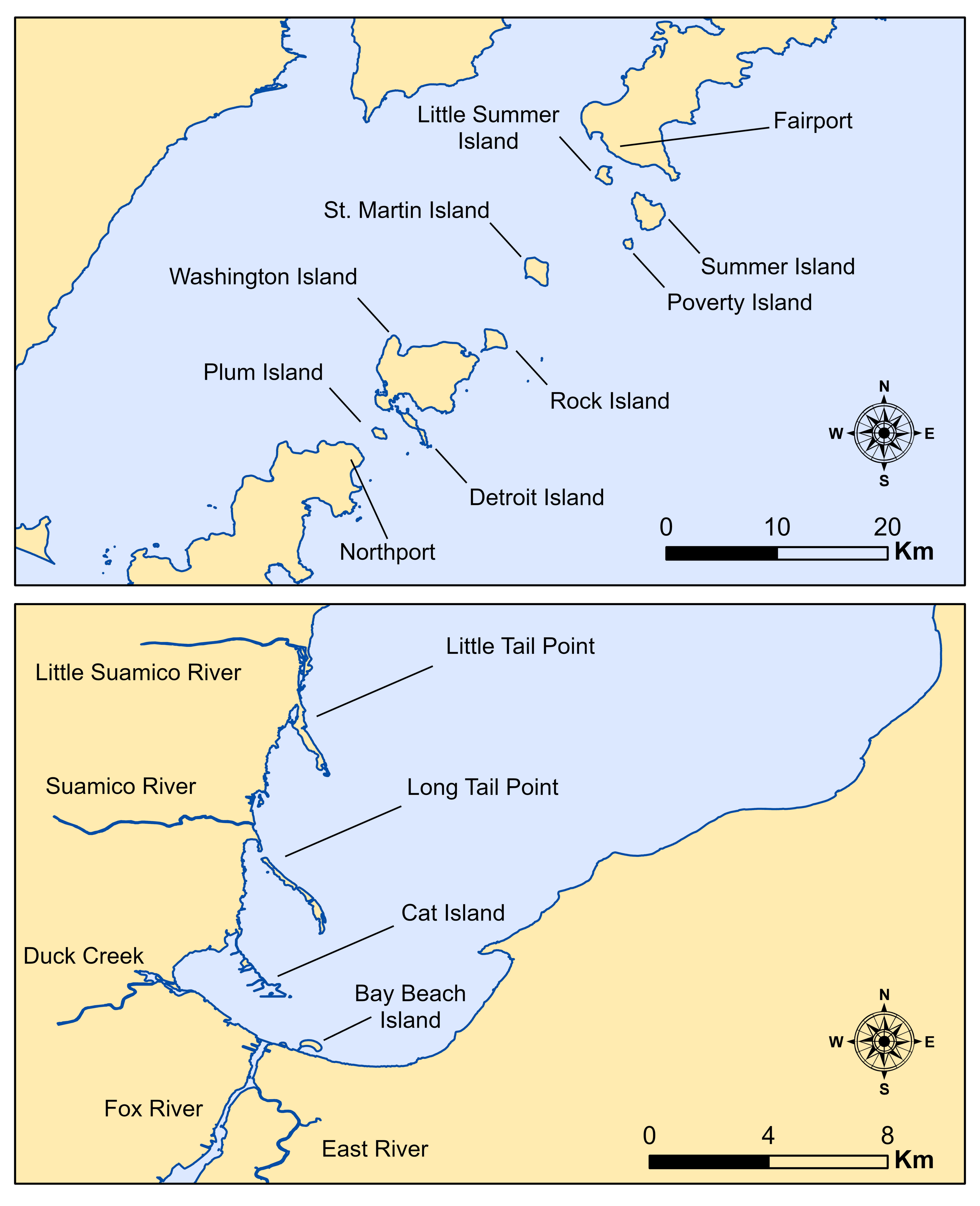
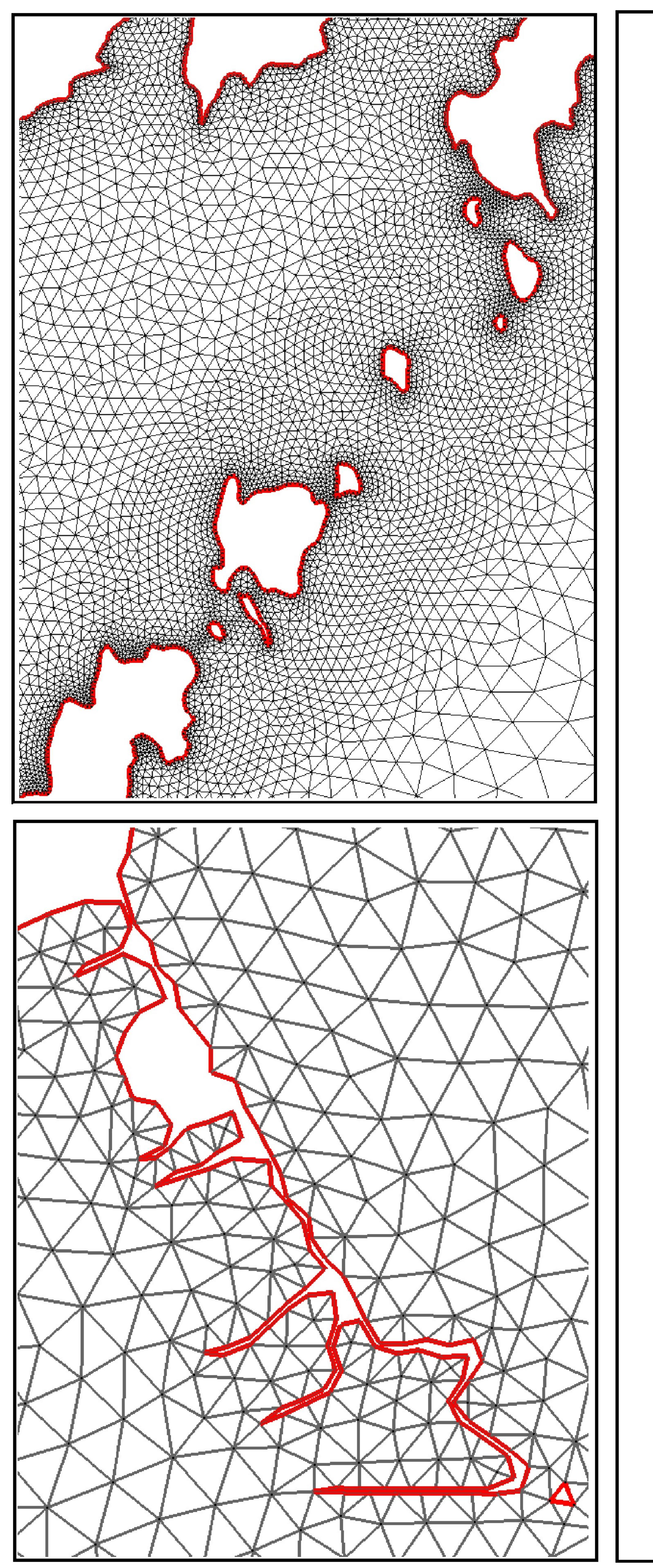


Figure S3.



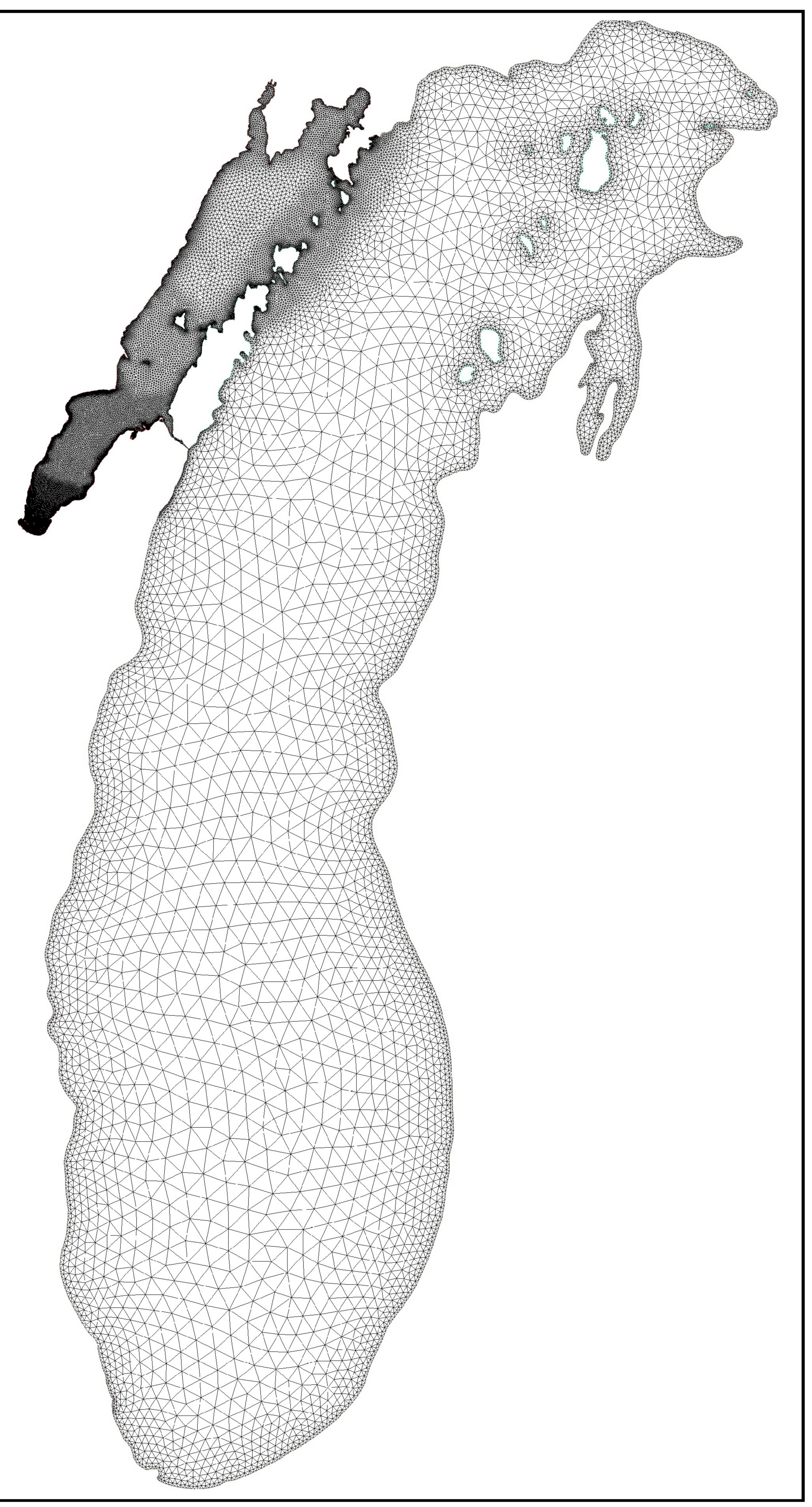


Figure S4.

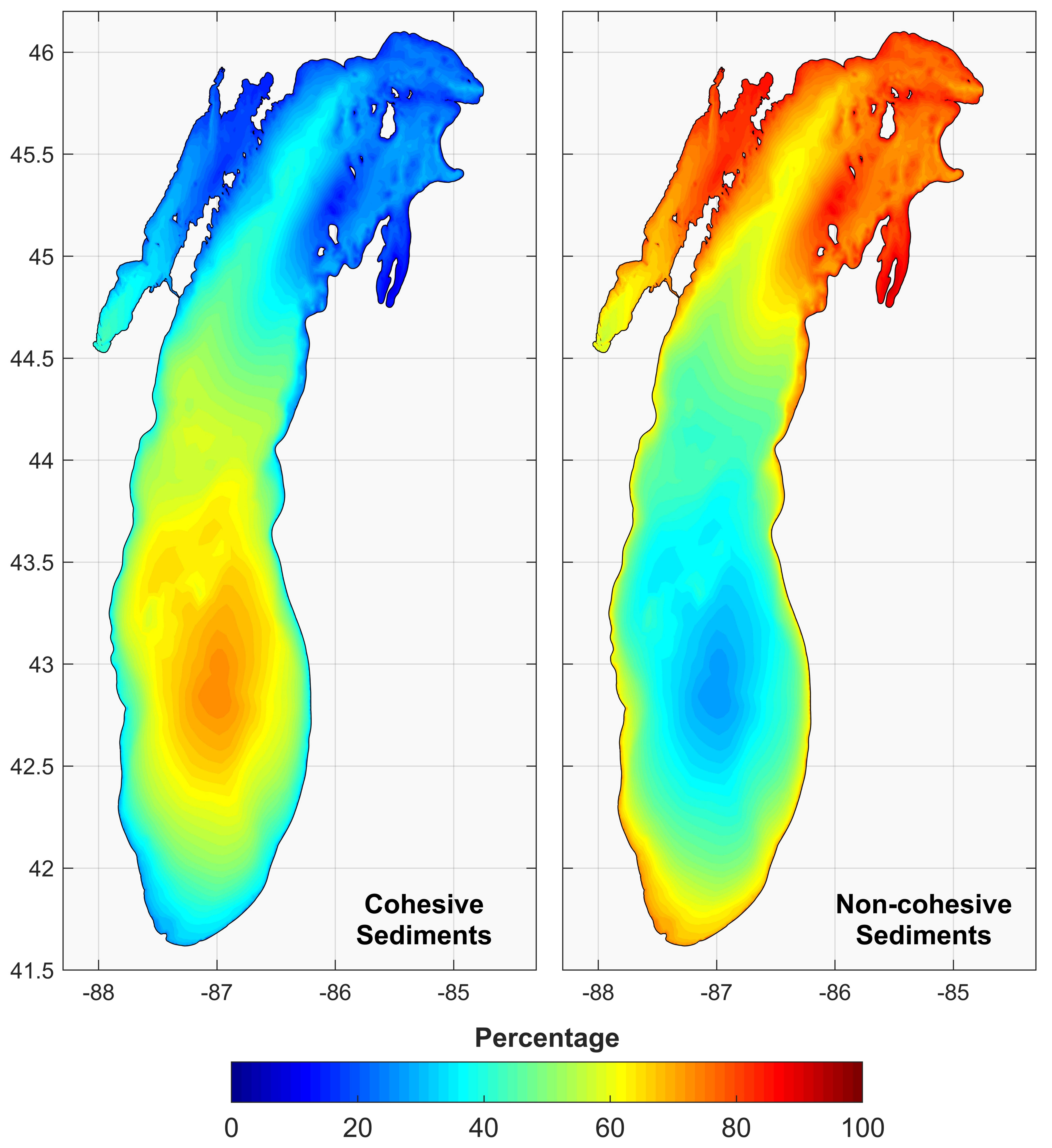


Figure S5.

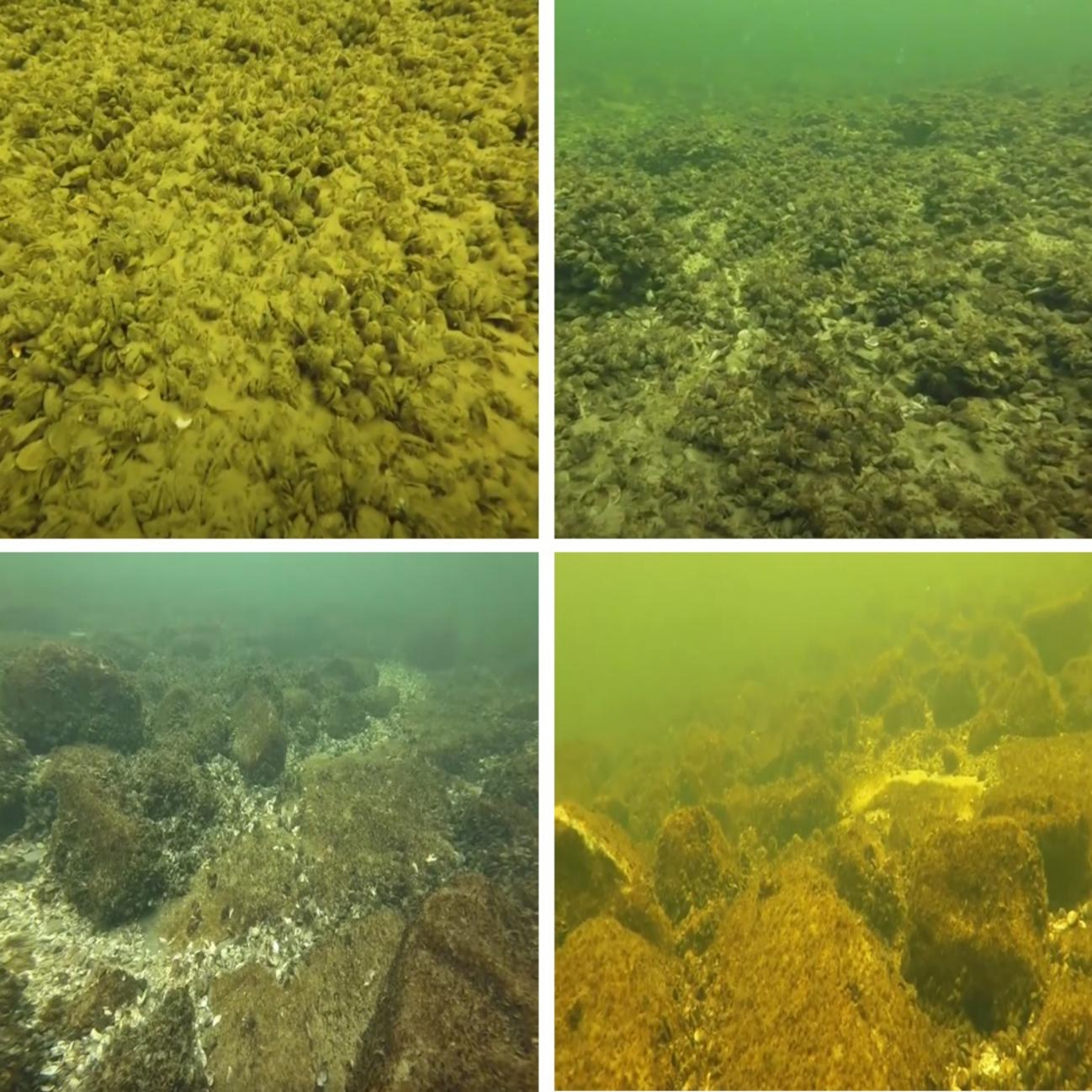
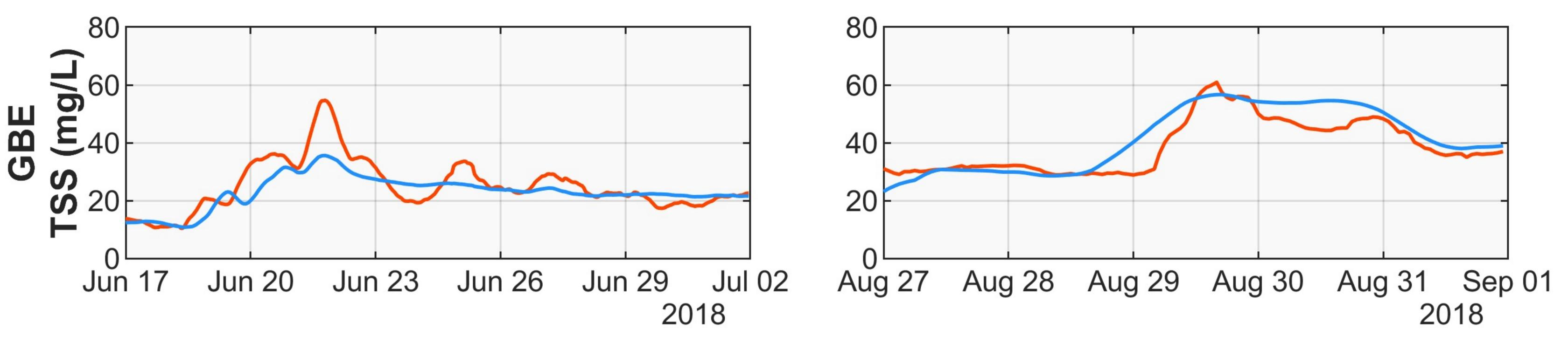
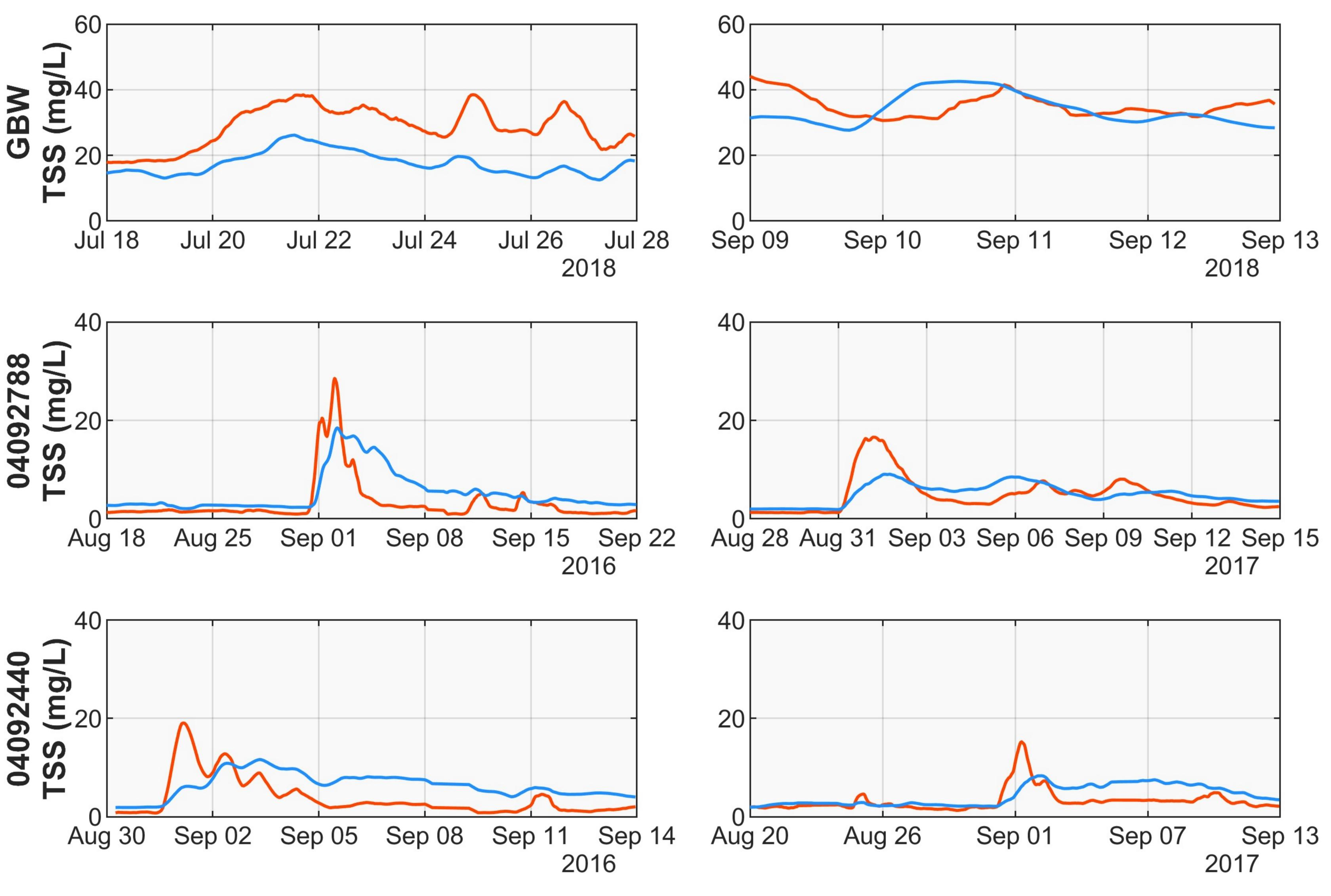
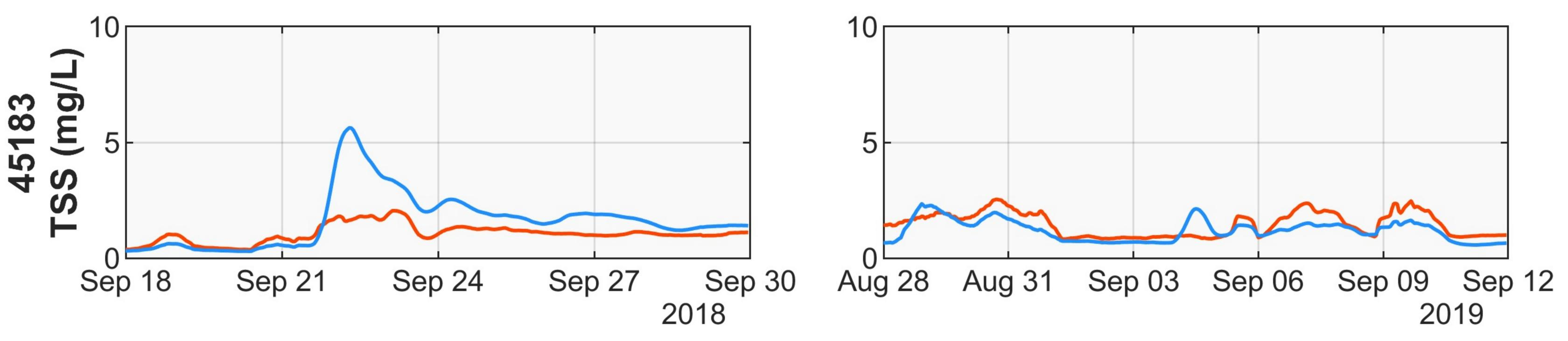


Figure S6.







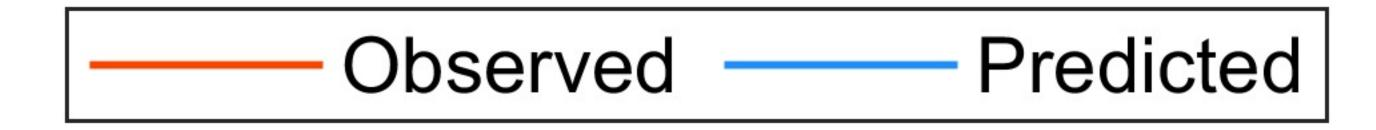
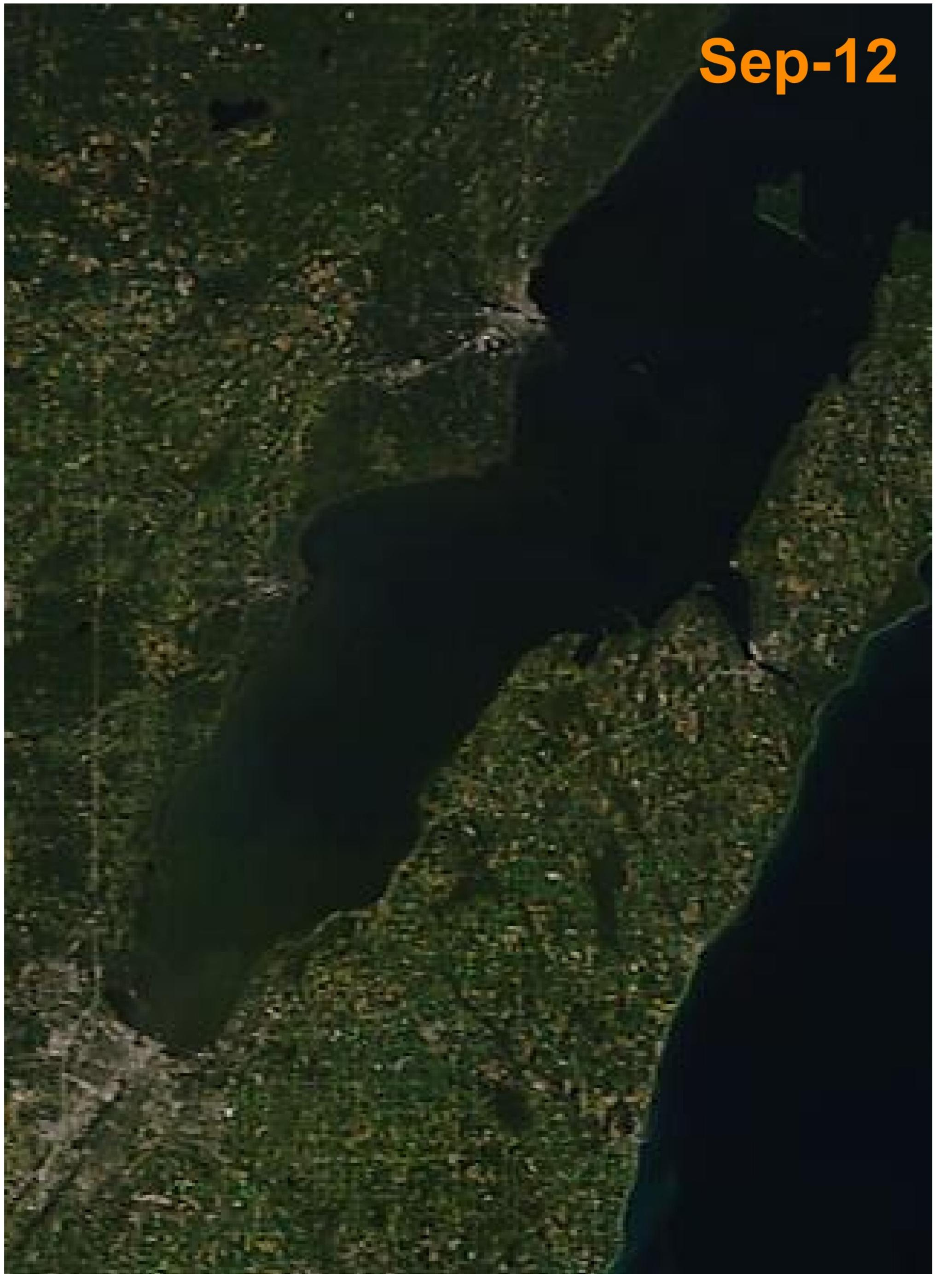


Figure S7.







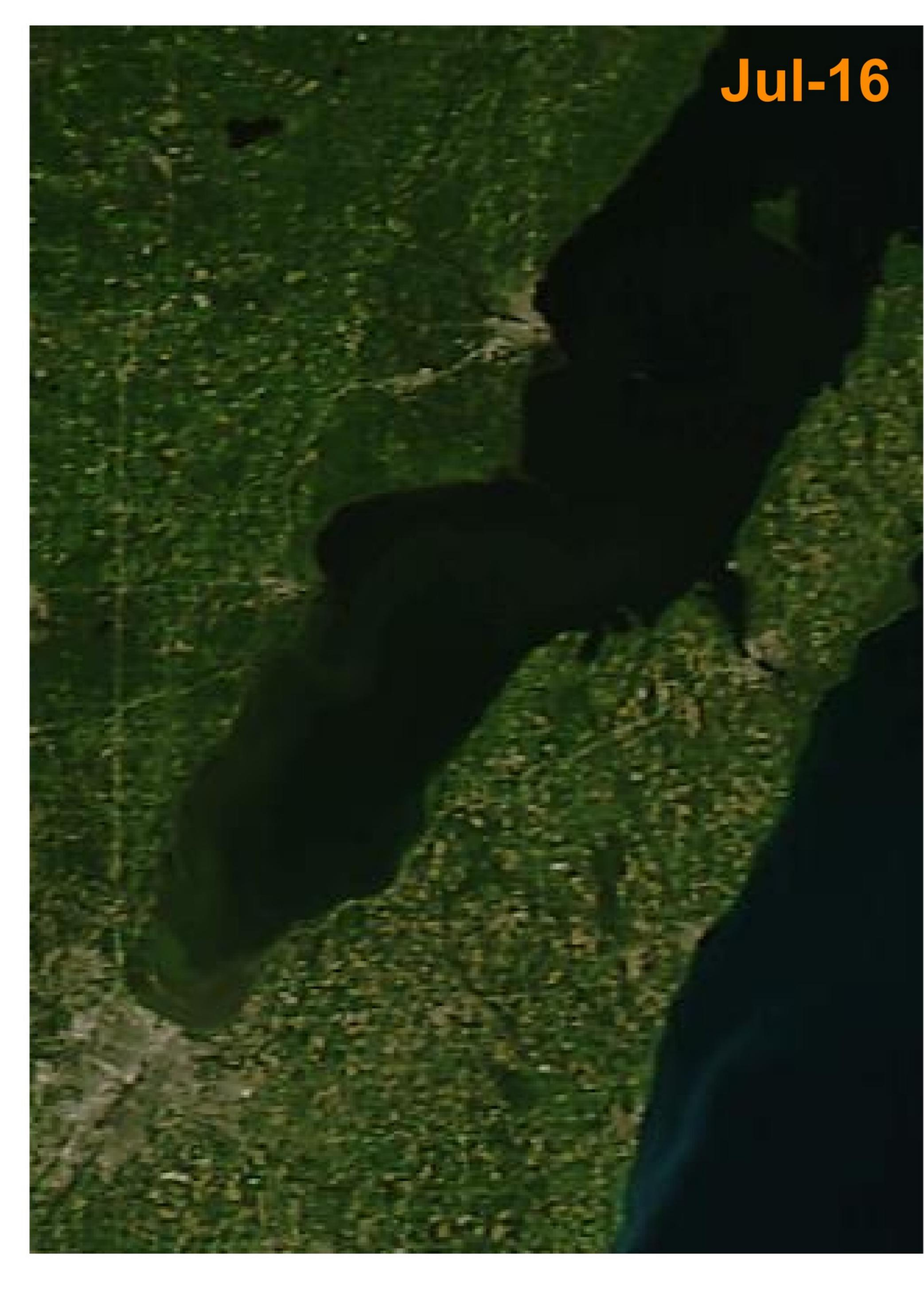
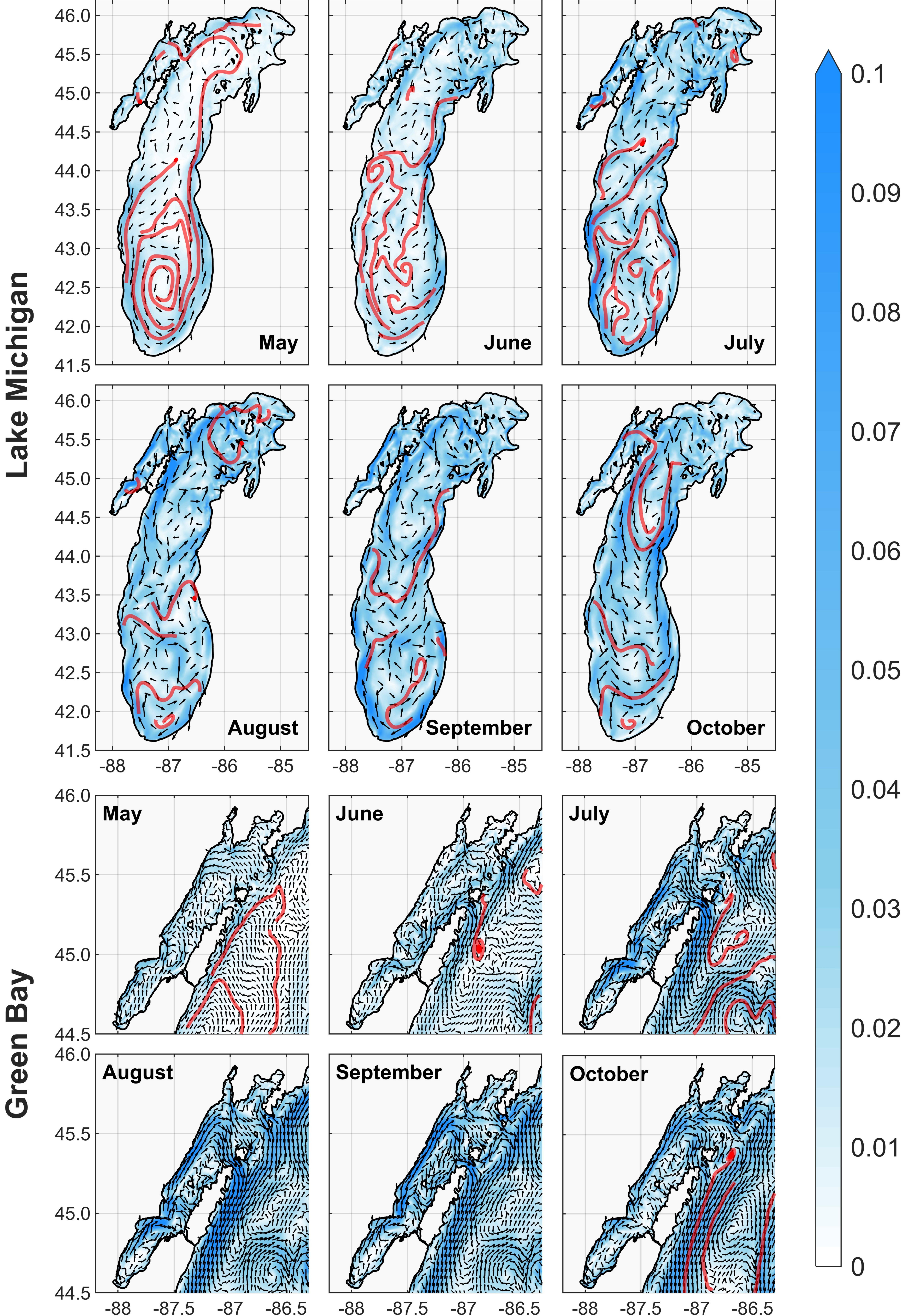




Figure S8.













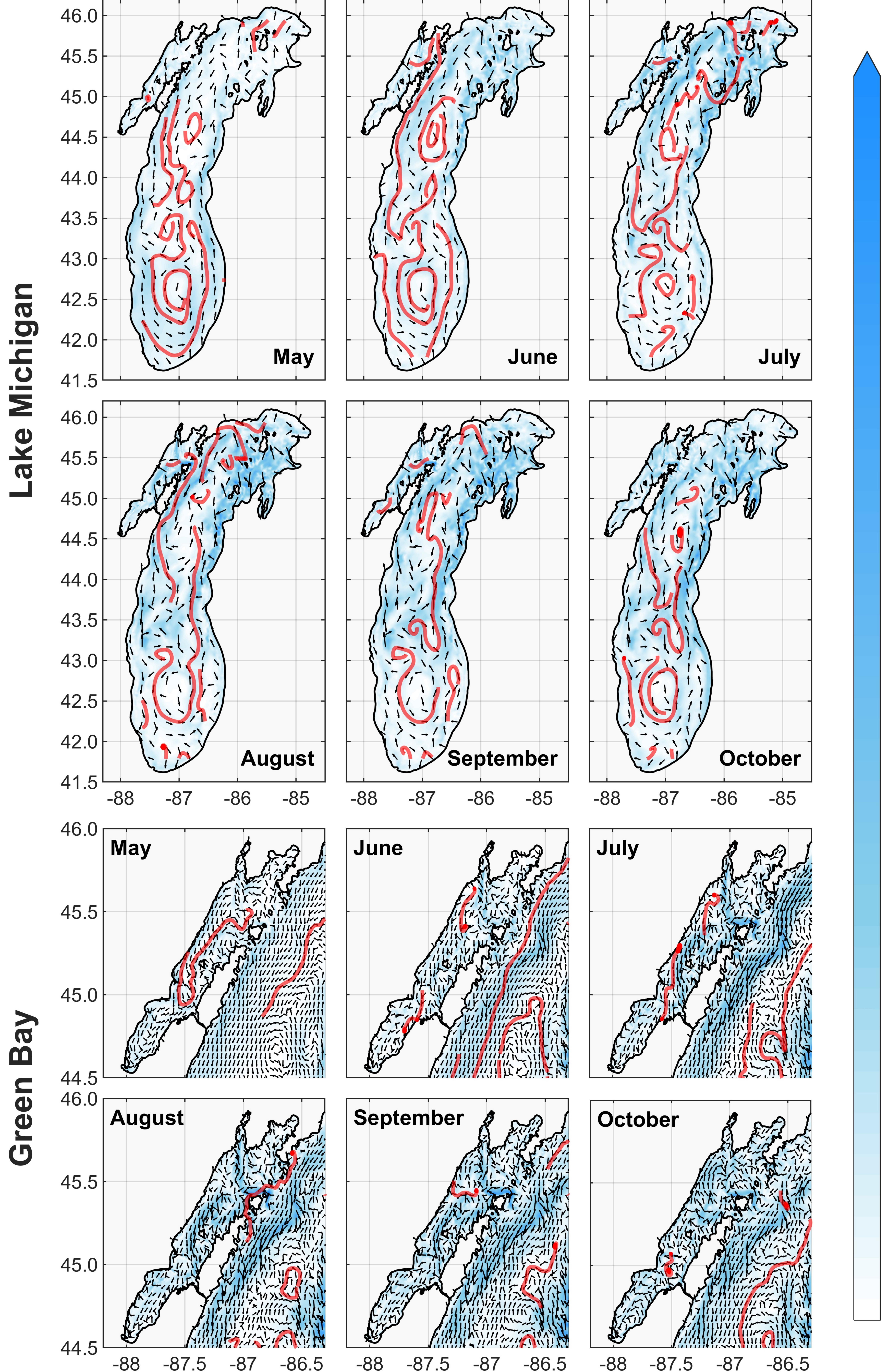
σ **D**S

.04

0.03

0.02

Figure S9.



0.1





0.07





0.05 J

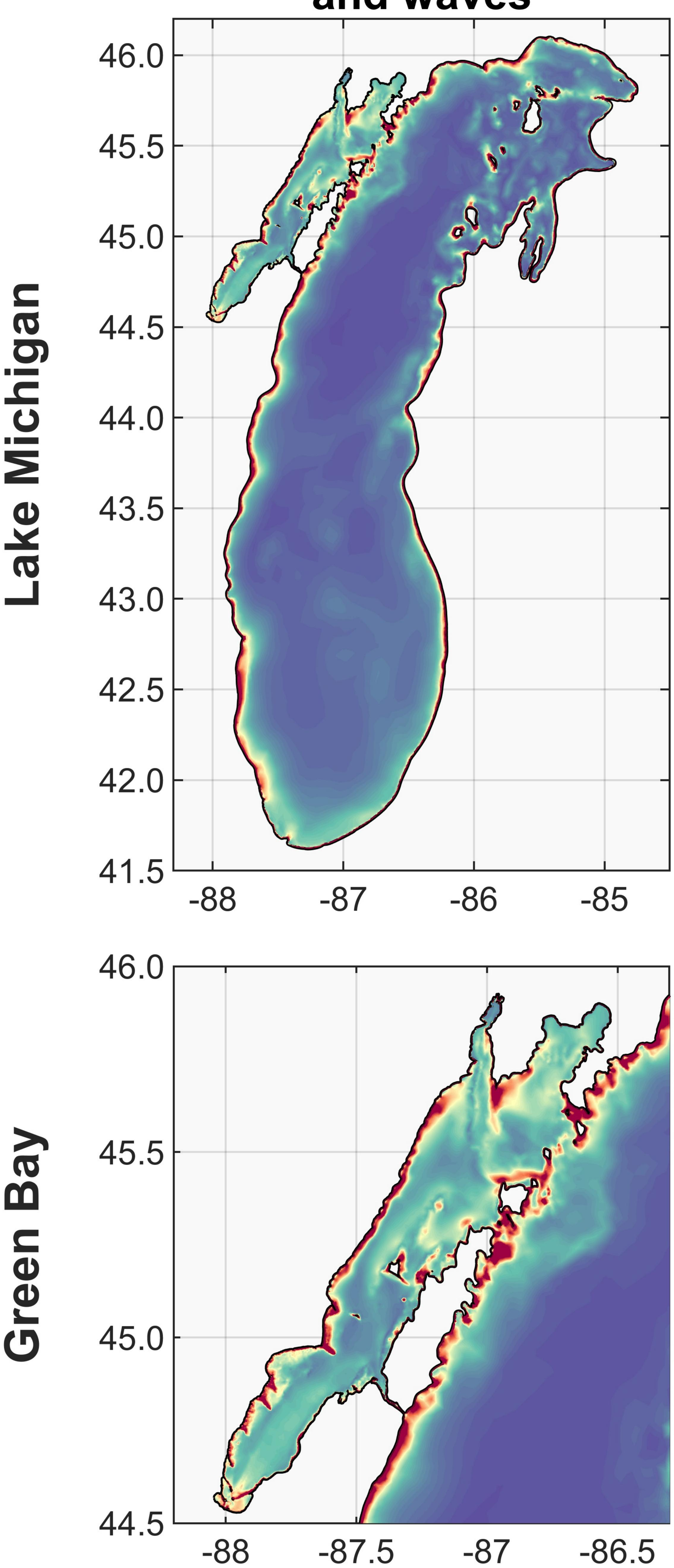
0.04

0.03

0.02

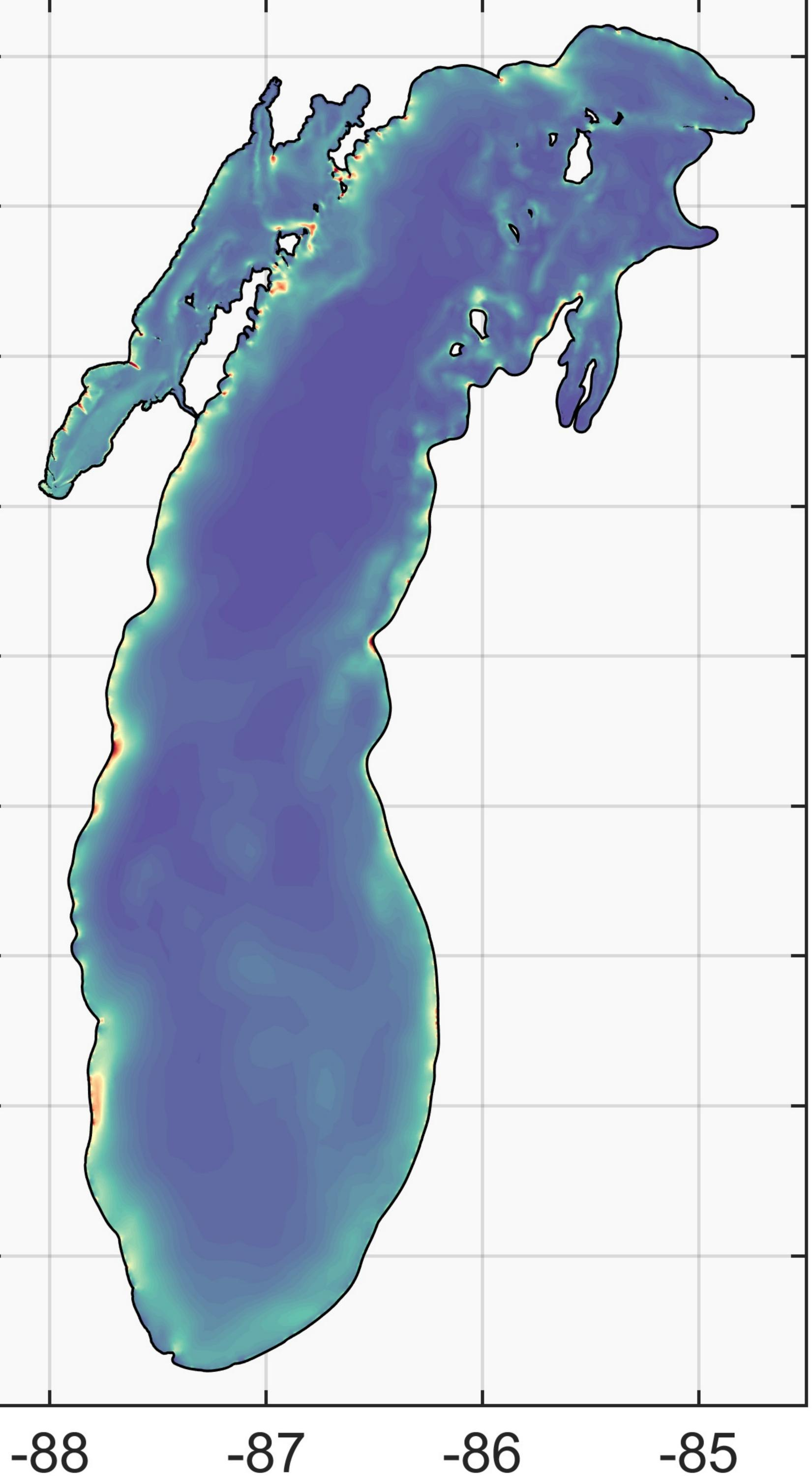
Figure S10.

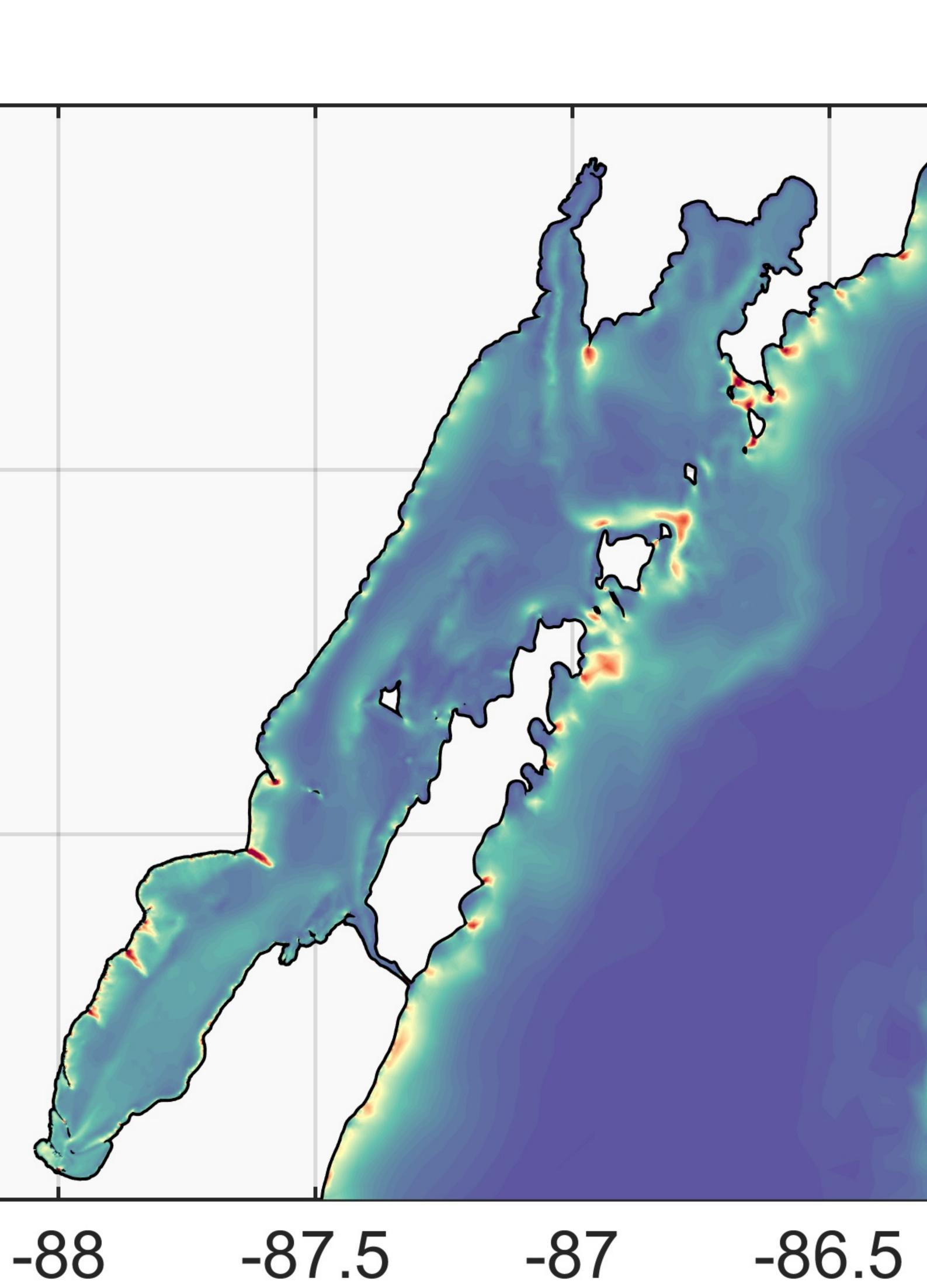
Combined currents and waves



ke Michigar

Currents only





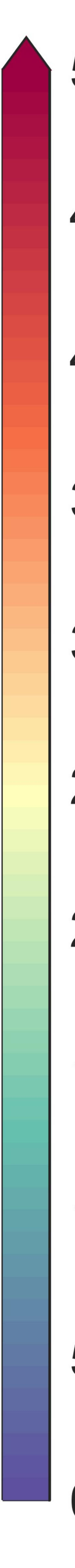
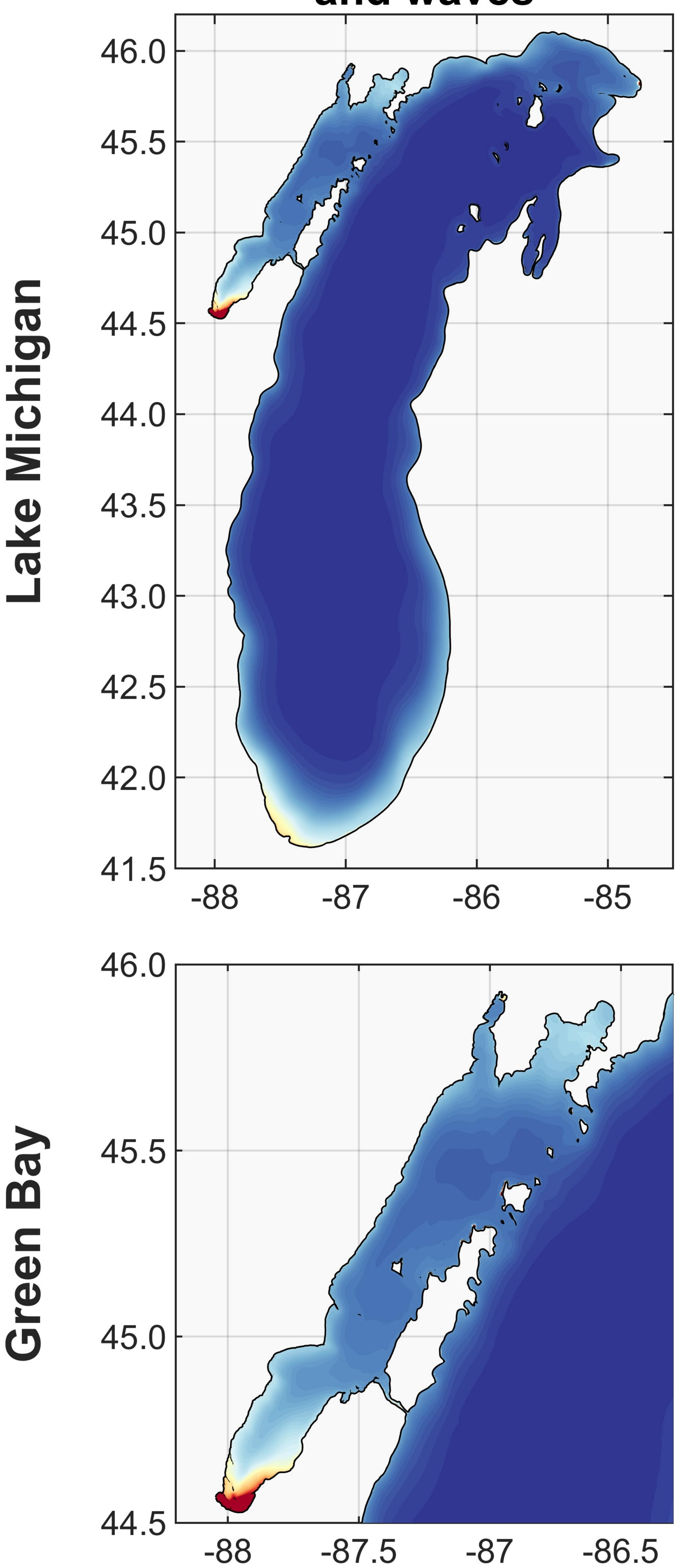


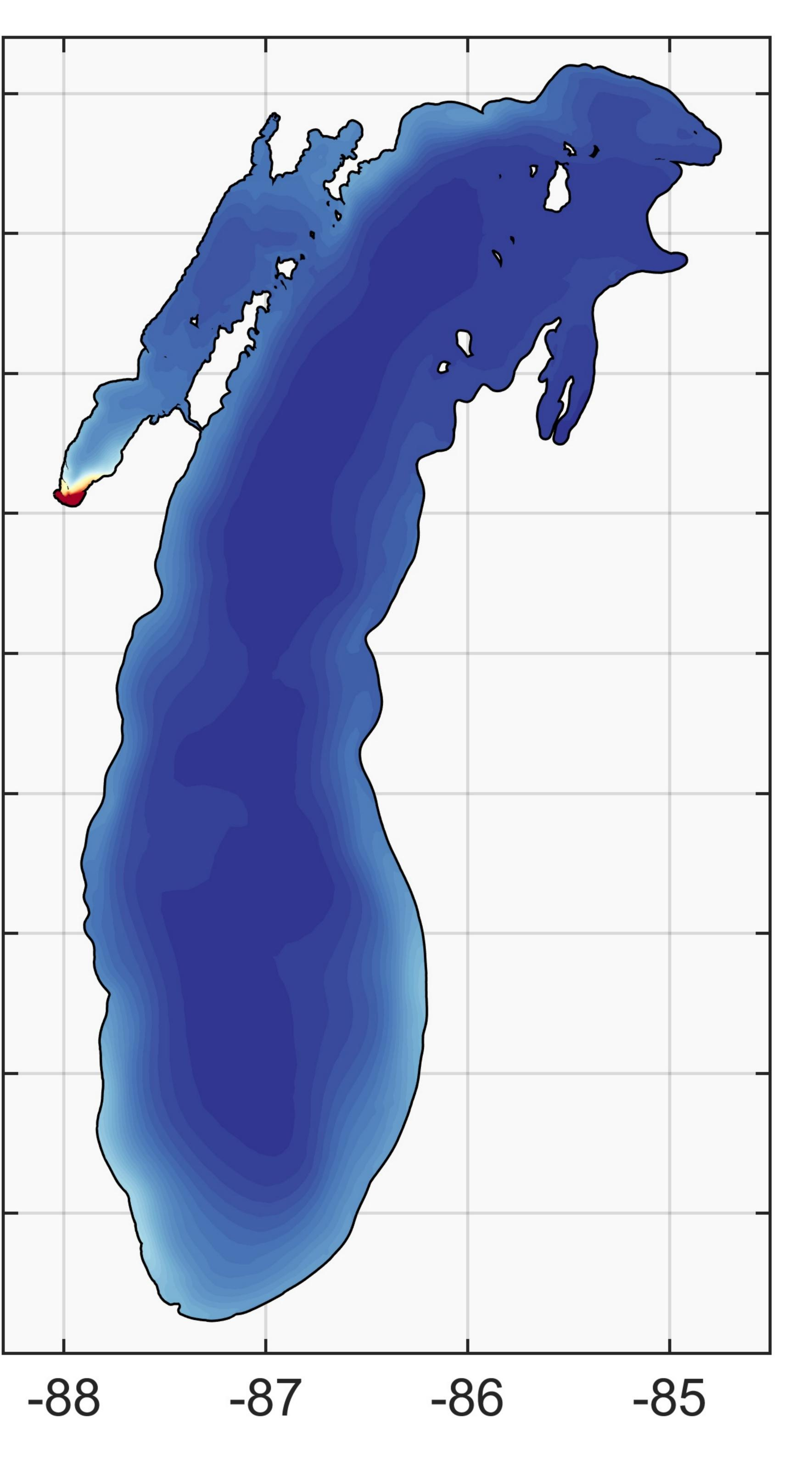
Figure S11.

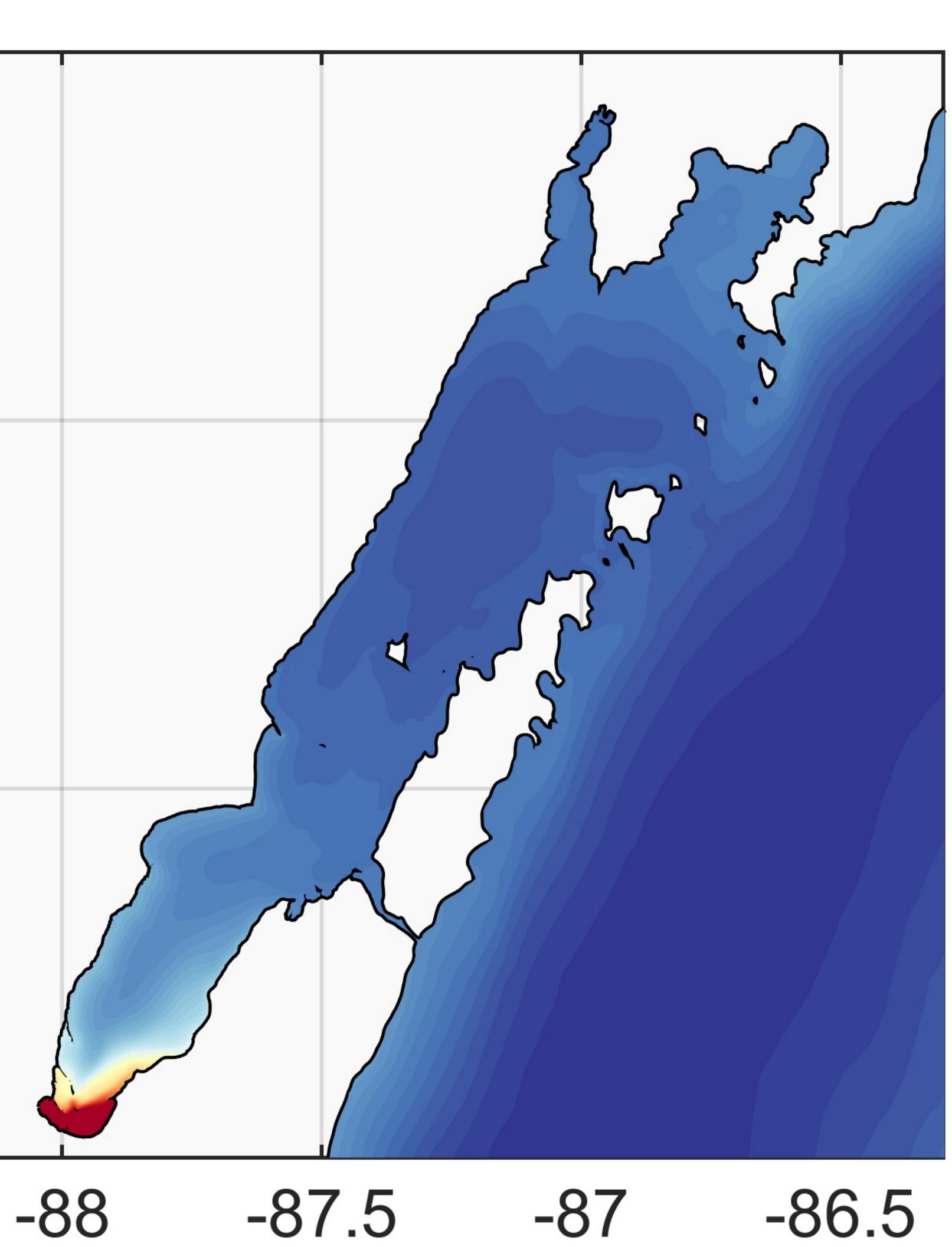
Combined currents and waves

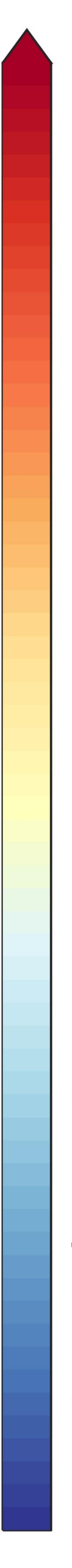


Lake Michigar

Currents only







20 Q 1 IO 16 14 10 10 8

Figure S12.

